MAGNETO-RHEOLOGICAL (MR) DAMPER DESIGN FOR OFF-ROAD VEHICLE SUSPENSIONS WITH FLOW BLOCKING ABILITY

RIAAN.F. MEESER

2015

Pretoria

South Africa

UNIVERSITY OF PRETORIA

UNIVERSITEIT VAN PRETORIA
UNIVERSITY OF PRETORIA
YUNIBESITHI YA PRETORIA

SUBMITTED IN PARTIAL FULFILMENT OF THE REQUIREMENTS FOR THE DEGREE: MASTERS IN MECHANICAL ENGINEERING IN THE FACULTY OF ENGINEERING, THE BUILT ENVIRONMENT AND INFORMATION TECHNOLOGY (EBIT).

Dissertation Summary

Thesis title:	Magneto-rheological (MR) Damper design for off-road vehicle suspensions with flow blocking ability
Author:	R.F. Meeser
Supervisor:	Prof. P.S. Els
Co-Supervisor:	Dr. S. Kaul
Department:	Mechanical and Aeronautical Engineering, University of Pretoria
Degree:	Masters in Mechanical Engineering

This study presents the design, development and testing of a magneto-rheological (MR) damper for an off-road vehicle. The MR damper developed in this study is expected to enhance the capability of the suspension system by allowing variable damping due to inherent properties of the MR fluid. MR fluids exhibit a reversible behaviour that can be controlled with the intensity of an external magnetic field, causing a change in the effective viscosity and thereby also in the force-velocity characteristics of the damper. The characteristic of this damper design distinguishes the damper developed in this study from the conventional damper used in the suspension system of a passenger car by having a controllable damping characteristic instead of a fixed one. The damper is designed to be used on the hydro-pneumatic 4 State Semi-active Suspension System ($4S_4$) that was developed by the University of Pretoria. Another additional feature of the damper developed in this study is the ability of the damper to act as a fluid flow blocking device so as to enable semi-active control of the suspension springs as required for the $4S_4$ system.

A mathematical model of the proposed damper has been developed using a modified Bingham plastic model. This model is used to determine the necessary geometry for the damper designed in this study, using the fluid flow rate and current to the electromagnet as the two main input variables. Furthermore, the model is used to compute the pressure drop over the MR valve as a function of the coil current and fluid flow rate. For manufacturing and size considerations, the proposed design incorporates a triple pass layout valve-mode damper with the MR fluid flowing through the three passages that are arranged in an S-shape so as to minimize the cross section of the electromagnet core while maintaining the required width and length of the valve to perform adequately.

An experimental setup has been built to test the validity of the analytical model. Experimental results confirm the applicability of the analytical model to accurately predict the pressure drop over the MR valve for given operating temperature and fluid properties. Experimental results show that the original MR damper designed for this study provides the required range of damping as compared to the reference system used for this study, with the only error being that the values of damping, both in the on-and off-state, are lower than expected. By using the validated theoretical model it has been seen that the whole range of damping characteristics can be shifted upwards by reducing the MR fluid passage height inside the valve which should yield the required characteristics.

Keywords

MR fluid, Magneto-rheological fluid, Blocking ability, Semi-active suspension damper.

Table of Contents

List of figures

List of tables

List of symbols/Abbreviations

Symbol/ abbreviation	Description	Unit
a	Quasi-Bingham behaviour constant, MR fluid	-
B	Flux density, magnets	Tesla
C	Carrier fluid correction factor, MR fluid	-
c	Empirical value for Dr. Dave Equations, MR fluid	-
C_0	Control voltage dependant variable, MR fluid	-
C1	Low flow rate curve fit constant 1, MR fluid	-
C2	Low flow rate curve fit constant 2, MR fluid	-
D	Active volume empirical factor, MR fluid	-
EMF	Electro motive force	Volt
F	Magneto motive force (MMF), magnets	Ampere. Turns
f	Friction factor, MR fluid	-
f	Bouc-Wen factor, MR fluid	-
Hz	Frequency	Cycles/second
H	Field intensity, magnets	A/m
i	Electric current, electric	Ampere
L	Volume	Litre
l	Magnetic path, magnets	meter
MR	Magneto-rheological	-
MMF	Magneto motive force	Ampere.turns
m	Distance	meter
N	Number of windings, magnets	-
n	Shear thinning constant, MR fluid	-
P	Pressure	N/m^2
R	Resistance, electrical	Ohm
R	Reluctance, magnets	Ampere.turns/weber
t	Time	second
T	Temperature	°C
V	Electrical voltage, electric	Volt
V	Velocity	m/s
W	Weighing factor, MR fluid	-
z	Evolutionary variable, MR fluid	-
α	Control voltage dependant variable, MR fluid	-
β	Temperature-viscosity constant, MR fluid	-
$\dot{\gamma}$	Shear rate, MR fluid	1/s
η	Viscosity, MR fluid	Pa.s
μ	Magnetic permeability, magnets	$Weber/m^2$
μ_r	Relative permeability, magnets	-
μ_0	Magnetic permeability of free space, magnets	$4\pi 10^{-7}$
σ	Material conductivity, electrical	Siemens/meter
τ	Shear stress, MR fluid	N/m^2
τ	Time constant, Magnets	second
Φ	Particle volume fraction, MR fluid	-
$\Delta P_{headloss}$	Head loss pressure drop, MR fluid	N/m^2
ΔP_{rheo}	Rheological pressure drop, MR fluid	N/m^2
Vol_{active}	Active MR fluid volume	m^3

1. INTRODUCTION

This chapter provides an overview as well as the main motivation for the research performed as part of this study. A brief description of spring-damper systems, used in vehicle suspensions is provided. The focus is on the different types of force elements and their key characteristics. Some details of the 4 State Semi-active Suspension System ($4S_4$) that has been developed at the University of Pretoria are also provided.

1.1. Background

Ride comfort and safety are two very important considerations in vehicle design. The vehicle suspension system is a very crucial component of a vehicle that significantly influences ride comfort as well as safety. The suspension system enhances ride comfort by isolating the vehicle body from the disturbances experienced when moving over a rough terrain. Furthermore, the suspension system is also expected to enable a vehicle to travel in a safe and predictable manner over a certain terrain, this is typically expressed as handling behaviour in the relevant literature. However, there is an inherent compromise associated with the two requirements as far as suspension design is concerned. Vehicle suspensions that are designed for superior ride comfort often lack the ability to behave in the required manner for adequate handling performance.

Suspension systems need to be designed for a vehicle-specific application that takes into consideration the type of handling required, while providing the best possible ride comfort for the terrain over which the vehicle will need to operate. This can be a potential problem since the optimal suspension settings can vary substantially for different operating conditions. Good handling on tar surfaces generally require stiff suspension springs with high damping to limit body roll, whereas ride comfort usually requires a softer, more forgiving, suspension system. The optimal suspension settings for these two cases generally contradict each other (Els, 2006).

This is especially true for vehicles that travel both on- and off-road where good handling as well as good ride comfort is required. Off-road vehicle suspension systems are usually characterised by their larger suspension travel to allow the wheels to move freely without reaching their bump and rebound stops. These suspensions also exhibit higher suspension velocities due to the increased roughness of the off-road terrain as compared to a smooth road surface. The designer of an off-road vehicle suspension is, therefore, faced with the challenge of compromising the designed suspension characteristics between a suspension system that will yield good handling characteristics, and that of a suspension that will yield good ride quality. Another aspect that needs to be considered is that off-road vehicle suspensions with higher travel usually result in locating the centre of mass of the

vehicle higher off the ground so as to allow for large travel. This can be detrimental to high speed handling on a flat surface and increase the rollover propensity (Els, 2006).

A satisfactory solution to the compromise in suspension settings cannot be obtained by using passive (fixed spring and damping characteristics) suspension systems. By implementing a controllable suspension on a vehicle where the ride height, spring stiffness and damping of the suspension can be altered without stopping the vehicle, it would be possible to select the optimal settings required for the vehicle handling and ride comfort over a specific terrain as the vehicle travels over that terrain. To obtain optimal spring rate and damping values for a vehicle suspension over a given terrain, controllable suspension systems have been developed that may be classified as fully active suspension systems, semi-active/adaptive and self-levelling suspension systems (Gillespie, 1992).

Fully active suspension systems incorporate actuators to both supply and absorb the desired forces in the suspension, these actuators can be hydraulic, pneumatic, or electromagnetic. Fully active suspension systems need to be designed for very high reliability, and require high energy levels to satisfactorily supply the required suspension forces. As a result, these suspension systems are very expensive and complex to implement. Fully active suspension systems also pose a high safety risk since the suspension would be able to overturn the vehicle in case of a controller failure or malfunction.

Semi-active suspension systems contain spring and damping elements with properties that can be changed through an external control system, these elements can only dissipate energy (damping) or temporarily store energy (spring). External power is required to change the properties, but this power is orders of magnitude less than the power required in fully active suspensions. Furthermore, a controller failure does not lead to a safety risk since the suspension becomes passive. This has made semi-active suspensions particularly appealing. Semi-active suspensions may further be categorised into slow-active/adaptive or low/high bandwidth systems. In the slow-active systems the spring rate and damping settings may be switched between different levels, in either discrete steps or continuously, using a control system which takes variables such as steering angle, braking and suspension motion into account. Switching on occurs very quickly so that the system may control dynamic effects such as pitch, bounce and roll motions of the sprung mass; with the switching back to softer settings occurring after some time has passed. This means that the system does not continuously adjust the spring and damper characteristics during individual suspension oscillation cycles. These systems are also called “adaptive suspensions”. Low and high bandwidth semi-active suspensions have the ability to vary spring rate and damping in individual cycles of

suspension movement with low bandwidth reacting to low frequency sprung mass motions and high bandwidth to both sprung and un-sprung mass movements.

Self-levelling/adaptive suspensions are just a variation of passive suspensions where the ride height may be adjusted according to the load that the vehicle experiences. Reaction time is slow, usually greater than 5 seconds and is typically implemented by means of an air spring to add the required force to level the vehicle (Gillespie, 1992).

It can be argued that the most feasible controllable suspension design would be a semi-active/adaptive suspension. This is due to the relatively high level of control, and compared to fully active suspension systems, at relatively low cost and complexity. For a semi-active suspension system, the change in spring stiffness may be realised by using an air spring where the volume and pressure of the air inside a bladder may be changed, or by having more than one air accumulator which can be switched from one to another, or both. The change in damping may be realised by having more than one specially designed hydraulic damper pack which can be selected or bypassed using a solenoid valve, or by having a proportional valve to yield a continuously variable damping. For off-road vehicles, which experience higher levels of suspension velocity, the use of higher flow rate valves becomes essential but these valves have relatively high reaction times due to their larger size, making their use in a semi-active suspension inadequate.

An alternative means of achieving semi-active damping is by using magneto-rheological (MR) fluid in an appropriately designed damper. The apparent viscosity of MR fluid can be continuously varied by means of varying an externally applied magnetic field over the working volume. An adequately designed valve could yield the required variable damping that is required to control a suspension satisfactorily. The advantage of using MR fluid is that the damping effect has a fast response, is reversible, and is a relatively simple method to achieve variable damping.

1.2. The 4 State Semi-active Suspension system ($4S_4$)

A prototype semi active suspension system that is capable of varying both the spring rate and damping between two discrete settings has been developed at the University of Pretoria (Els, 2006). The system is called the Four State Semi-active Suspension System, abbreviated $4S_4$. A schematic of the $4S_4$ system is shown in Figure 1. This system uses a hydraulic cylinder containing hydraulic oil to work as a strut and exert the required forces on the axle of an off-road vehicle. This hydraulic cylinder is coupled to two gas accumulators, accumulator 1 and 2, shown in Figure 1, via two hydraulic dampers respectively. The accumulators act as springs by compressing the working gas in

the accumulator. To move from the low to the high spring rate, valve 3 may be closed, forcing all the fluid to flow into accumulator 1 through damper 1. This provides the high stiffness, high damping setting. The spring rates can be individually tailored by changing the volumes of the two accumulators. If valve 1 is opened it effectively short-circuits damper 1, thereby yielding high stiffness and low damping. With valve 3 open and valves 1 and 2 closed, the system achieves the low stiffness, high damping setting. Finally, a low stiffness and low damping setting is achieved if all three valves are open. The ride height of the system may be adjusted by adding or removing hydraulic fluid from the cylinder.

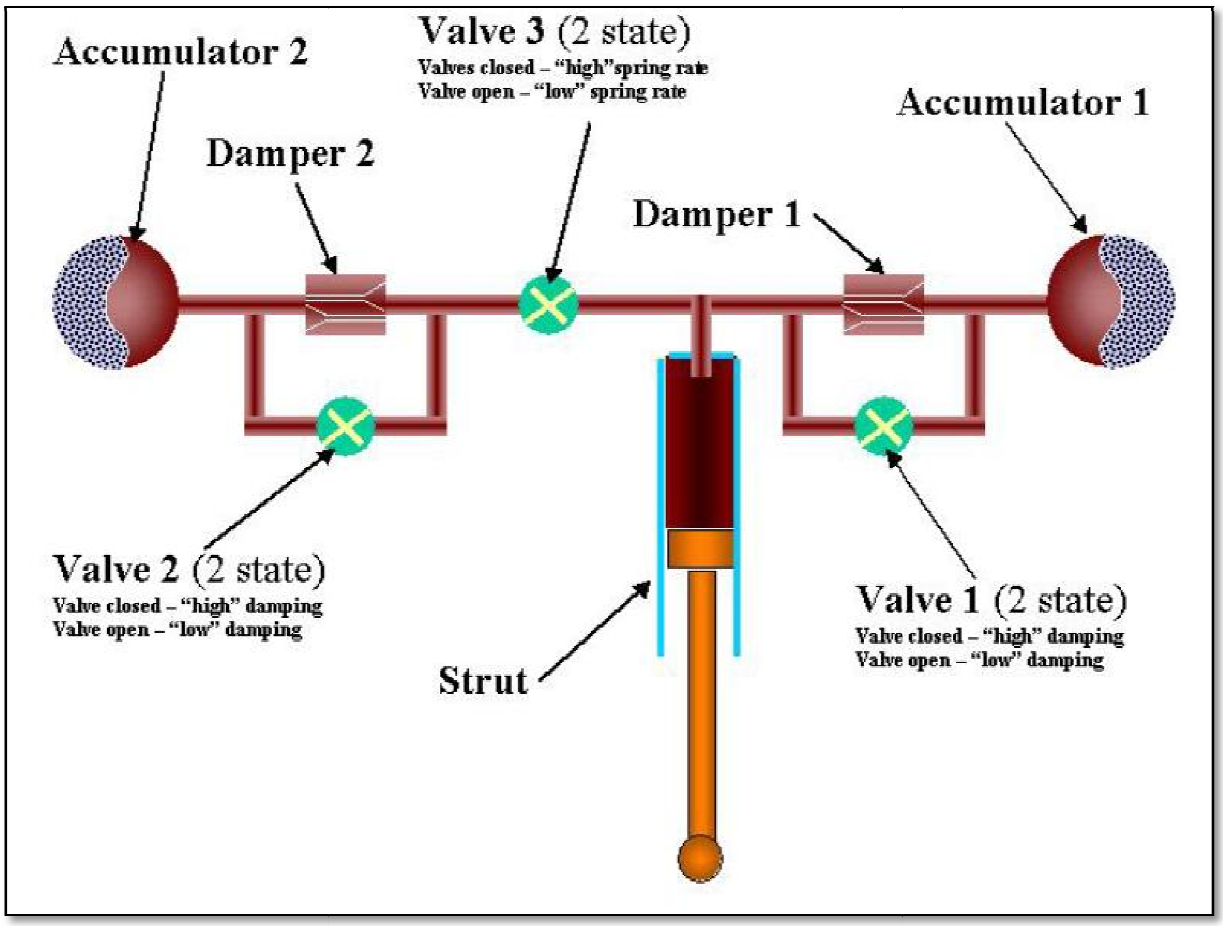

Figure 1: The Four state Semi-active Suspension System, $4S_4$(Els, 2006)

The main characteristics of the $4S_4$ system may be summarised as follows:

1. Maximum relative suspension velocity of 2m/s, translating to a fluid flow rate of 236 l/s
2. Valve response time to the order of 50ms
3. Low damping characteristic, less than half the baseline damper characteristic
4. High damping characteristic, 2 to 3 times the baseline damper characteristic

One of the most significant characteristics of a damper is the force-velocity curve. The force-velocity curves for the $4S_4$ system in high stiffness and damping as well as low stiffness and damping modes are shown in Figure 2. These two modes are also compared to a baseline passive damper in Figure 2.

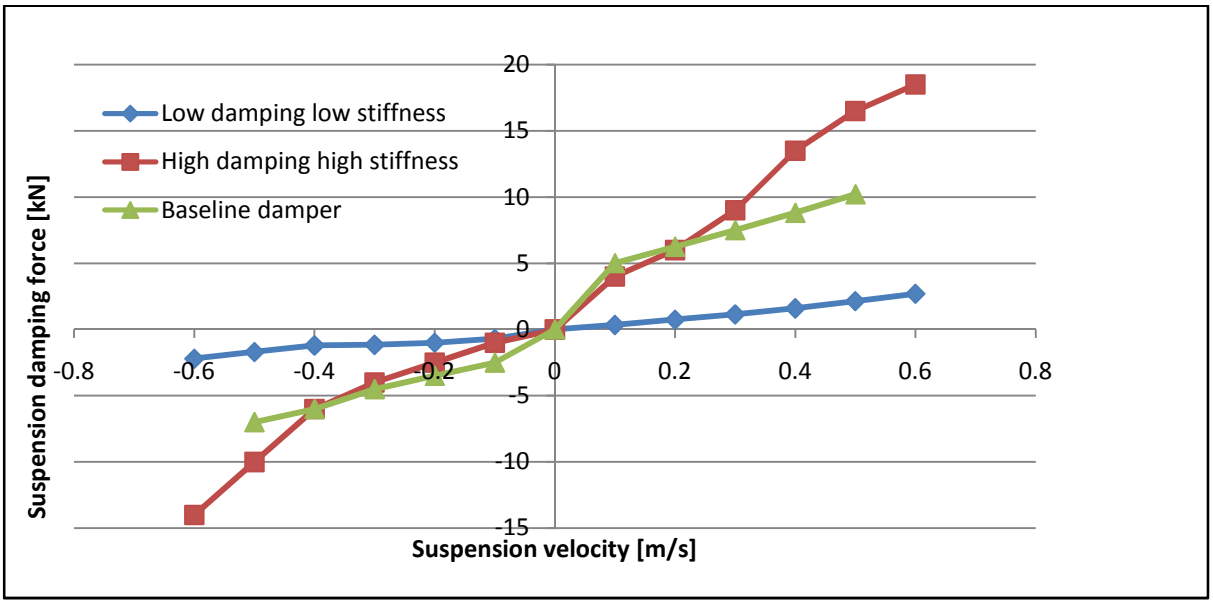

Figure 2: $4S_4$ force velocity curves for low and high settings (Els, 2006)

The baseline force-velocity characteristic was derived from testing of the standard damper pack found in the Land Rover vehicle's dampers. The standard damper has a piston diameter of 35mm, as compared to the 50mm $4S_4$ piston diameter. The baseline damper characteristic is then scaled for both force and velocity to be able to use its values for the $4s_4$.The results shown in Figure 2 demonstrate two discrete damper settings from the performance of the $4S_4$ system with an ability to vary from damping forces that are much lower than the baseline damper to damping forces that are higher than the baseline damper at higher suspension velocities. The lower level significantly enhances ride comfort while the higher level improves vehicle handling. This suspension system has been proven to greatly increase the vehicle handling as well as ride comfort during testing (Els, 2006).

The damper developed for the $4S_4$ system has also been optimised and it has been found that the damper characteristic is 1.35 times the baseline damping value for handling and 0.55 times the baseline value for ride comfort in combined handling and ride quality (Thoresson et al., 2009). Figure 3 shows this new operating range for the optimal semi-active suspension damper characteristics.

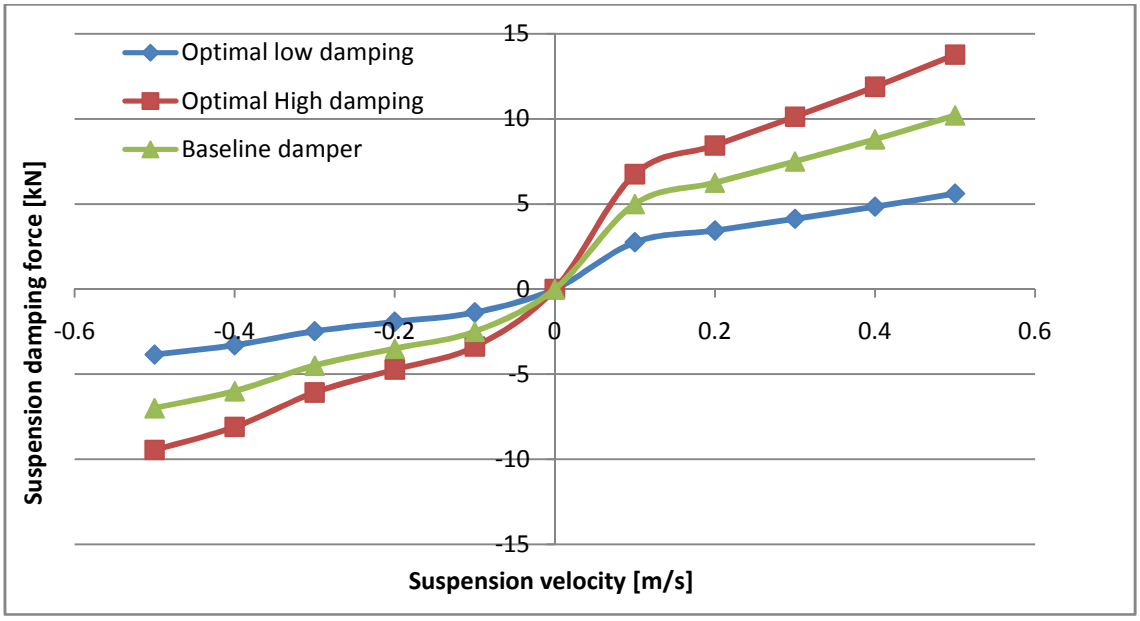

Figure 3: Optimal force velocity characteristic for 2 damping states (Thoresson et al., 2009)

It has been observed that if the values for damping are optimised for handling and ride comfort separately, they tend to move to their upper and lower bounds for handling and comfort respectively, as expected. This may lead to some unsafe situations as these individually optimised values show a severe increase in the suspension RMS value for body roll for the very low damping value when comfort is optimised (Thoresson et al., 2009).

1.3. Problem statement

The discussion in this chapter provides a background for the problem statement for this study. This study seeks to answer the following questions pertaining to the use of MR fluid in an off-road suspension system:

1. Can MR fluid be used to yield controllable damping when implemented in the $4S_4$ system?
2. Can the required damping force range from the minimum to the maximum values for the optimized suspension damping characteristics, as shown in Figure 3,be practically realized by making use of MR fluid?
3. Can a MR fluid damper produce a high enough pressure drop so as to effectively block any flow of the fluid, facilitating the use of the MR damper valve to replace the solenoid valve 3, as shown in Figure 1, in order to enable semi-active spring control?

In summary, the main aim of this thesis is to investigate an enhancement of the existing $4S_4$ system by using a MR fluid based damping system. This is done by specifically answering the three questions listed above.

For the design of a MR valve, the optimised force-velocity damper characteristics shown in Figure 3 may be scaled to a more convenient form by plotting the effective (required) pressure drop over the MR valve as a function of the fluid flow rate. The area that was used for the calculation is from the $4S_4$piston diameter of 50mm. The scaled values for damping can be seen in Figure 4, where the grey shaded area indicates the required range of operation for pressure drop versus flow rate that the proposed MR valve needs to be designed for.

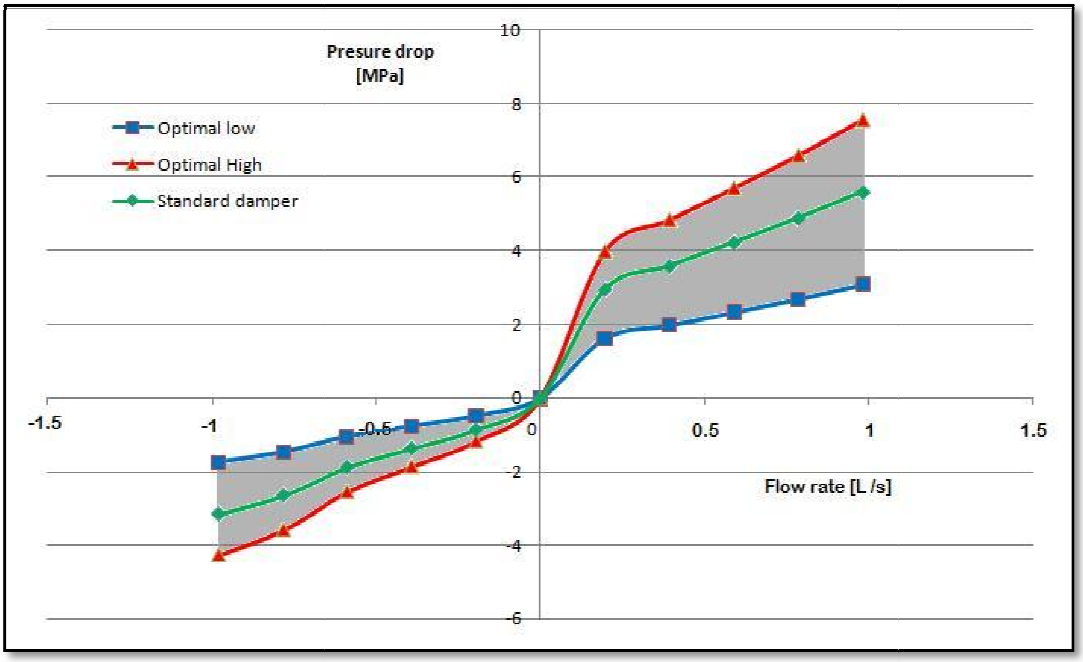

Figure 4: Optimised pressure drop vs. flow rate operating bandwidth shaded in grey

1.4. Thesis summary

This chapter summarises the background for this study and also provides a problem statement that this study will seek to answer. This thesis is divided into six chapters. Chapter 2 provides a literature study on MR fluid and the use of MR fluids for damping. Chapter 3 presents the theoretical model that has been used to study different aspects of the MR damper. This model has also been used to determine the required geometrical parameters of the MR valve in order to meet the necessary design requirements. Chapter 4 discusses the results obtained from testing and experimentation performed to support the findings of the theoretical model. Chapter 5 draws conclusions and lists some recommendations for future work and suggestions for improving the design of the MR valve developed in this study.

2. Literature study

The literature study investigates the operating principles of MR fluids, how to model them and how they may be used in damper designs. Commercial MR devices are investigated to gain an understanding of the operation of such devices. The sealing of MR devices is also researched at after which a study into the modelling of magnetic circuits is done.

2.1. MR fluids

This section covers MR fluid composition and the theoretical models used for MR fluids, firstly looking at viscous models and then going on to the modelling of the magnetic field dependant characteristics.

Rheology is the branch of physics that describes the deformation and flow of matter. A magneto-rheological fluid is a fluid where flow and deformation properties are dependent on the intensity and direction of an externally applied magnetic field.

MR fluids consist of a carrier fluid filled with micro-sized magnetically polarisable particles (usually soft iron based) and stabilising agents to help keep the magnetic particles in suspension. The concentrations of the particles usually vary from about 20% to 40% by volume (Carlson, 2004) or 2% to 50% by weight (Levin et al., 1997). These particles usually have a mean diameter of around 5µm. When an external magnetic field is applied, the particles become polarized and align to the applied field's direction in only a few milliseconds forming chains of ferrous particles, which cause a restriction to the flow of the fluid, and thus increases the fluid's apparent viscosity (Tao, 2001). The carrier fluid is usually hydrocarbon based oil although MR fluids are also made using silicone oil or water for specific applications. The yield strength of MR fluid usually varies from 50 to 100 KPa in normal shear mode (Carlson, Catanzarite and St.Clair, 1995). The process has a very fast reaction time (to the order of milliseconds) and usually depends mostly on the magnetic field build up time. The forming and breaking down of the chains is completely reversible (Tao, 2001).

When there is no external magnetic field present the fluid acts like a normal Newtonian fluid with the viscosity comparable to that of the carrier fluid. A Newtonian fluid is a fluid that acts according to Eq.(1).

$$\tau = \eta \frac{dv}{dt} = \eta \dot{\gamma} \quad (1)$$

In equation 1 τ is the shear stress, η is the fluid viscosity and $\frac{dv}{dt}$ or $\dot{\gamma}$ is the velocity profile (shear strain) between the surfaces moving relative to each other (Hersman et al., 2006). When an external magnetic field is applied the magnetized particles form thin chains along the field lines, which cause an increase in the apparent viscosity due to the increased restriction of the flow. This can be seen in Figure5. Figure 5ashows the magnetic particles (2% volume fraction, 50µm in diameter) before application of an external magnetic field, Figure 5b shows the particles aligned to a magnetic field applied in the direction of B.

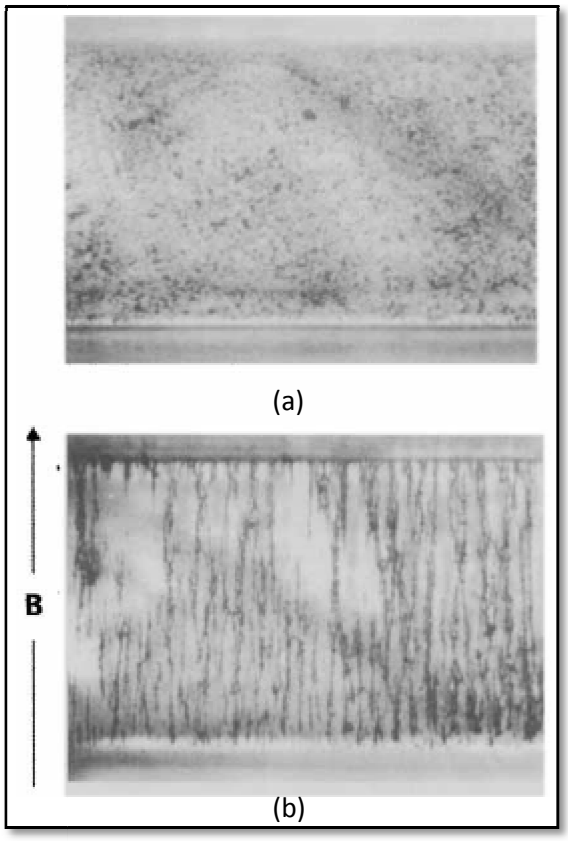

Figure 5: MR particles aligning to an external field (Klingenberg, 2001)

When the fluid is in this magnetized state it starts to act as a solid material and the fluid behaviour is described as classical Bingham fluid behaviour which means that the material does not flow unless the applied stress exceeds the material yield stress (Klingenberg, 2001). This material yield strength is a function of the magnetic particle type, concentration, size, shape and the applied magnetic field strength (Spencer et al., 1996).

When in the magnetized state, MR fluids usually show only small variations in apparent viscosity with a change in temperature. Some recent research reported that variations in damping force for an MR damper of less than 10% were measured when the temperature was varied from -40°C to +150°C showing that these fluids are very stable with respect to varying temperature (Carlson et al., 1995).

As indicated in Figure 5b, the introduction of a magnetic field quickly aligns the particles in the direction of the field forming thin chains of particles, only one particle wide. Tao, (2001), shows that the forming of an MR structure has two developmental stages, the first being the quick forming of the thin chains and the second the aggregation of chains to form thicker columns consisting of a single chain surrounded by four other chains that are slightly offset to it. The forming of the thicker columns is a much slower process than the initial stage, taking several seconds, or even to the order of minutes for larger MR devices (Tao, 2001). With no magnetic field the particles are randomly distributed. This new structure has the body-centred tetragonal lattice (BCT) structure which is a stronger structure than the single chain structures found before aggregation due to the fact that thicker columns are more difficult to bend. Due to the fact that the thicker the column the more difficult it is to bend, the chains only group up to about 10-15 chains in a column after which the

resistance to joining other groups becomes too big. Tao, (2001), found that by applying a compressive stress to the fluid in the direction of the magnetic field one is able to encourage the forming of columns. The chains formed in the tests performed had a diameter of 8µm, with the diameter of the columns formed by compression having a diameter of 60µm. The forming of the columns showed an increase in the yield strength of the fluid, from around 80KPa up to 800KPa, for an applied pressure of 2MPa. Figure 6 shows the BCT structure, where the green (central chain) particles show the original chain and the red (outer 4 chains) particles represent the chains which were added due to settling/aggregation (Olabi and Grunwald, 2007).

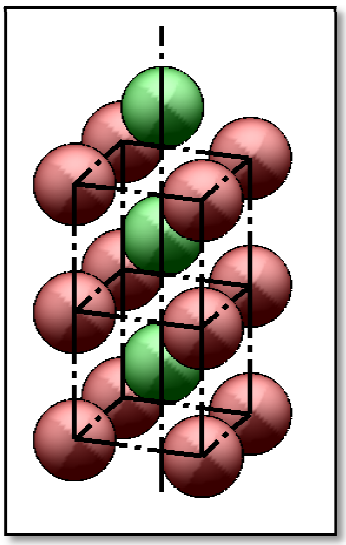

Figure 6: An example of a BCT lattice structure (Olabi and Grunwald, (2007)

Control of the shear properties of the MR fluid in any device therefore relies on the control of the magnetic flux applied to the fluid using a magnetic circuit. For steady state designs permanent magnets can be used, but electromagnets make it possible to dynamically control the flux and therefore the flow properties. For commercially available MR fluids information regarding the field dependant properties of a MR fluid can be found in the specific MR fluid's data sheet obtained from the fluid manufacturer. Information such as the fluid flux density vs. field intensity properties, yield stress versus strain rate and the fluid yield stress versus magnetic field intensity usually appear in graph form. Empirical equations have been derived to approximate these graphs (Carlson, 2005). Once the magnetic field requirements for the application are known, a magnetic circuit can be designed to supply the needed magnetic flux over the working fluid gap to yield the desired device characteristics (Carlson, 2004).

2.2. Mathematical modelling of MR fluids

Several models have been developed to describe the behaviour of MR fluids in their working environment. This section gives a description of some of these models, the first of which is the Bingham model.

The Bingham model makes use of the Newtonian fluid model which was mentioned earlier, but it also adds the dynamic shear stress component as a function of the externally applied magnetic field. For zero magnetic field the fluid reacts like a Newtonian fluid, but as the field is increased the

shear stress increases with the field induced stress value. The following formula describes the Bingham fluid behaviour.

$$\tau = \tau_{yd}(B) + \eta\dot{\gamma} \quad (2)$$

Where τ is the Bingham shear stress, τ_{yd} is the dynamic yield stress as a function of the magnetic field and the $\eta\dot{\gamma}$term is the shear stress as is described by the Newtonian fluid model. The Bingham model combines the shear due to magnetic field with the shear due to the fluid viscosity (Li and Du, 2003, Jingnan et al., 2003).Daniela Susan-Resiga, (2007), and Occhiuzzi et al., (2003), found that the Bingham model is not accurate in describing the fluid behaviour when exposed to very low shear rates, also called the "roll-off state", but it becomes more accurate as the shear rate is increased. They also found that the dynamic stress is a function of the applied shear rate replacing the term $\tau_{yd}(B)$ with the term $\tau_{yd}(B)sgn(\dot{\gamma})$ to account for shear thinning of the fluid.

Another model named the Bouc-Wen model was also developed to model the behaviour of MR fluid in the shear mode between parallel plates especially for use in modelling of structural dampers (Jansen and Dyke, 2000). This model indicated in Figure 7, is made up of a viscous damper and a history dependent function to account for the hysteresis in the system.

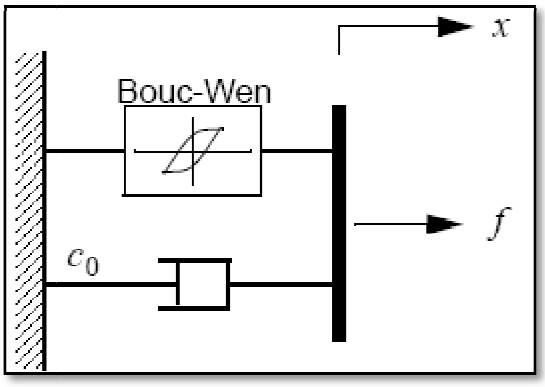

Figure 7: Bouc-Wen model for MR shear behaviour (Jansen and Dyke, 2000)

The equations governing the damper force predicted by the Bouc-Wen model are:

$$f = C_0\dot{x} + \propto z \quad (3)$$

And

$$\dot{z} = -\gamma|\dot{x}|z|z|^{n-1} - \beta\dot{x}|z|^n + A\dot{x} \quad (4)$$

From (Jansen and Dyke, 2000)

The variable z is an evolutionary variable that takes the history dependence of the response of the fluid into account. Where α and C_o are control voltage (voltage over the coil) dependent variables.

Jansen and Dyke, (2000), reported that this model can be used to accurately predict the behaviour of the MR fluid for shear applications over a wide range of inputs.

2.3. MR dampers

There are many possible designs for MR fluid dampers. MR fluids can be applied in three possible modes, as is shown in Figure 8. The first mode is the so-called valve mode, Figure 8a, where the fluid is passed between two stationary elements with the magnetic flux flowing from the one element to the other, perpendicular to the flow of the fluid. The second mode, Figure 8b, is the direct shear mode where the fluid is sheared between two plates moving relative to each other with the magnetic flux perpendicular to the shear direction. The last mode, Figure 8c, is the squeeze mode, where the fluid is compressed between two plates with a magnetic flux flowing from one plate to the other. The squeeze mode is the least popular mode of the three modes for use in MR devices.

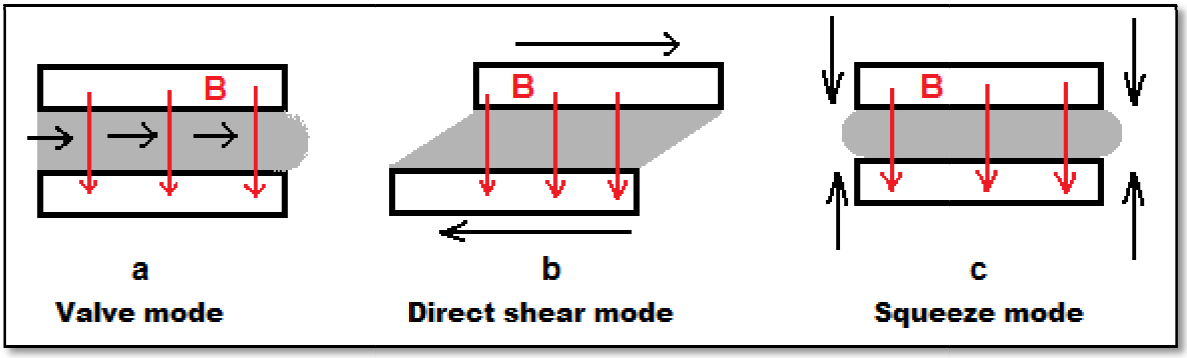

Figure 8: MR fluid application modes

Some Magneto rheological dampers use MR fluid in a shear mode (or a combination of shear and valve mode) to dissipate energy in order to damp motion. The damping force can be controlled by varying the applied magnetic field intensity. One application for these dampers are used in modern big buildings to dampen seismic vibrations caused by earthquakes, this does not make the building earthquake proof, but it does dampen motion to minimize deflection and reduce resonance, thus increasing the building's ability to survive a certain size earthquake with minimum damage. Figure 9a shows an 180kN damper made by Lord Corporation; this damper is designed for use in civil structures. Figure 9bshows the inside of such a damper. This damper has a piston rod that protrudes both sides so that there is not a need to account for change in volume due to the piston rod's movement; the small accumulator is there for thermal expansion only.

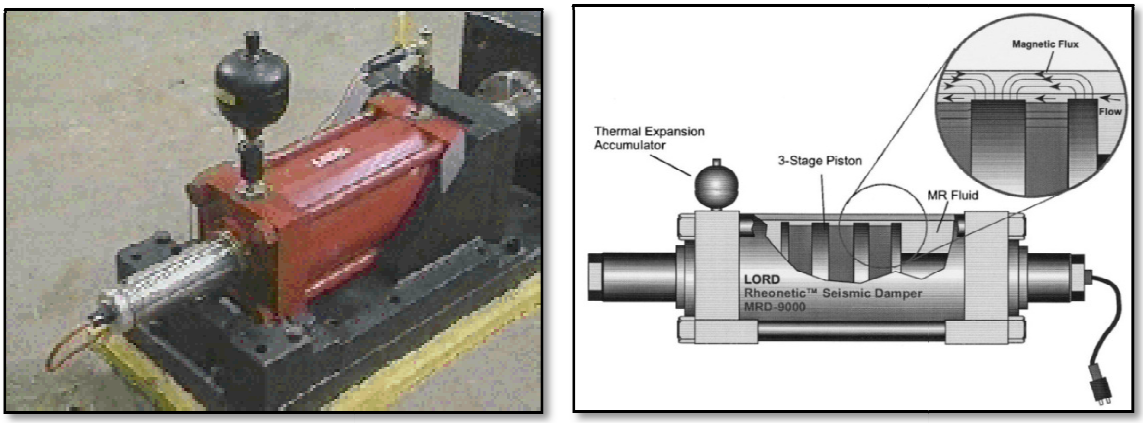

a b

Figure 9: 180kN MR damper (Lord_Corporation, 2008)

For smaller damping applications (such as washing machines), damper designs that use the shear mode of the fluid exist, but instead of having a whole chamber filled with fluid, the working volume consists of MR fluid filled foam. When subjected to a magnetic field the resistance to movement between the foam and the opposite wall increases, thus increasing the resulting force. An example of such a device can be seen in Figure 10. The advantage of this type of device is that the amount of MR fluid needed for the device and the device complexity is greatly reduced, thus reducing the cost of the product.

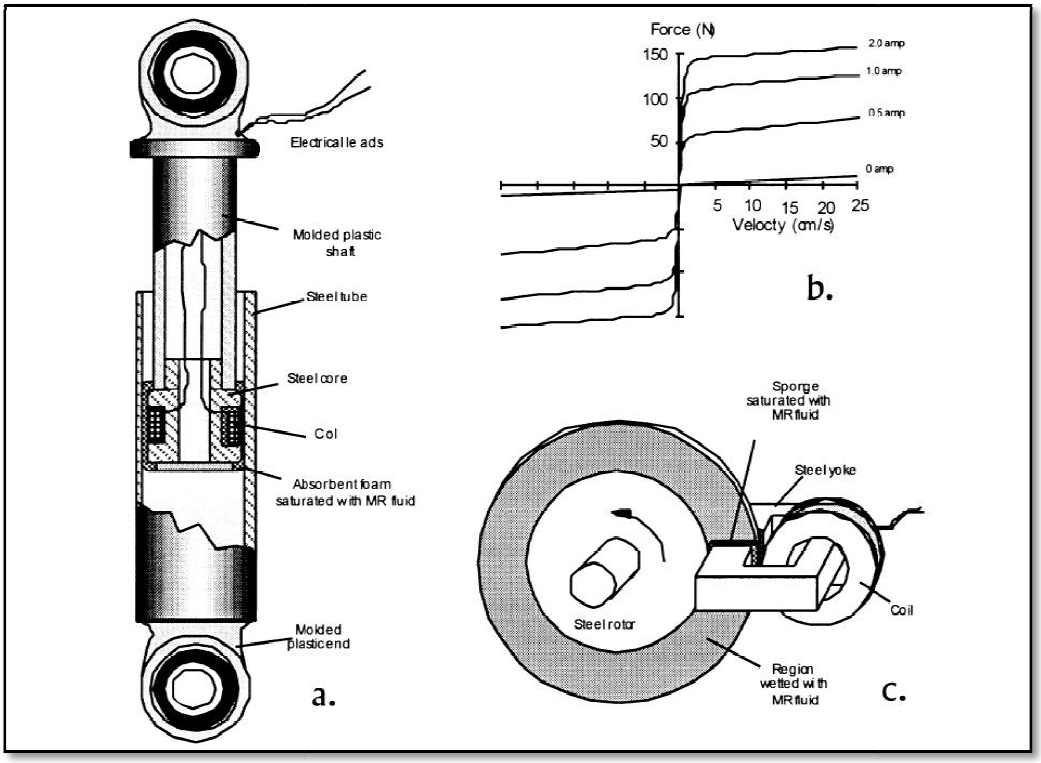

Figure 10: MR foam devices and characteristic curve (J. David Carlson, 2000)

Figure 10a shows a linear MR foam damper, Figure 10b shows a characteristic curve and Figure 10c a rotary MR damper.

MR dampers also find their application in damping of seat motion in on-and off-highway vehicles. These small dampers have the ability to generate a damping force in excess of 2000 N and an energy dissipation rate of 600W. An input power of up to only 4W is needed to control this device, meaning that the power required to operate the device is much less (150x) than the device dissipation rate (Carlson et al., 1995). An example of such a device can be seen in Figure 11.

Figure 11: Small 2,4kN MR damper (Lord Corporation, 2008)

The main application of MR dampers, of interest for the present study, is vehicle suspension systems. The majority of vehicles are fitted with passive dampers. The characteristics of these dampers are fixed at the design stage and remain almost constant for the life of the damper. With the introduction of semi-active MR dampers in the automotive industry it became possible to control the damping of the suspension system continuously and very quickly, allowing the onboard computer of the vehicle to optimize the suspension damping for each road profile to reduce the handling vs. ride comfort compromise. Developed by Delphi, the Magneride™ dampers became commercially available in 2002 and are currently implemented in over a dozen cars. Cars implemented with MR suspension systems include the Audi TT and R8, various Cadillac models and even the Ferrari 599GTB (Magneride, 2014). Figure 12shows one of these MR dampers.

Figure 12: Delphi Magneride™ MR damper(Lord-Corporation, 2008)

These dampers work in the same way as ordinary dampers in that a fluid is passed through an orifice in the moving piston. The difference is just that where normal dampers have springs and valves to restrict the flow of fluid, MR dampers have electromagnets around the orifice, which, when activated cause an increase in apparent viscosity thus increasing the damping force. These dampers usually implement MR fluid in valve mode.

One specific vehicle that uses the third generation Magneride™ dampers is a Sport Utility Vehicle (SUV) manufactured by Land Rover, named the Range Rover Evoque. These third generation dampers employ two smaller electromagnetic coils instead of the previous generation's single coil, and is said to be twice as fast reacting as the previous generation. The response time is said to be 10ms. By sampling the applicable variables at 1 kHz the ECU continuously calculates the required

damping by means of the MR dampers. What makes the Evoque unique is its terrain sensing ability which can sense a terrain surface in less than 2 seconds and correspondingly apply the best damping for that terrain, be it on or off-road. These dampers are said to be able to generate 3 kN of damping force for a velocity of 1 m/s (Land Rover Evoque's magnetic attraction, 2011).

A special MR damper prototype has been developed by Lord Corporation under contract for US Engine Production Inc. for use in the US Military High Mobility Multipurpose Wheeled Vehicle (HMMWV, or Humvee). The MR dampers that are implemented in the HMMWV and other military vehicles have reached 5 million cycles of durability testing, which exceeds the military requirement to last 1 million cycles at 120°C, and have also undergone 10,000 miles of durability testing on a US Army test truck on an accelerated durability test course in Nevada. Figure 13 shows the difference between the vehicle body displacements for a HMMWV fitted with standard dampers and one with MR suspension. From Figure 13 it can be seen that a substantial decrease in vehicle body displacement is achieved using the MR suspension. This test was done over a test track with a 2.7" (69 mm) RMS displacement at 15 Mph (24 km/h). These dampers are reported to show increased speed, handling and safety over terrain (Lord.com, 2013).

Figure 13: Comparison between the standard damper and MR damper on a HMMWV (Lord.com, 2013)

Tests results showed that the vehicle ride limiting speed over rough terrain was improved significantly by the application of the MR suspension to the HMMWV vehicle. For a terrain with a RMS displacement of 1.5" (38mm) it was found that an increase of 35% in the limiting speed was reached for the MR suspension as compared to the standard setup. As the RMS value increases the difference between the MR suspension and the standard became smaller, yielding 25% for a 2" (51mm) and 10% for 3.4" (86mm) (Wray et al., 2003).

Prototype MR damper applications for larger vehicles also exist; one example is the Stryker, shown in Figure 14. The system used 8 MR dampers and controllers to control the vehicle's suspension damping. The system used 80 watts in idle mode and an estimated 250 watts cross country, with a theoretical peak of 800 watts. The MR system proved itself over a range of off-road courses, yielding a maximum increase in vehicle speed of 72%, from 22 Mph to 38 Mph for the same level of driver dissipated energy, 6 watts. The system also showed an improvement in the vehicle's handling, with a 30% reduction in vehicle roll rate. The maximum lane change speed was also increased from 38 Mph to over 50 Mph with the MR suspension as compared to the standard

vehicle. This increase in ride quality is also beneficial to increase platform stability, which aids battlefield effectiveness over the rough terrain (Wray et al., 2005).

Figure 14: Stryker military vehicle (Wray et al., 2005)

From the research done the advantages of implementing a MR suspension have become evident.

2.4. MR fluid sealing

Although MR fluid is based on normal hydraulic fluids, the presence of iron particles in the fluid makes it potentially abrasive. The sealing of MR fluid is a special concern as normal hydraulic seals do not necessarily work very well for the required service life of the device. According to Lord Corporation, the seal and wear surfaces need to be optimised for the specific design at hand (Lord Corporation, 2004). With the increased cost of these dampers compared to normal dampers an increased life would be beneficial.

The use of o-rings to seal off pistons or any dynamic sealing application for MR fluids is discouraged. These types of seals form a wedge between the seal and the cylinder, trapping the ferrous particles and forcing them against the cylinder wall causing scrape marks and increasing the wear inside the cylinder. The use of o-rings for stationary components is said to work very well (Poynor, 2001). Poynor, (2001), recommends the use of “U” type, or scraper seals that scrape against the surface of the cylinder, instead of o-ring type seals, dramatically reducing the amount of particles trapped between the cylinder wall and the seal, and thus reducing the wear inside the cylinder. There is no special requirement on the seal material.

Guide strips for the moving parts can be placed behind the seals where the particles will not be able to enter into. The guide strip material used for the design of the guide strip material is also to be chosen such that it is capable of embedding foreign objects in its surface which should lower the risk of damage to the cylinder wall.

2.5. Electromagnetic circuits

In order to apply a controllable varying magnetic field to the MR fluid, electromagnets are used. A magnetic field can be generated by passing an electric current through conductor coils wound on Ferro-magnetic materials. From Ampere's law the line integral of the magnetic field intensity (H) around a closed path is equal to the total current linked by the contour. (Sen, 1997)

$$\oint \mathrm{H.dl} = \sum \mathrm{i} \quad (5)$$

The magnetic field intensity (H) produces a magnetic flux density (B) everywhere it exists. The magnetic flux density (B) is related to the field intensity (H) by the following equation:

$$\mathrm{B}=\mu\mathrm{H}\ (\mathrm{Weber/m^2})$$

$$=\mu_r\mu_0\mathrm{H}\ (\mathrm{Weber/m^2}) \quad (6)$$

Where:

μ = Magnetic permeability of the medium, a measure of the ability of the medium to carry magnetic fields. (Henry/meter)

μ_r = Relative permeability of medium with respect to free space (air)

μ_0 = Permeability of free space = $4\pi.10^{-7}$

The value of μ_r is 1 for non-ferrous conductors.For ferrous metals used in magnetic machines the value of $\mu_r$can range from 2000 to 6000. The larger the value of μ_r the lower the current required to produce a certain flux density in the magnetic circuit (Sen, 1997).

Magnetic circuits can be modelled with an equivalent electric circuit, where the electro motive force (EMF) can be replaced by the magneto motive force (MMF), electric current (I=EMF/R) by the Flux (ϕ=MMF/*R*), and the resistance R (*length*/σA) by the reluctance *R (length/μA)*.The variable σ represents the conductivity of the material, and μ the medium permeability.

After some mathematical manipulation the field intensity can be rewritten as:

$$\mathrm{H} = \mathrm{Ni/length\ (At/m)} \quad (7)$$

And the flux density can be written as:

$$\mathrm{B} = \mu\mathrm{Ni/length\ (Tesla)} \quad (8)$$

(Where N is the number of windings in the coil and i the current)

Each ferrous material has a corresponding magnetization curve which relates the field intensity (H) with the flux density (B), as can be seen in Figure15 (magnetization curve)(Sen, 1997)

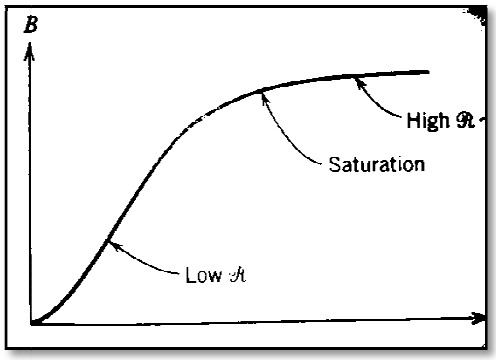

Figure 15: A typical magnetization curve (Sen, 1997)

Magnetic circuits can also be expanded to cater for different types of magnetic applications, or more than one magnetic media. Consider the case where the magnetic circuit is comprised of a core and an air gap, now the equation H = Ni/length (At/m) can be rewritten to account for the air gap as follows:

$$Ni = H_c l_c + H_g l_g \quad (9)$$

Where l_c and $l_g$represent the lengths of the core and air gap respectively.

The magnetic material used is up to the designer. A material with a high flux density for specific field intensity is preferred, as lower currents are needed and saturation is less prevalent. Goncalves, (2005), recommended the use of 12L14 steel for the core of his electromagnet.

Thus by using the above equations and catering for each material's magnetic properties one can model a magnetic circuit using this equivalent electric circuit analogy. To test the magnetic field intensity a device called a hall-effect meter is used. This device measures the magnetic flux in a certain direction. This device will be used to verify the magnetic core modelling.

2.6. Summary of literature study

From the literature studied it was seen that Magneto Rheological fluids are able to change their rheological properties as a function of an externally applied magnetic field. Modelling of MR fluids can be done with careful consideration of all the variables in the system. Research done into commercial MR vehicle dampers has shown that these dampers have the ability to improve on vehicle handling as well as driver comfort. MR damping has been applied to damping problems ranging from seat damping devices to vehicle suspensions and even civil structures. MR suspension damping ranges from standard road vehicles up to big military off-road vehicles. The sealing of these fluids can be easily done by using scraper type seals in optimised configurations. Magnetic circuits can be modelled by using an equivalent electrical circuit model. The necessary information has now been reviewed to continue with the design of the MR damper system.

A successful damper design will require the following to be known:

- ✓ Fluid properties
- ✓ Magnetic circuit analysis
- ✓ MR valve geometry
- ✓ Core material and geometry specification
- ✓ Flow rate of MR fluid
- ✓ Appropriate sealing

3. Theoretical modelling and design

This section covers all the theory needed to facilitate the modelling of the performance of a MR damper.

3.1. Modelling of the pressure drop over a MR valve

This section explains the methodology used to design the MR valve so as to achieve the required operating parameters for the damper. Other related details associated with the design are also discussed in this section.

From research it was found that MR fluid can be modelled for two separate regimes (Olabi & Grunwald, (2007). The first regime being the flow of the fluid without the presence of an external magnetic field, also termed the viscous flow regime, which is a function of the fluid viscosity, and the shear rate applied to the fluid. The second operation regime is the change in shear strength of the fluid as a function of the applied magnetic field. For the fluid flowing as a normal Newtonian fluid without the presence of an external field, the shear-force developed by the fluid can be expressed as is shown in equation 10.

$$\tau = \eta \frac{dv}{dt} = \eta \dot{\gamma} \quad (10)$$

In Eq.(10), η is the fluid viscosity and $\dot{\gamma}$ is the shear rate that the fluid experiences.

The suspension device in consideration works as a hydraulic cylinder which pumps its fluid through some type of flow restrictor or valve; this means that the valve mode for MR fluid operation is the mode that will be implemented in this research study as the fluid is pumped through the MR device, instead of having surfaces that move relative to each other in the presence of an external magnetic field, as in the direct shear and squeeze modes of MR operation.

3.1.1. Rheological pressure drop (off-state pressure drop)

The rheological pressure drop can be divided into two contributors, namely the rheological pressure drop over the MR valve, and the feeder pipes respectively. The pressure drop over the MR valve for fluid in the valve mode due to the rheological effects of the fluid can be determined as follows (Olabi & Grunwald, (2007) (R. Ay, 2000):

$$\Delta P_{rheo} = \frac{12 \times \eta \times \text{flow rate} \times \text{passage length}}{\text{MR fluid gap}^3 \times \text{passage width}} \quad (11)$$

From eq. (11) it can be seen that the rheological pressure drop over a valve mode MR channel is a function of the geometry of the channel, the fluid viscosity, and linearly proportional to the flow rate of the fluid.

It can now be noted that the fluid will cause a viscous pressure drop over the MR channel, as stated above, as well as the feeder pipes that transport the fluid from the actuator into the MR channel. The severity of the effect of this viscous flow is not known at this stage, since the geometry

of the valve and pipe diameters haven't been chosen, so it will be taken into account in the design later so as to try and model the MR valve as accurately as possible.

The rheological pressure drop in the feeder pipes that supply the MR valve with the fluid can be calculated as is shown in eq.(12).

$$\Delta P_{head\ loss} = \frac{\text{Fluid density} \times \text{Friction factor} \times \text{Pipe length} \times \text{fluid velocity}^2}{2 \times \text{Pipe diameter}} \quad (12)$$

The friction factor in Eq. (12) is calculated for laminar flow as follows:

$$\text{Friction factor} = \frac{64}{\text{Reynolds number}} \quad (13)$$

If the Reynolds number exceeds 2100, the flow is seen as being in the transitional or turbulent regime and the friction factor needs to be determined empirically by making use of the Moody Chart (Metzger and Willard, 2011). This now concludes the theory for the prediction of the pressure drop over the MR valve assembly for the "off-state" MR operation. Figure 16 shows the sensitivity of the pressure drop to the feeder pipe's diameter and length.

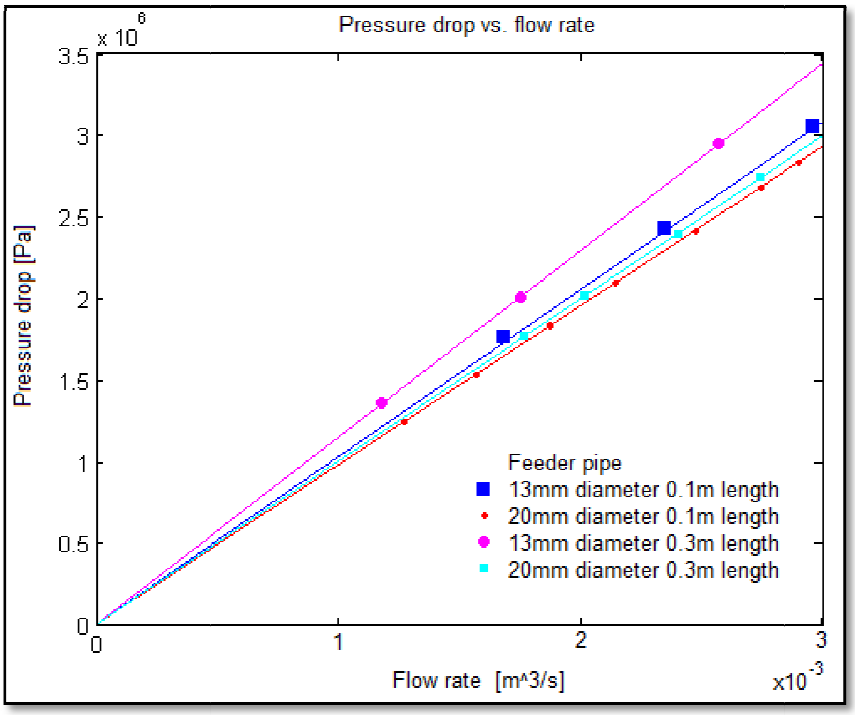

Figure 16: Rheological pressure drop for various feeder pipe options

From Figure 16 it can be seen that the length and diameter of the feeder pipe does in fact need to be considered when designing a MR valve to be used in a suspension system as diameter and length both influence the pressure drop. With a variation in diameter from 13mm to 20mm it is noted that the pressure drop decreases with about 5 percent. An increase in the pipe length from 0.1m to 0.3m for the 13mm diameter pipe increases the pressure drop from over the valve and feeder pipes from 3.1MPa to 3.4MPa, which is an increase of approximately 10% and directly influences the performance of the MR valve in the off-state by the same value. The geometry of the

MR valve itself will also, as stated in Eq. (11) influence the total pressure drop as well. Both the feeder pipe length and passage geometry are needed to be able to predict the off-state damping that the MR valve system will yield. By carefully choosing the valve geometry the off-state (minimum) damping may be tailored for the given system requirements.

3.1.2. Prediction of fluid shear strength as a function of magnetic field

The second distinct regime for the MR valve calculation is analyzed through the determination of the shear strength of the fluid for an applied magnetic field. This can be calculated empirically using the equations derived by Carlson (Carlson, 2005).

$$\tau_0 = C \times 271700\Phi^{1.5239} \times \tanh\left(6.33 \times 10^{-6} \times H_{mr}\right) \quad (14)$$

In Eq. (14), C is a factor that depends on the type of carrier fluid used. A factor of 1 is used for hydrocarbon oil, 1.16 for water and 0.95 for silicone oil; Φ is the volume fraction of iron particles in the fluid, and H_{mr} is the magnetic field intensity. Figure 17 shows these equations plotted for a 0.32 volume fraction of iron particles for different carrier fluids. A volume fraction of 0.32 was chosen for the figure as it is one of the stronger fluids available on the market and which is recommended for use in damper devices.

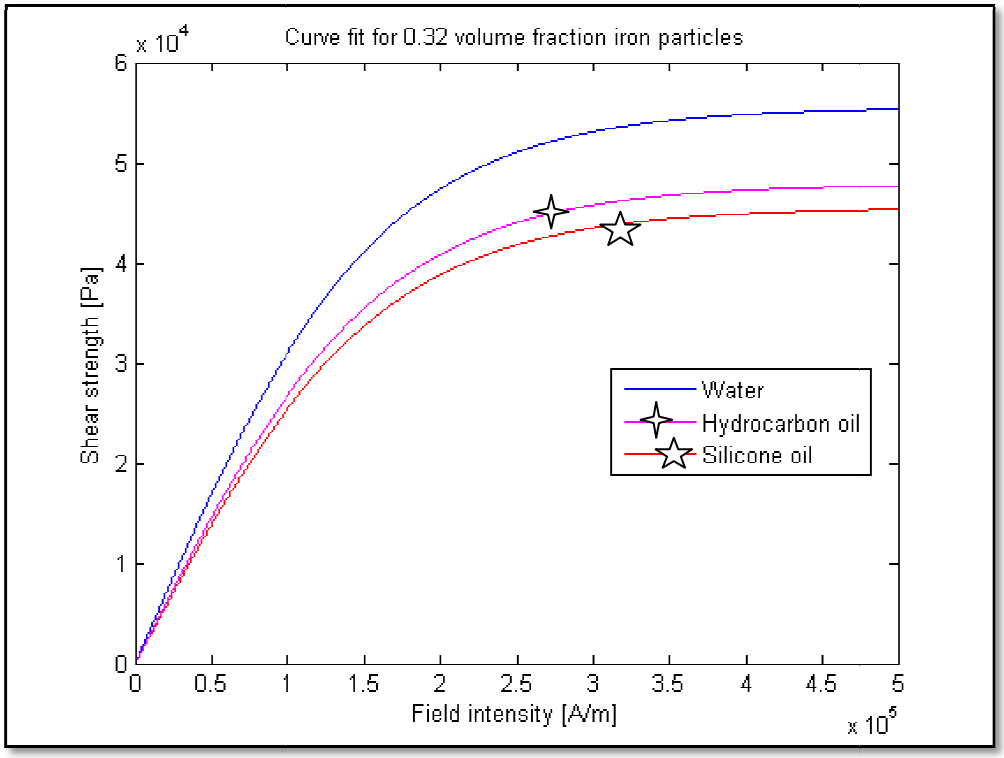

Figure 17: Empirical plots for MR fluid yield strength vs. Magnetic field intensity

From Figure 17 it is seen that a magnetic field intensity around 350 kA/m is needed to saturate MR fluid with a volume fraction of 0.32. This is now a design input variable for the magnetic circuit, a field intensity higher than the saturation value will mean that no meaningful increase in the fluid shear strength will be noted, while a field intensity lower than this will not yield the maximum shear strength that the fluid can yield, thus not using the fluid to capacity.

3.1.3. Superimposed model

The two models for MR fluid operation, rheological and magnetic field dependant shear strength can now be superimposed to determine the combined effect of two. This superposition is commonly referred to as the Bingham Plastic Model, and is expressed as:

$$\tau = \tau_{yd}(B) + \eta\dot{\gamma} \quad (15)$$

In Eq. (15), the first component is the shear in the fluid as a function of the external magnetic field, and the second component is the shear of the fluid as a function of the shear rate and viscosity of the fluid.

For implementation in the analytical model the magnetic field dependant component of the total pressure drop is calculated using Eq. (16)

$$\Delta P_{MR} = \frac{D \times \tau_0 \times \text{MR Passage length}}{\text{Passage height}} \quad (16)$$

In Eq. (16) the constant D has an empirical value of 2 for $\Delta P_{MR}/ \Delta P_{rheo} \approx 1$, and a value of 3 for $\Delta P_{MR}/ \Delta P_{rheo} \approx 100$ (Olabi and Grunwald, 2007). By using an equivalent form of the Bingham model the pressure drop over the valve can now be calculated by summing the rheological pressure drop and the magnetic field dependent pressure drop to obtain the total pressure drop. This now concludes the modelling of the pressure drop over the MR valve as a function of the valve geometry, pipe length and externally applied magnetic field for normal shear rates.

3.1.4. Flow blocking ability

An important aspect of this research is to investigate the possibility of using the MR valve that is used for damping to block off the flow of MR fluid. According to the normal Bingham model the shear yield is a function of the shear rate and the shear strength as a function of an externally applied field, as was shown in equation 15. Resiga, (2007), found that this equation does not hold for very low shear rates, as is the case when trying to block off flow. It was found that the fluid acts as a normal quasi-Newtonian fluid for very low shear rates and then starts to follow the shear thinning Hershel-Bulkley model as shear rate is increased. It was proposed that the following relation be used:

$$\tau(\dot{\gamma}) = \tau_N(\dot{\gamma})W_1(\dot{\gamma}) + \tau_{HB}(\dot{\gamma})W_2(\dot{\gamma}) \quad (17)$$

Where the quasi-Newtonian behaviour is given by

$$\tau_N(\dot{\gamma}) = \eta_0\dot{\gamma} \quad (18)$$

And the field dependant part from the Hershel-Bulkley equation

$$\tau_{HB}(\dot{\gamma}) = \tau_0 + c\dot{\gamma}^{1-n} \quad (19)$$

With W_1 and W_2chosen such that $W_1 >> W_2$ when the shear rate is small and $W_2 >> W_1$ when the shear rate is larger, also with $W_1 + W_2 = 1$. Farjoud, (2011), proposed that the weighing factors be set up such that

$$W_1(\dot{\gamma}) = e^{-a\dot{\gamma}} \text{ and } W_2 = 1\text{-}W_1 \quad (20)$$

With the constant “a” in Eq. (20) being a value used to scale the transition time from where the shear value goes from the Newtonian model to the Hershel-Bulkley model. The value for the constant “a” is to be determined experimentally. Figure 18 shows the effect of increasing the value for “a” on the low shear rate characteristic, note that this figure is just shown to indicate the effect of the value “a” and is not intended to show any accurate information.

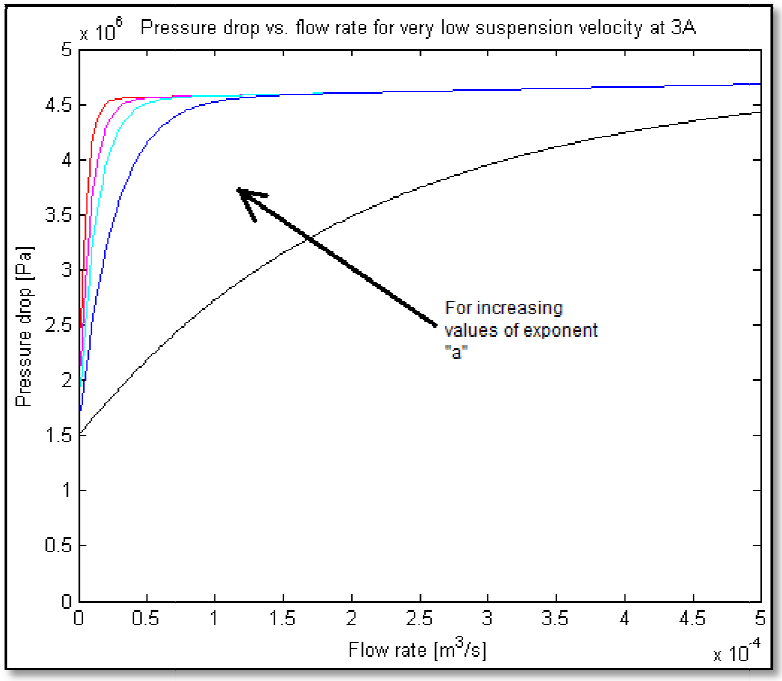

Figure 18: Low shear rate curve fit

Due to the fact that the shear thinning exponent, n, in Eq. (19) also needs to be determined experimentally it was chosen to use the normal Bingham model instead, and use the shear thinning model only if a bad fit for the data was evident from testing. The resulting model shown in Eq. (21) is applied for the calculation of the shear strength:

$$\tau(\dot{\gamma}) = \eta_0 \dot{\gamma} e^{-a\dot{\gamma}} + \tau_B(1 - e^{-a\dot{\gamma}}) \quad (21)$$

The value for “a”, and the fluid viscosity, are the only values that will need to be determined experimentally. From Eq. (21) it can be seen that the fluid shear strength is now a function of the fluid viscosity, shear rate and the magnetic field dependant component, which, when manipulated correctly can yield the total pressure drop over the MR valve. It may be noted that the fluid viscosity is a function of temperature, of which the relation may be found by testing.

The total pressure drop that the hydraulic cylinder will experience is calculated as the sum of the pressure drop due to flow losses in the feeder pipe, the rheological pressure drop over the valve due to the flow of fluid through the MR passage, and the pressure drop over the valve due to the shear resistance of the fluid as a function of the externally applied magnetic field.

3.2. MR passage geometry

The fluid modelling needs to be followed up by the determination of the required geometry of the MR valve. As mentioned earlier, for the damper designed in this study, the mode of operation will be the valve mode. As a design input for the determination of the valve geometry, the minimum

damping in the off state, the maximum damping in the on state and the maximum flow rate for the suspension needs to be specified.

The first parameter to calculate for the design of the MR valve is the active volume of the MR fluid. This is the minimum volume of MR fluid that will be needed to yield the desired MR effect, and can be determined as follows:

$$\mathrm{Vol}_{\mathrm{active}} = \left(\frac{12}{\mathrm{D}^2}\right) \times \frac{\eta}{{\tau_0}^2} \times (\mathrm{x.Q.}\Delta \mathrm{P_{MR}}) \qquad (22)$$

In Eq. (22),η is the fluid viscosity, τ_0 is the shear strength due to the applied magnetic field, Q is the fluid flow rate, and ΔP_{MR} is the pressure drop over the valve due to the MR effect. The factor D in this case has an empirical value of 2 for τ_{MR}/τ_{Rheo} ~ 1 and a value of 3 for τ_{MR}/τ_{Rheo}~ 100, where τ_{MR}/τ_{Rheo} is the ratio of the MR effect to the Newtonian fluid effect, also equal to the variable x in Eq. (22)(Yang et al, 2002). The constant D is the same one as was used in Eq. (16).

Figure 19 shows the effect that the passage width and length have on the rheological pressure drop for a constant gap size of 2.5mm, viscosity of 0.107 Pa-s and a flow rate of 1.2 *l/s*.

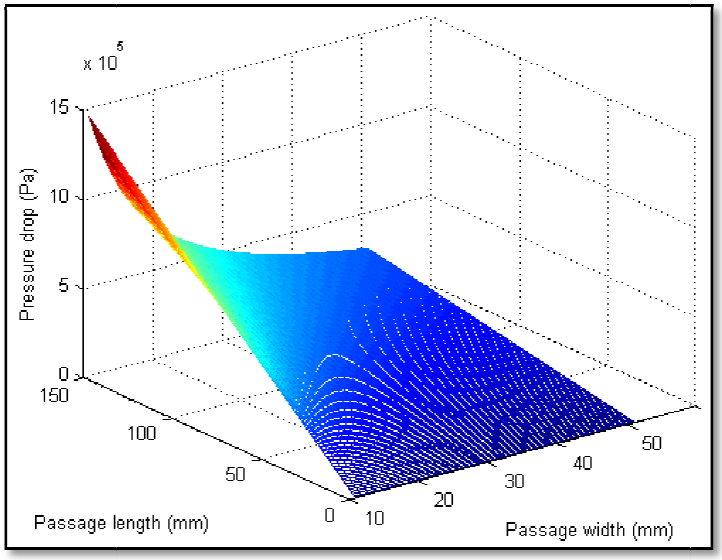

Figure 19: Rheological pressure drop as a function of geometry for 2.5mm MR gap

It can be seen from Figure 19 that the rheological damping force in the MR passage approaches zero as the length of the MR passage approaches zero due to the decreasing shear area, this relationship is linear with respect to the length of the valve. The pressure drop over the valve is inversely proportional to the width of the passage. As the width decreases the effective area through which the fluid can flow also decreases, thereby increasing the pressure drop. If the width keeps increasing, the effect of the width on the pressure drop becomes smaller, thus yielding the non-linear behaviour.

Using the calculated active fluid volume as a function of the type of fluid and the on-and off-state pressure drops, the geometry of the MR passage can be determined. An iterative process has been followed with the appropriate gap size chosen and the corresponding width and length of the MR passage found so as to satisfy the minimum active fluid volume and pressure drop requirements. Figure 20 shows the line of solutions for the MR passage geometry that will yield the required on

and off state characteristics. It shows the passage height (termed gap size in the figure) as a function of passage width and length. All units are in meters.

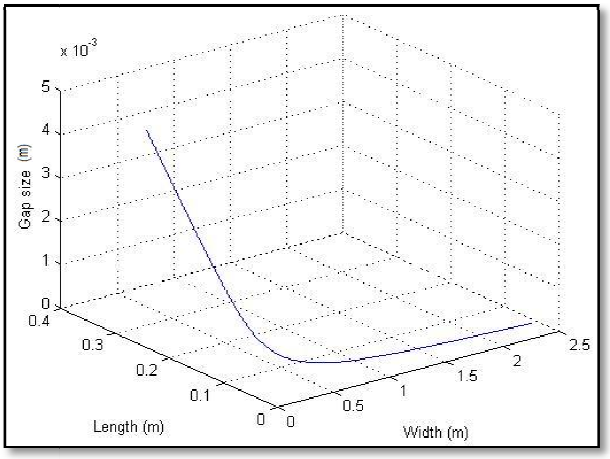

Figure 20: Solutions to geometry that will comply with requirements

From Figure 20 one can note that an infinite number of solutions to the problem exist. The most practically implementable one of these solutions was used for the damper design. As the MR gap increases the passage length increases and the width decreases, and vice versa. For a large MR gap the manufacturing tolerances become less stringent, but the length of the valve becomes excessively high, especially when considering the magnet needed to effectively magnetize the area, which now limits the maximum gap that can be used. As the gap is decreased the width increases rapidly, which will also be a limiting factor with respect to size and magnet design.

It is found that a width of 40mm, passage length of 120mm and a gap of 2.5mm would be a viable solution, which meets the requirements for on-and off-state damping. However, the calculated passage size (120mmx40mm) will require a very large magnet core to supply the magnetic field. This problem has been solved by designing three 40mm x 40mm passages that are in series with one another, one beneath the other. The effective passage length and width remains unchanged (3x40mm x 40mm), but the core cross section is reduced drastically from 120mmx40mm to 40mmx40mm. Figure 21 shows a cross-sectional view of the layout with three lengths of 40mm. The magnetic flux has to effectively travel through the core (top and bottom blocks in Figure 21), three 2.5mm MR fluid sections and two steel cores inside the valve, which guide the fluid and transmit the magnetic field.

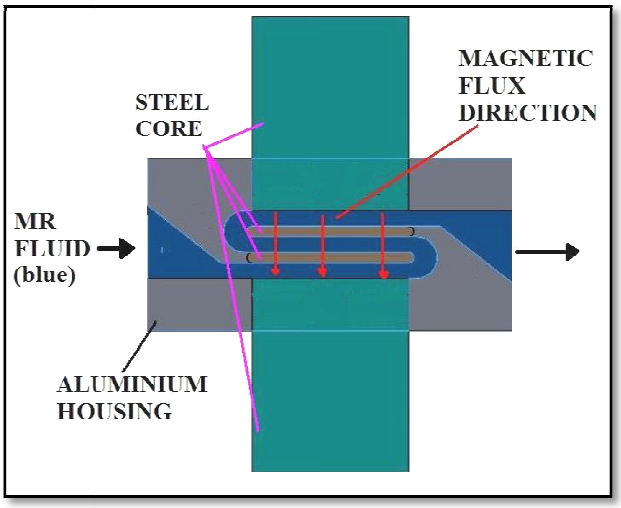

Figure 21: MR valve layout, cross sectional view

The proposed layout will meet the required damping characteristics for the various states according to the theoretical model.

3.3. Magnetic circuit design

It is important to model the magnetic circuit that would be able to provide the magnetic field intensity capable of bringing the fluid up to its maximum shear yield strength/close to its saturation value.

The modelling of the magnetic circuit has been done by using an equivalent electric circuit analogy (Sen, 1997). The equivalent circuit approach treats the path of the magnetic field through the core and MR fluid as analogous to electric current flowing through an electric circuit containing various resistors. The EMF (electro-motive force), which is the driving force in an electric circuit is replaced by the MMF (magneto-motive force), the analogous driving force in a magnetic circuit. The driving force in an electric circuit produces electric current ($i = E/R$) with corresponding flux ($\Phi = F/\mathcal{R}$) in the magnetic circuit, and is limited by resistance ($R = l/\sigma A$) and reluctance ($\mathcal{R} = l/\mu A$) for the circuit models of the electric and magnetic circuits respectively. The variables σ and μ represent the conductivity and permeability respectively. Using this analogy, the magnetic circuit for the designed MR valve will have a magneto-motive force (F) that is provided by an electromagnetic coil carrying electric current. The flow of the flux is restricted by the reluctance created by the outside core, internal core elements and MR fluid respectively. The equivalent magnetic circuit for the proposed MR valve design can be seen in Figure 22.One way in which to solve this magnetic circuit is to use the trial and error method (Sen, 1997).

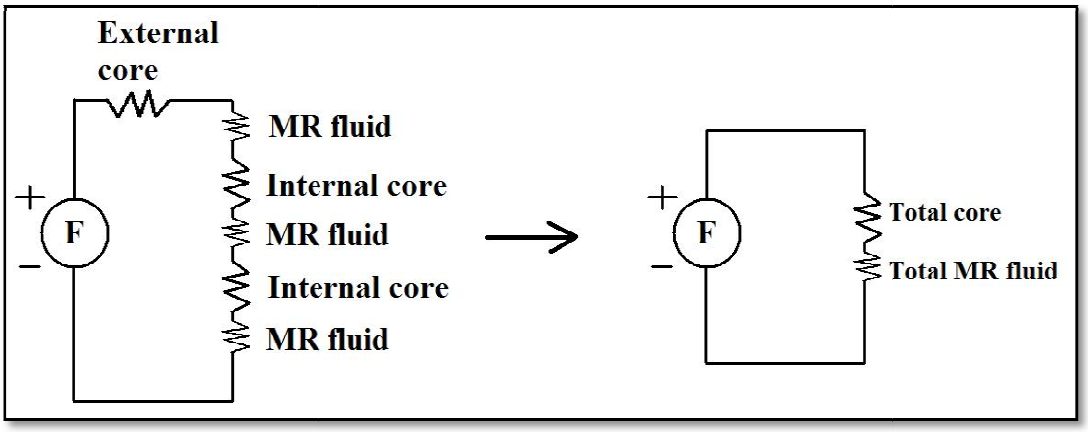

Figure 22: Magnetic circuit equivalent

Materials have distinct magnetic properties. Usually the relationship between the flux density B (Tesla) and the field intensity H (Ampere turns/meter) is given graphically for the material in the form of a magnetization curve. Thus, for a known value of flux density, the field intensity may be obtained from the material magnetization curve. It is assumed that the flux density (B) throughout the magnetic circuit is constant. Therefore, for a known value of flux density (B), the field intensity (H) may be obtained for each material in the magnetic circuit. Curve fitting is used for this calculation for the B-H curves from different materials. These variables of the magnetic circuit are required to calculate the shear strength of the MR fluid due to the magnetic field (τ_0). The MMF in the circuit is calculated by taking the product of the number of windings (N) and the coil current (i), MMF = Ni(Sen, 1997). A typical B-H curve for normal steel, similar to AISI 1018, is shown in Figure 23, with the B-H curve for a 32% particle volume fraction MR fluid shown in Figure 24(Lord-Corporation, 2008).

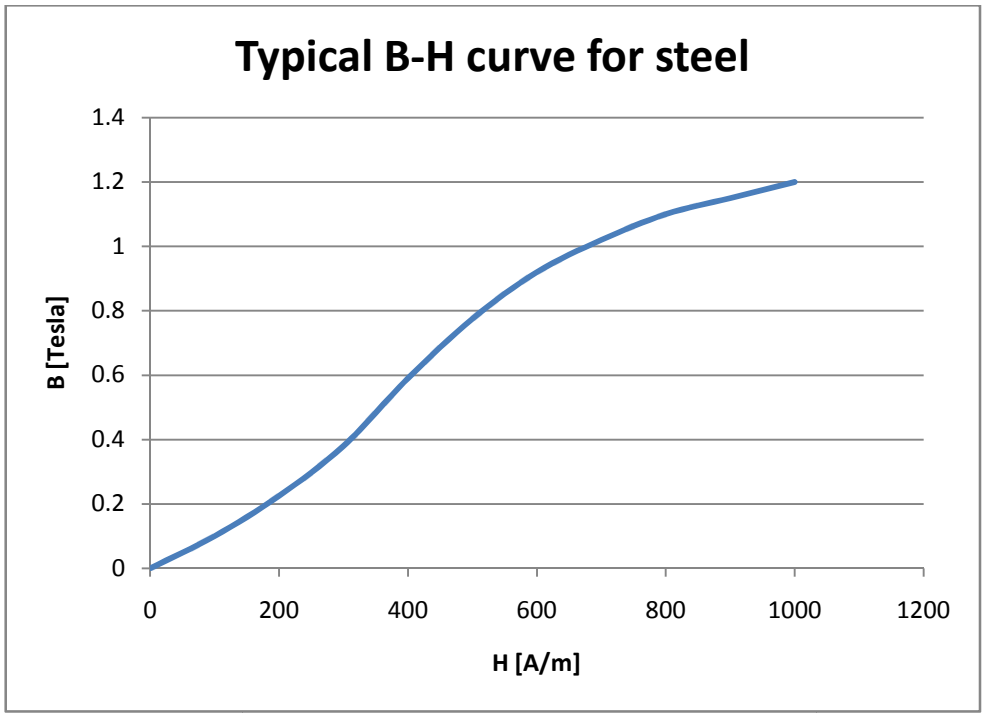

Figure 23: B-H curve for cast steel (Sen, 1997)

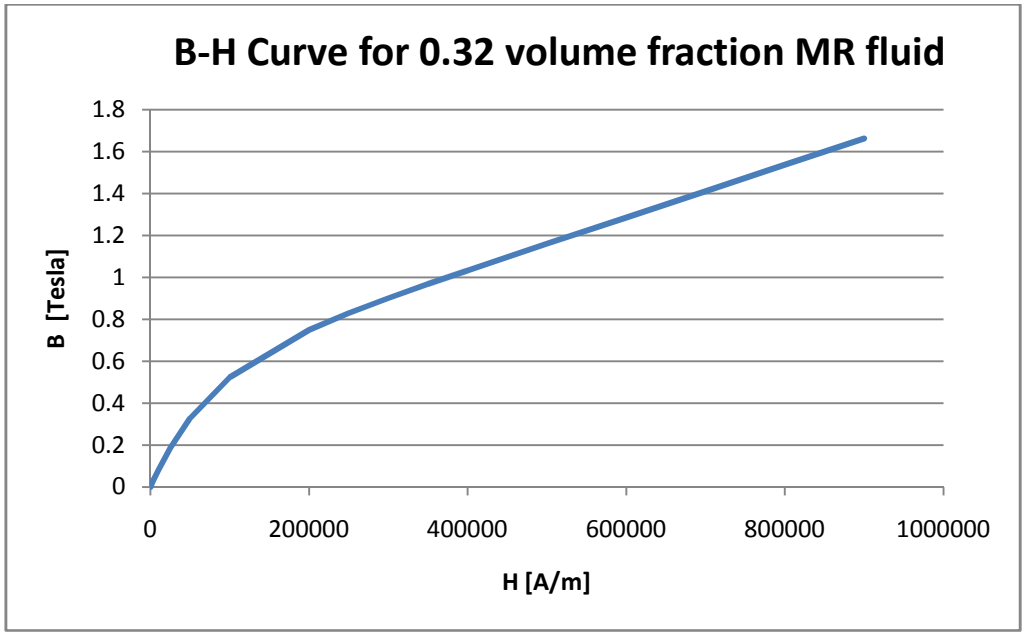

Figure 24: B-H curve for MR fluid (Lord-Corporation, 2008)

Using the current input to the coil, the field intensity is determined by solving the magnetic equivalent circuit for the MR damper design. This is done iteratively using an initial estimate for the flux density (B) in the circuit, and then solving for the field intensity (H) throughout the various materials in the magnetic circuit. These values are then used to recalculate the flux density that will cause the field intensity that is known now, and the process is repeated until the values for field intensity in the various materials as well as the flux density throughout the magnetic circuit converge.

From the fluid modelling discussed in Section3.1.2 the required field intensity in the MR fluid is identified to be around 350 KA/m, and the core cross section is set at 40mmx40mm from Section3.2.These input variables have been used to design the magnetic supply circuit.

This resulted in a magnetic core having a cross section of 40mmx40mm, an overall length of 0.52m with an electromagnet having 1400 windings and carrying a maximum current of 3A being able to fully saturate the MR fluid.

3.4. Pressure drop vs. Flow rate and coil current predictions

With the identified geometry and all the different aspects of the modelling covered in the previous sections of this chapter, it is now possible to predict the MR valve's overall pressure drop as a function of coil current and fluid flow rate. These are the variables that are required as the input for the use of the MR valve as a damping device for the suspension system considered. This model takes the following parameters into account in order to predict the pressure drop as a function of flow rate and current:

- Fluid viscosity (as function of temperature)
- Fluid particle volume fraction
- Magnetic core length
- Coil current

- Number of windings in the coil
- MR fluid and cast steel B-H characteristics
- MR passage geometry
- Feeder pipe diameter and length
- Flow rate
- Transition between quasi-Newtonian and Bingham model

Figure 25 shows a contour plot of the pressure drop over the proposed MR valve as a function of the coil current and flow rate.

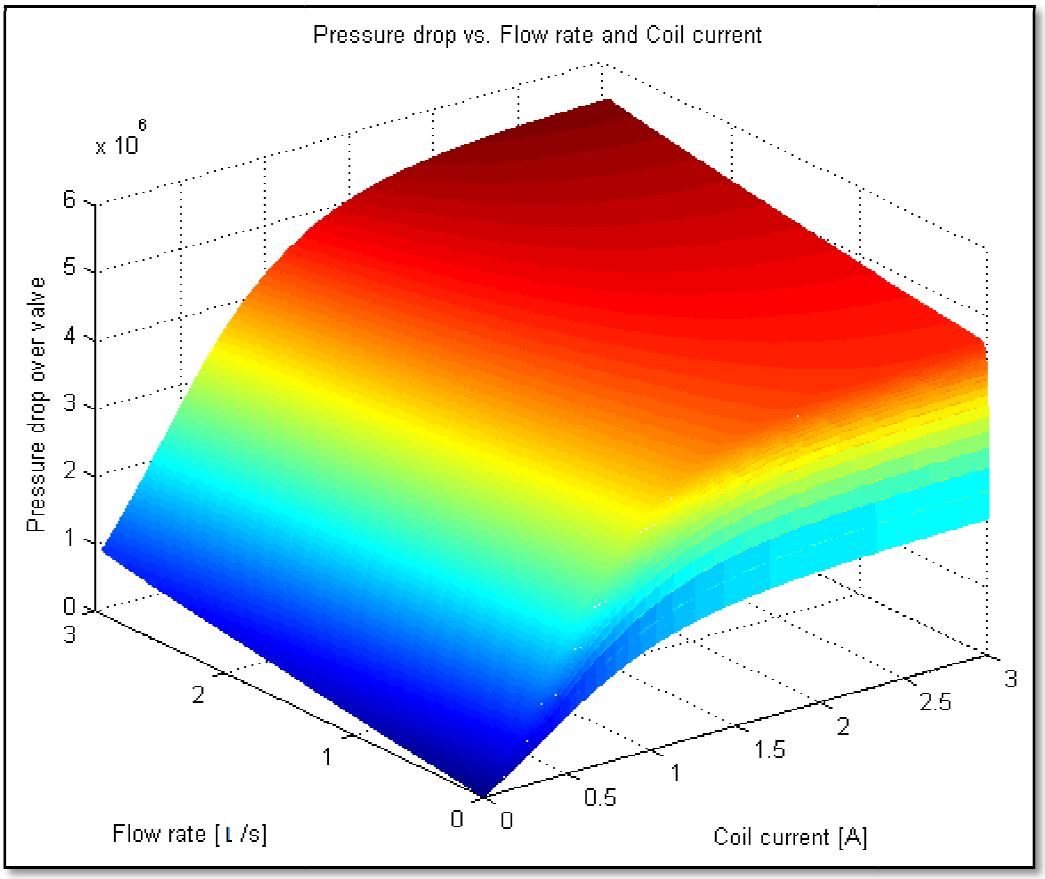

Figure 25: MR valve pressure drop vs. Coil current and flow rate

The sudden decrease in pressure drop for very low flow rates is due to the effect discussed in Section 3.1.4, when the fluid acts more like a Newtonian fluid than a Bingham fluid and then gradually changes to the Bingham behaviour as the fluid shear rate increases. The severity of this changeover will need to be determined by testing, which is associated with the value for the constant “a” in Eq. (20). Figure 25sums up the overall predicted performance for the MR valve, and will be used to compare experimental data with the theoretical model.

3.5. Flow blocking of the MR valve

This section reviews the specific case within the relationship between the pressure drop and flow rate predictions as discussed in Section 3.1.4. To evaluate the flow blocking ability of the device only the maximum current will be considered, as this will yield the highest shear strength in the fluid

and lower currents will thus show a lower pressure drop than what could be achieved. The maximum, or saturation current for the fluid has been determined from the model to be around 3 Amps. The specific case to be considered, therefore, corresponds with the furthest right hand plane for very low flow rates in Figure 25 for a constant maximum current of 3A. Figure 26 shows the pressure drop versus flow rate curve for 3A coil current and a low flow rate. It may be noted that the severity of the change from quasi-Newtonian to Bingham fluid behaviour needs to be investigated through testing.

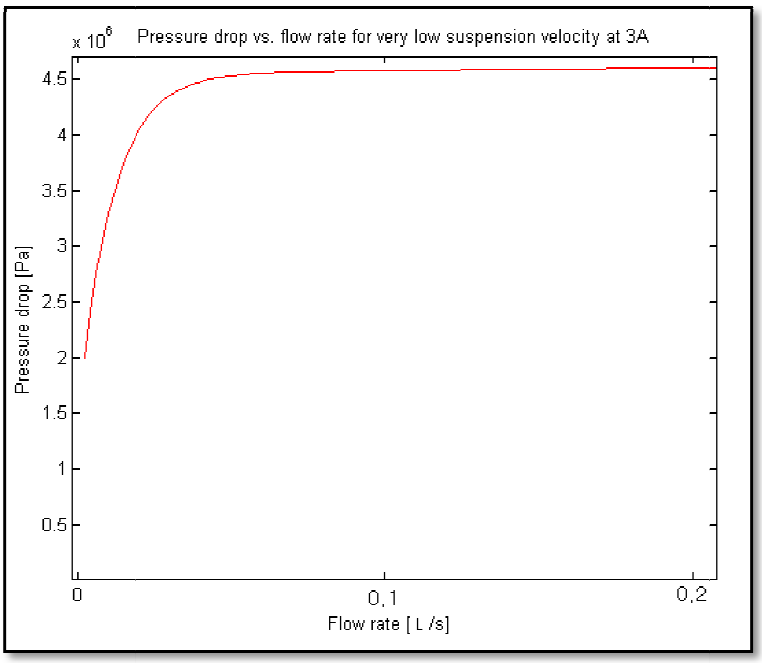

Figure 26: Low flow rate model initial predictions

From figure 26 it can be seen that the theoretical model predicts that the pressure drop approaches zero as the flow rate approaches zero, so, blocking the MR fluid flow out indefinitely or allowing the flow rate to approach zero under load would theoretically not be possible. This will require an evaluation of the pressure drop for very low flow rates in order to determine the lowest flow rate at which the fluid flow can still be effectively blocked, that will be adequate to enable the use of the MR valve to replace solenoid valve 3 in the $4S_4$ system depicted in Figure 1.

3.6. Summary

This chapter provided the relevant theoretical background required for modelling and predicting the behaviour of the valve mode MR device as a function of the fluid flow rate and coil current. The model developed in this chapter was used to select multiple design parameters and finalize the valve geometry. Chapter 4 will present the details of the test setup that is developed according to the dimensions determined in this chapter, Section 3.2. Chapter 4 also presents the test results from experiments used to fully characterize the MR valve for validating the theoretical predictions about the performance of the valve as a function of coil current and flow rate.

4. Experiments and results

This chapter presents the experiments carried out as part of this research. The test results are compiled and compared with the results obtained from the theoretical model. The testing of the magnetic circuit is presented first to validate the theoretical model for the performance of the coil. After the magnetic circuit has been validated, the MR valve's pressure drop as a function of flow rate and coil current can be determined. The low flow rate characteristics for the blocking ability predictions are also analysed.

4.1. Magnetic core testing

In this section the modelling of the magnetic core is evaluated so as to obtain an accurate theoretical model that may be used for predicting the performance of the coil, and that would allow the core to deliver the required flux density to properly activate the MR fluid.

To characterise the magnetic coil's magnetic flux relationship with the input current while carrying the MR fluid would be difficult, because that would require the magnetic field strength testing probe to be inserted into the MR fluid. This would be quite messy and time consuming, and would also risk damage to the sensitive probe and yield inaccurate measurements. It was, therefore, decided to build a small scale setup to test the theoretical model for the prediction of the magnetic flux as a function of coil current without the MR fluid. As a result, the flux density was measured in the atmospheric air to characterise the performance of the electromagnet that has been developed for this study. The goal of this test is to determine whether the theoretical model for the flux delivered is accurate, given a known core length and MMF. Replacing the medium with atmospheric air (from the MR fluid) is not expected to cause any unforeseen change in the model apart from changing from the MR fluid curve to the atmospheric air curve. After the core has been modelled and tested, the term used for atmospheric air will be replaced by the term corresponding to the MR fluid. It may be noted that the characteristics for the MR fluid is well documented in the existing literature (Lord, 2013).

4.1.1. Magnetic core characterisation

A small magnetic core was built with an air gap of 5mm and 500 windings. The theoretical model is used to predict the field intensity in the air gap as a function of the coil current, the number of windings and for the steel that was used as core material.

A Hall Effect probe together with a display device was used to measure the strength of the magnetic field [Tesla] in the 5mm gap. The magnetic flux density is measured as a function of the coil current. Table 1 shows the results of these measurements and compares the measured values with the theoretical.

Table 1: Magnetic core testing

Coil current (A)	Theoretical (T)	Measured (T)	% Error
0.25	0.0289	0.037	28
0.5	0.0574	0.062	8
0.75	0.0861	0.085	1.3
1.0	0.1150	0.103	10
1.25	0.1441	0.113	22

From Table 1 it can be noted that the model is reasonably accurate in the central range of the magnetic field intensity, and starts to diverge at low and high flux densities. The divergence at low flux density may be attributed to residual magnetic fields. The divergence at higher flux densities could be due to the saturation of the core as well as an increase in fringing of the magnetic field in the air gap. Fringing occurs when the flux starts to bulge outwards from the gap and effectively increases the area through which it flows, thus reducing the magnetic flux intensity in the gap. At this stage the model for determining the flux density in the MR fluid will be based on the model that was used for the test discussed above and the test results for the MR device will confirm the applicability of this model.

The magnetic flux for the core that has been built for the full scale test setup of the MR valve was also measured so as to verify proper functioning of the coil, and investigate whether hysteresis will be a concern in the physical MR valve tests. After the probe was inserted from the opened side of the MR valve into the passages where the MR fluid will flow, the magnetic flux density was recorded as a function of current. This was done manually in increments of 0.2A from zero up to the maximum rated current of 3.6A, and then reduced to zero and up to -3.6A, and repeated through a few cycles. The reason for providing both a forward and reversing current is to also evaluate the hysteresis properties of the magnetic core and verify the application to the MR fluid device. Figure 27 shows the average measured flux density as a function of current for three 2.5mm air gaps.

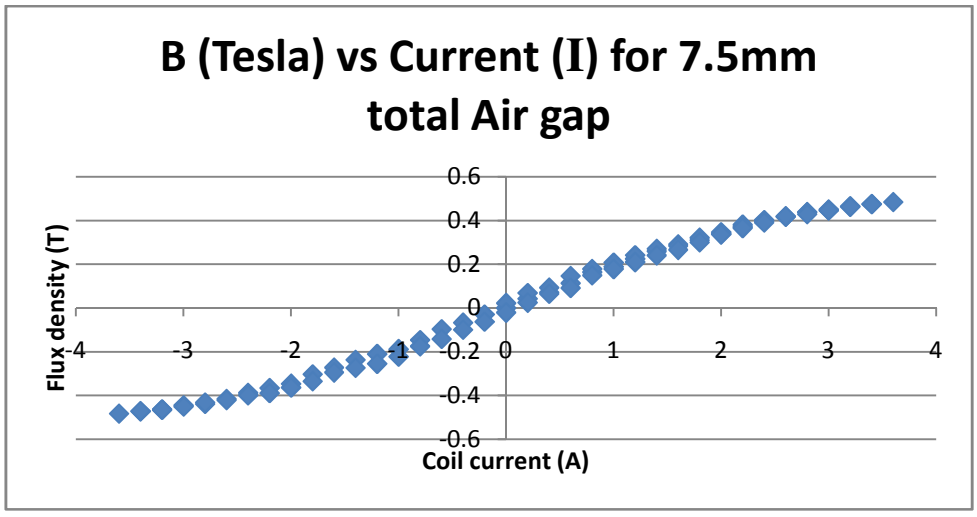

Figure 27: B vs. I for magnetic core

From Figure 27it can be seen that the maximum flux density for an air gap of 7.5mm is 0.48T at a current of 3.6A with minimal hysteresis effects. It is expected that the flux density value will increase when the air gap is replaced by the MR fluid due to the fluid being a better conductor of magnetic flux than atmospheric air.

4.1.2. Magnetic core results discussion

From the tests performed in this section it can be concluded that the model used for predicting the magnetic flux in the MR fluid is accurate, provided that the magnetic core is not saturating. The value of flux at saturation is known and saturation of the magnetic circuit can be tracked so as to ensure that it is not taking place during normal operation of the MR valve, meaning

that the magnetic circuit is designed such that the MR fluid should saturate at maximum yield strength before the electromagnetic circuit saturates in flux.

It can be concluded from Figure 27that the effect of hysteresis is quite small when operating the core with normal direct current, and it will thus be considered negligible in the operation of the MR device developed in this study.

4.2. MR valve pressure drop versus flow rate testing

This section covers the test procedures followed to determine the MR valve's pressure drop as a function of coil current and flow rate. The outcome of these tests should be a data set from which the pressure drop over the MR valve can be stated as a function of flow rate and coil current. Firstly, the experimental design and equipment required for this test will be discussed, after which the experimental setup, procedure, testing, results and discussion will follow.

4.2.1. Experimental design

The design and manufacture of a MR valve is a task with many key features that need to be carefully considered. This section describes the test setup that has been designed and built for validating the theoretical model by testing. An overview of the design and assembly of the MR valve is provided here, followed by the details of the experiment to investigate the fluid pumping equipment.

In a MR valve the MR fluid is activated by using an electromagnet to supply magnetic field intensity to the MR fluid, which causes the fluid to change its apparent viscosity yielding the controllable damping effect. This implies that a magnetic circuit will need to be designed using a ferrous core material that can supply the magnetic field intensity from the coil to the fluid, as discussed in Section 4.1. The housing of the valve on the other hand will need to be manufactured from a non-ferrous material so that the magnetic flux will flow through the MR fluid instead of the housing. If a ferrous material is used for fabricating the housing, short-circuiting of the magnetic flux past the MR fluid will take place thus failing to yield the desired MR effect.

As mentioned in Section 3.2, the geometry of the valve has three MR passages 40mmx40mm with a height of 2.5mm connected in series with each other and stacked such that the flux flows through all three at the same time. Figure 21 section 3.2provides the details of the layout. The magnetic core has been manufactured from 40mm thick steel(AISI 1018) that is CNC flame cut roughly into shape, after which it is milled flat to manufacture the required core profile, and given the calculated required number of 1400 windings of copper wire, capable of handling 3A. Hot rolled steel has been chosen for the core material as it has one of the best abilities for carrying a constant magnetic field, and the only reason for going to more specialised steels would be if a rapidly varying magnetic field is required, which might cause problems due to hysteresis of steel. This is, however, not an issue for the design presented in this section, so normal steel is the chosen material for the core. This core now needs to extend all the way into the MR valve such that the fluid is in direct contact with the core. This is ensured by the design so that no "air" gap between the core and the

fluid, yielding the maximum intensity of the magnetic field. The two small cores inside the valve that separate the three channels are also made from normal steel.

The housing for the valve needs to be made from a non-ferrous metal, so that the flux will not travel through the housing instead of the MR fluid. Aluminium (2024) has been chosen for its ease of manufacturing and moderate strength. Since it results in the assembly having two different materials, careful design and manufacturing is required to mitigate possible leakage of the fluid. Figure 28 shows an exploded view of the designed MR valve including the core and valve housing/body.

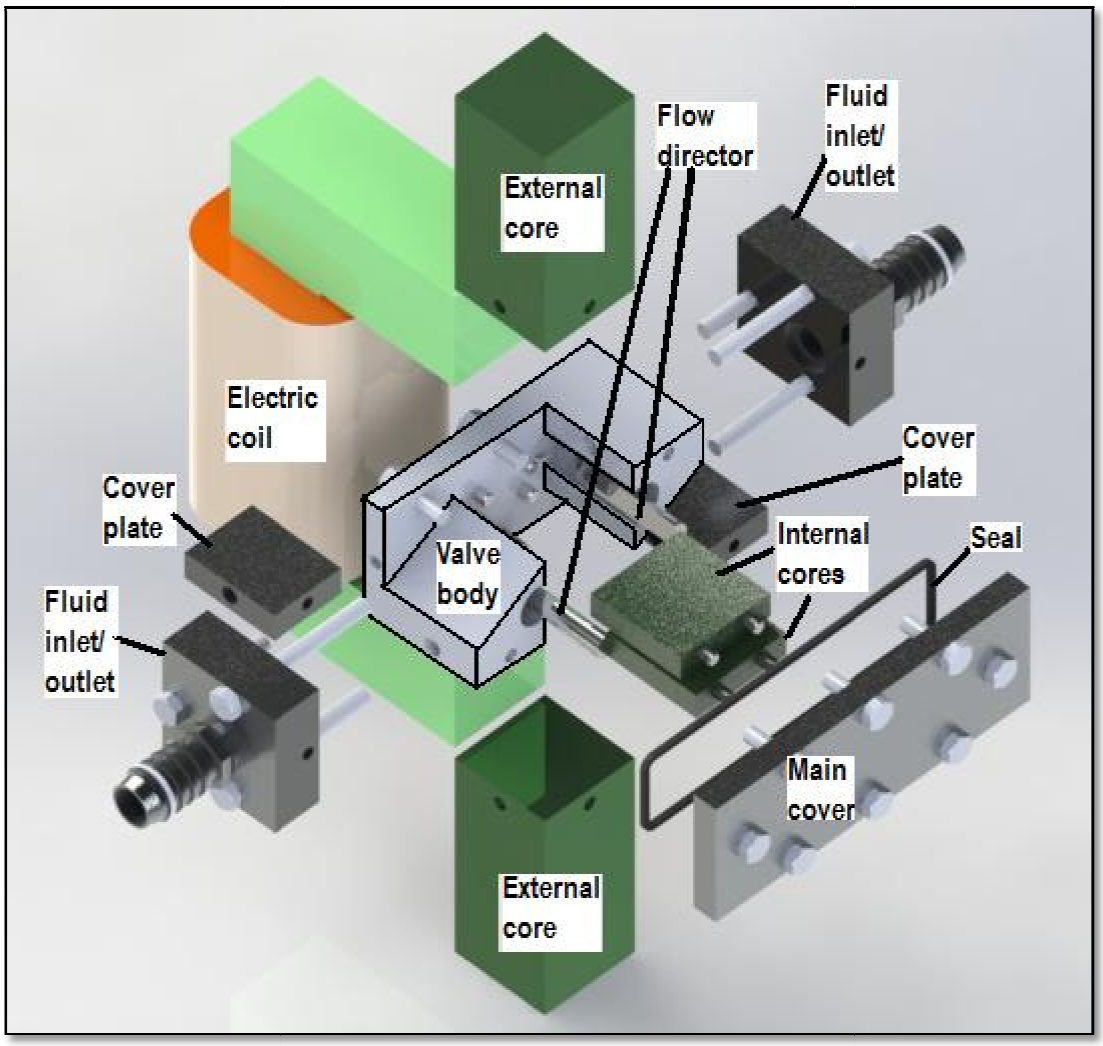

Figure 28: Exploded view of conceived valve design

In Figure 28 the external cores are used to take the magnetic flux into the MR fluid, these are loose so that better accuracy may be obtained during machining and assembling.

The sealing between most of the metal surfaces in the design shown in Figure 28 is ensured by tight machining tolerances, as well as the use of a copper based gasket making sealant in aerosol form, without the use of conventional seals. Using conventional sealing would have been very challenging in the proposed design due to many points having three components meeting in one corner making use of o-ring type seals impractical. The only place where an o-ring type seal has been

used is on the main cover plate because both this plate and the surface it needs to seal onto are flat parallel surfaces.

4.2.2. Assembly procedure

The assembly procedure for the proposed design is important and is discussed briefly in this section with the use of an assembly sequence shown in Figure 29. The first step in the assembly of the MR valve is to press the dowel pins into the internal cores so that they may be accurately located in the valve body, Figure 29a. These internal cores are then inserted into the valve body's locating holes for the dowel pins, Figure 29b. The flow directing semi-cylindrical dowels are then inserted adjacent to the internal cores, Figure 29c. Next, the vertical cores are moved into place after being sprayed with a layer of copper gasket maker, Figure 29 d and e. The top and bottom covers for the valve are now inserted, after getting a layer of the copper gasket maker, Figure 29 f and g. The valve body end caps may then be put into place, also with the copper gasket maker, Figure 29 h and i. The last items for the valve are the o-ring and main valve cover that need to be inserted as shown in Figure 29 j. All fasteners are then assembled and incrementally tightened at the same time so that the parts can nest together as perfectly as possible, Figure 29 i. The only components that are required to complete the assembly of the MR valve are the end pieces (y-shape) for the fluid to flow in and out, and the external magnet core. The end pieces are used such that one side of the Y-shape is connected to the fluid line from the hydraulic cylinder and the other side of the y-shape is used to insert a pressure transducer. The final model of the MR valve assembly can be seen in Figure 30. The physical assembly that has the lid removed as well as the final MR valve assembly may be seen in Figure 31 and Figure 32 respectively. The power supply used to provide the input current can also be seen in the background in Figure31 and Figure 32.

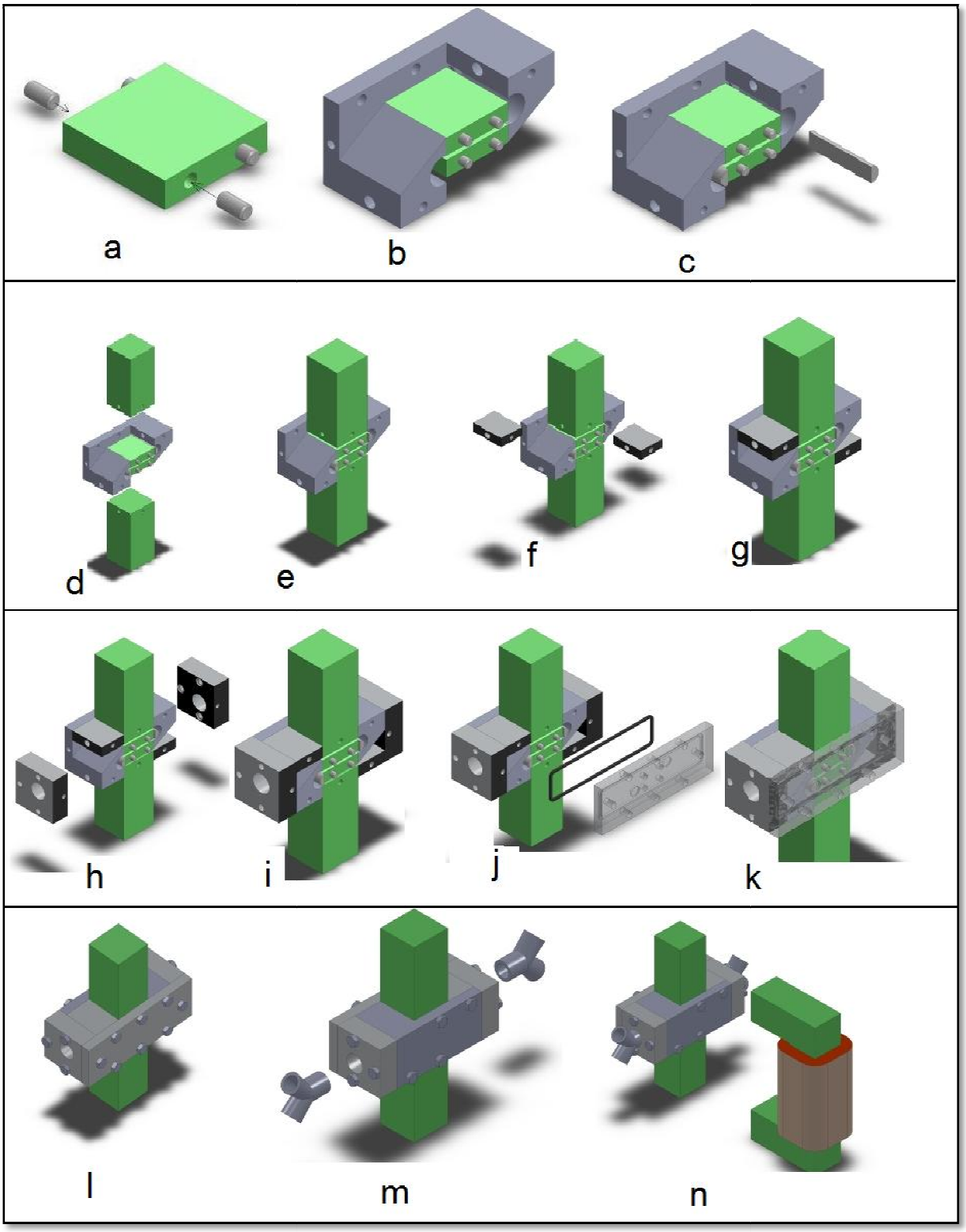

Figure 29: MR valve assembly sequence

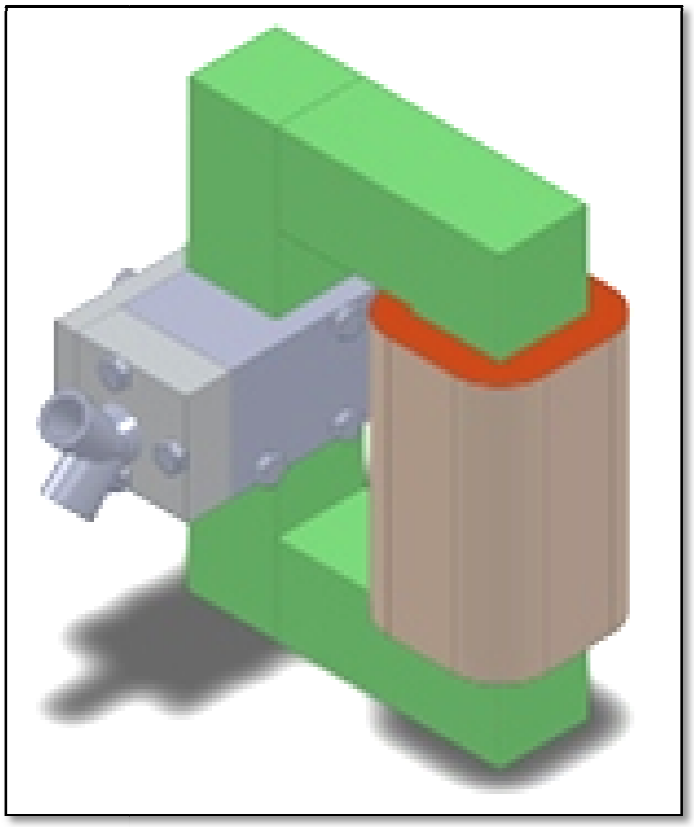

Figure 30: Assembled MR valve CAD

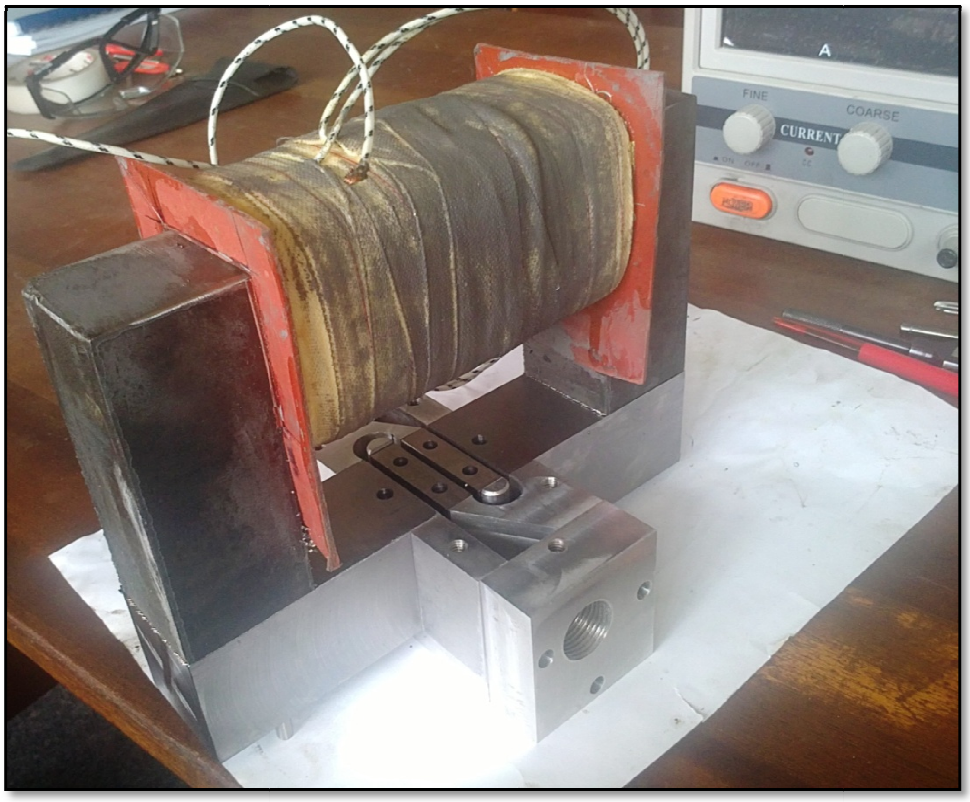

Figure 31: Partially assembled MR valve

Figure 32: Complete assembled MR valve

4.2.3. Actuation equipment

To supply the fluid flow to the valve a double acting hydraulic cylinder containing the fluid is coupled to a servo hydraulic actuator. The hydraulic cylinder has a double acting design with the cylinder rod exiting on both sides. With the cylinder rod exiting on both sides, the volume of the fluid inside the system does not change as the piston is displaced, as is the case of a cylinder with the rod exiting on one side only. This simplifies the design of the supply circuit and alleviates the necessity for a pressurised accumulator in the system. The hydraulic cylinder has a piston diameter of 70mm and rod diameter of 35mm. To achieve the required maximum flow rate of 1.2l/s this hydraulic cylinder requires an actuation velocity in excess of 0.42m/s. The maximum pressure drop over the valve was calculated in Section 1to be 8MPa, meaning that the actuation force to the hydraulic cylinder will need to be somewhere to the order of 23kN, with some margin of error to account for piston friction and model errors as well.

The hydraulic cylinder is actuated by a 25kN servo hydraulic actuator. The servo hydraulic actuator system has velocity capabilities in excess of 2m/s, which means that it is capable of supplying both the required force as well as the velocity needed for successful testing of the MR valve. The hydraulic cylinder that has been used for the testing can be seen in Figure 33a with the servo hydraulic actuator coupled to the rod-end at the bottom, a closer look at the clevis attachment is shown in Figure 33b. It can also be noted that the hydraulic actuator has been mounted using a 90mm spherical bearing on the cylinder and a 30mm spherical rod end on the cylinder rod (Figure 33b and Figure 34). The advantage of having the spherical joint on both sides is that any unnecessary friction from radial forces on the cylinder rod are minimised, also accounting for any issues with assembly tolerances and misalignment.

For the sealing of the hydraulic cylinder it has been decided to use scraper type seals in the end caps of the cylinder where it seals on the shaft, these seals are placed toward the inside of the sliding rings and external dust covers to keep the ferrous particles out of those sensitive regions. These scraper type seals help keep the shaft surface free from wearing by the ferrous particles that

will cause damage when they get stuck between the cylinder rod and a seal (Poynor, 2001). The same philosophy was implemented on the piston, using scraper type seals to scrape the ferrous particles from the cylinder wall before any sliding components pass over them.

(a) (b)

Figure 33: Fluid supply circuit

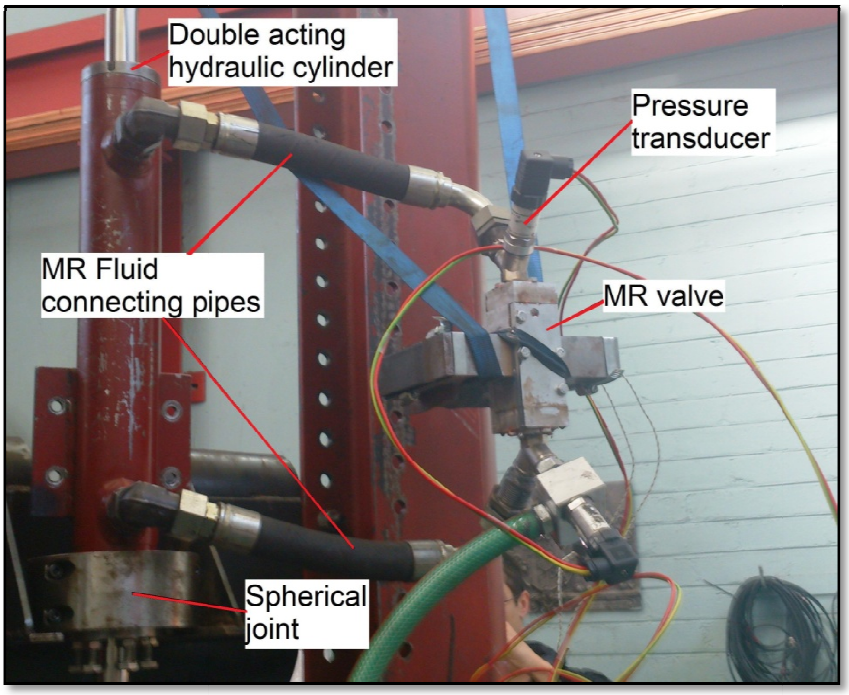

Figure 34: MR valve on test setup

The complete MR valve assembly is then attached to the MR fluid supplying hydraulic cylinder as can be seen in Figure 34.It may be noted that the pressure transducers are also inserted at this stage as well.

This concludes the section on the design and assembly of the MR valve as well as the assembly of the complete test setup. This setup is used for testing the MR valve to verify the validity of the theoretical models presented in Chapter 3.

4.2.4. Equipment for measurement of valve characteristics

With the MR valve and fluid pumping setup now ready it is time to look at the measurement equipment that will be needed to complete the testing. The variables that are important to obtain from testing include the coil current, the pressure drop over the MR valve and the flow rate. The coil current for the experimental setup is supplied by a power supply, the value of which is read off the digital display.

4.2.4.1. Pressure transducers

To measure the pressure drop over the valve it will be necessary to measure the line pressure before and after the fluid passes through the MR valve. This has been done by using two 400bar Wika™ pressure transducers. These two transducers are mounted in the open end of the ½ inch BSP thread y-pieces that connect the fluid from the hydraulic cylinder to the MR valve. Locating the pressure transducers here allows measurement of the pressure drop over the valve only.

Before any pressure transducer can be used with accuracy it needs to be calibrated. Calibration has been performed on a purpose built hydraulic test bench, and the calibration data for the two pressure transducers can be seen in Figure 35.

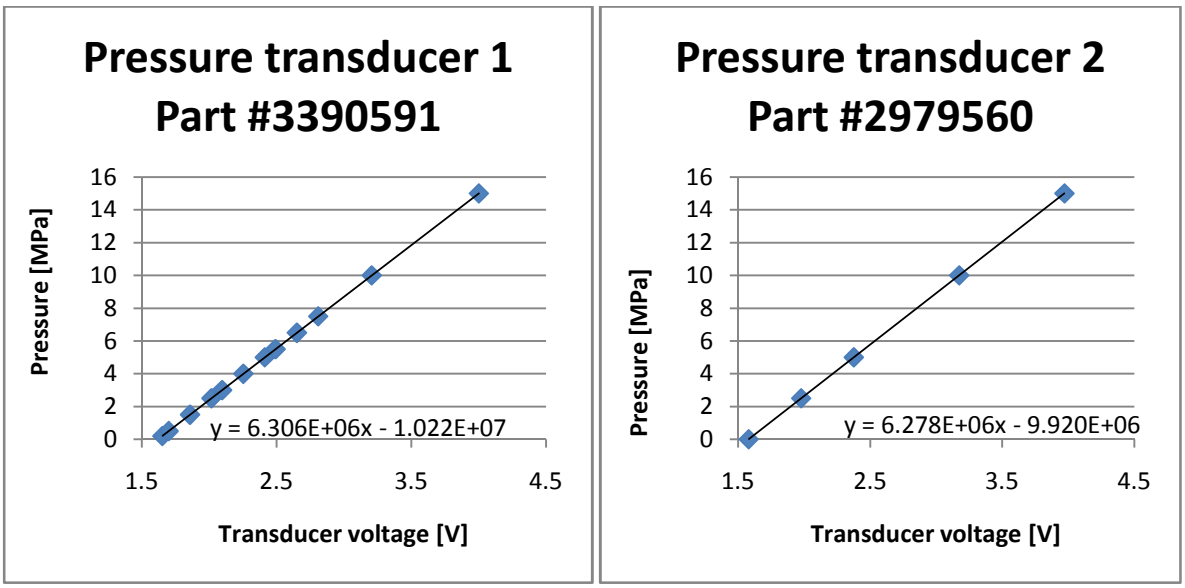

Figure 35: Pressure transducer calibration

From Figure 35 it is seen that the transducers perform as expected, yielding a linear pressure versus voltage relationship. These equations for calibration may now be used to obtain the pressure as a function of the recorded transducer voltage.

4.2.4.2. *Displacement measurement*

The servo hydraulic actuator control circuit has an output that is given as a voltage proportional to the displacement of the actuator. It reads linearly from -10V to +10V for a displacement centred around zero and moving up and down by a stroke of 125mm. Scaling the voltages appropriately will the result in a data vector for displacement as a function of time.

4.2.4.3. *Actuator load cell*

A load cell has been fitted between the servo hydraulic actuator and the MR fluid pumping hydraulic cylinder. This was done so that the effect of piston friction may be estimated. The load cell used has a maximum rating of 50kN. The load cell has been calibrated using standard masses and a voltage measuring device. The calibration data for the load cell can be seen in Figure 36.

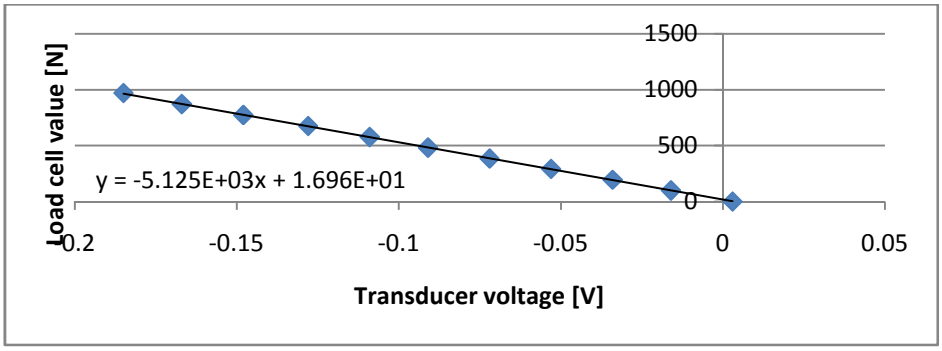

Figure 36: 50kN load cell calibration

From Figure 36 it can be seen that the load cell exhibits a linear characteristic, as is expected. The force applied to the load cell can thus be calculated by using the curve fit equation shown on Figure 36.

4.2.4.4. Data acquisition

The voltage signals obtained from the pressure transducers, load cell and servo hydraulic actuator are recorded using a multi-channel data acquisition device. The device used was a HBM Spider 8, which has the ability to measure up to 8 channels simultaneously at an adjustable sampling frequency of up to 1200Hz and gives the results as a ASCII or spreadsheet file with the columns in the resulting file corresponding to the voltages measured per input channel, as a function of time. The data sampling rate for the tests was set to 100Hz, which is two orders of magnitude higher than the highest expected frequency. The high sampling rate was chosen to so as to aim to accurately read any spikes in the pressures that may be caused by loose physical connections, so that they may be fixed before excessively high pressure spikes cause damage to the valve or sensors.

4.2.5. Experimental procedure

For the testing of the MR valve a specific procedure was conceived. It was decided to start with a constant velocity and signal amplitude input to the actuator, starting at a low frequency/actuation velocity, and increasing the frequency only after the whole coil current range was covered. This will result in a set of data for pressure drop as a function of coil current and actuation frequency, with the frequency and amplitude relationship being linearly proportional to the flow rate of the MR fluid.

The stroke of the actuator that has been used was set to 100mm, with a starting frequency of 0.1Hz, yielding an actuator velocity of 0.04m/s and hence a flow rate of 0.115 l/s (10% of maximum tested value). This triangular displacement input (constant velocity) was chosen so that the most accurate steady state pressure drop as a function of velocity, and thus flow rate, characteristic may be achieved. The actuation frequency was increased by increments of 0.1Hz. With the increasing triangular wave frequency it was observed that the shock loading on the system increased drastically when the actuator changed direction of travel. The shock loading is due to small amounts of free play found on the rod-end connection, which, after direction change, momentarily caused the actuator to move at a constant velocity without the hydraulic cylinder following. Figure

37 shows the spike due to the sudden change in actuation direction of the triangular displacement input. The figure is plotted for 0.5Hz, 100mm stroke and 0A coil current.

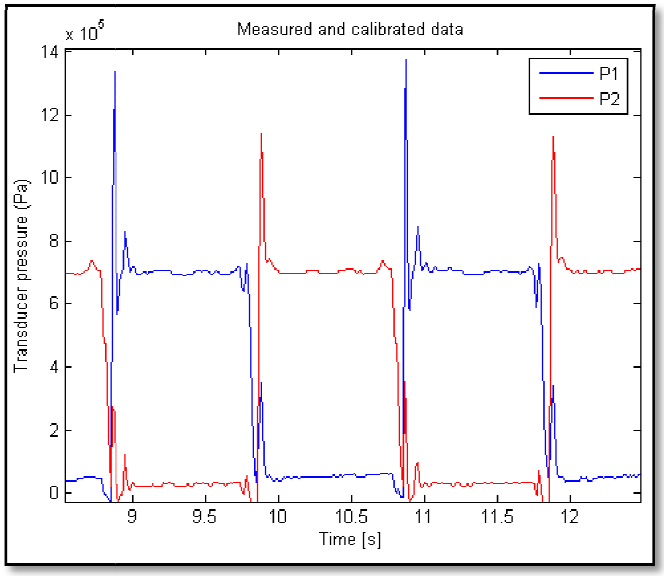

Figure 37: Shock in pressure due to triangular wave input

With this pressure spike in the system it was decided to rather switch to a smoother sine wave input for the higher flow rates that need to be tested. Another advantage of the sine wave is that for the same frequency and amplitude a higher velocity is achieved. The control circuit for the servo hydraulic actuator has a built-in function generator, triangular, sine and square, and at the time of testing could not take any external signals to supply a better suited displacement control function. The ideal displacement curve would typically be a triangular wave with rounded tips to soften the changing of direction; this would yield constant velocity data, without the harsh pressure spikes.

The predetermined maximum flow rate required was stated in Section 1 as 1.2l/s (236l/min), with a corresponding actuator velocity of 0.42m/s. This means that a sine wave with an amplitude of 100mm will need to be applied at a frequency higher than 0.67Hz to achieve the flow rate required for comparison of the MR valve with the standard $4S_4$ system. The displacement control sinusoidal wave of the hydraulic cylinder will thus be applied in steps of 0.1Hz from 0.1Hz up to 0.7Hz with amplitude of 0.1m.

As the displacement is applied and the pressure transducers' voltages are recording, the coil current will be set to the required value for that specific test. The reason for setting the current after the movement has started was to minimise the chance of the MR particles' chains forming into columns and yielding an excessively high initial pressure drop over the valve, which may cause damage or promote leakage in the valve (Tao, 2001). The current values were increased from zero, in increments of 0.2A up to 3A for the testing done. The pressure drop as a function of current was traced as current was increased and it was seen that saturation of the MR fluid had taken place around 2.4A already, thus meaning that an increase over the 3A stated above was pointless.

The next sections will show the results of the tests performed for the pressure drop as a function of flow rate and magnetic coil current.

4.2.6. Results of experiments

In this section the results of the pressure drop tests will be displayed. Firstly by evaluating the measured and calibrated data, from which the more relevant information including the pressure drop versus flow rate characteristic is derived.

4.2.7. Verifying that the test equipment works as intended

The first step in testing any device is to run a quick and simple test by which it may be verified that all the sensors/outputs of the system are functioning the way that they are supposed to. Firstly the displacement is plotted using the calibrated displacement to verify that the output works as expected. Figure 38 shows the displacement values for the data plotted against time for a triangular wave with 0.1m amplitude and 0.1Hz frequency.

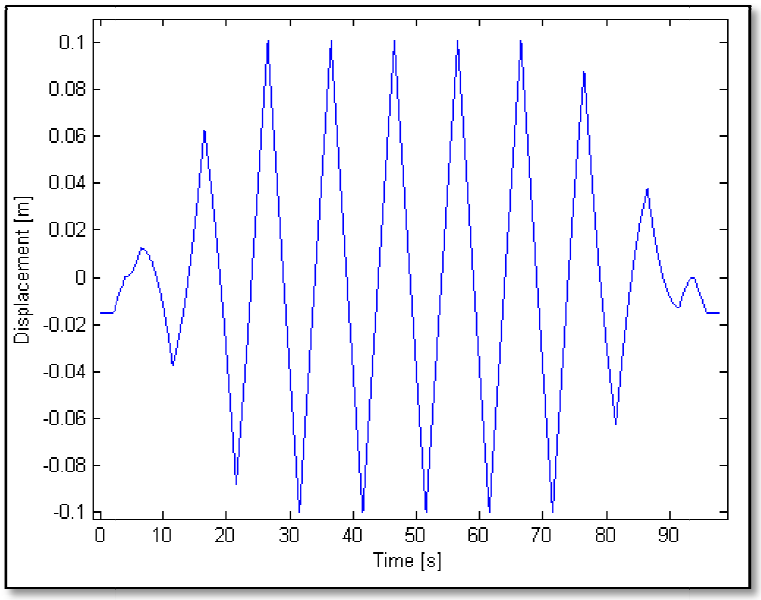

Figure 38: Triangular displacement input 0.1Hz, 100mm amplitude

From Figure 38 it can be seen that the servo hydraulic actuator does in fact displace as is specified by the input triangular wave, as it travels the correct distance at the correct frequency (10 seconds per cycle). This means that the actuator is performing according to the control circuit as expected.

Figure 39 shows the two pressure transducer measurements as a function of time. This test was performed using a triangular displacement input with a frequency of 0.1Hz, amplitude of 100mm and a coil current of 1A. The transducers are named P1 and P2 respectively, the information that is important will be the pressure difference between them. Figure 40 shows this difference in pressure, which is effectively the pressure drop over the MR valve.

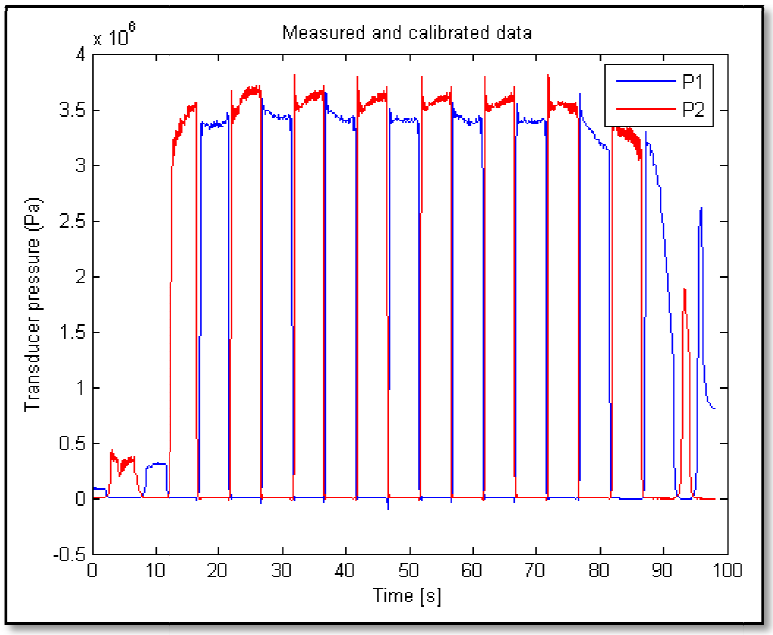

Figure 39: Pressure transducer measurements for 0.1Hz 1A

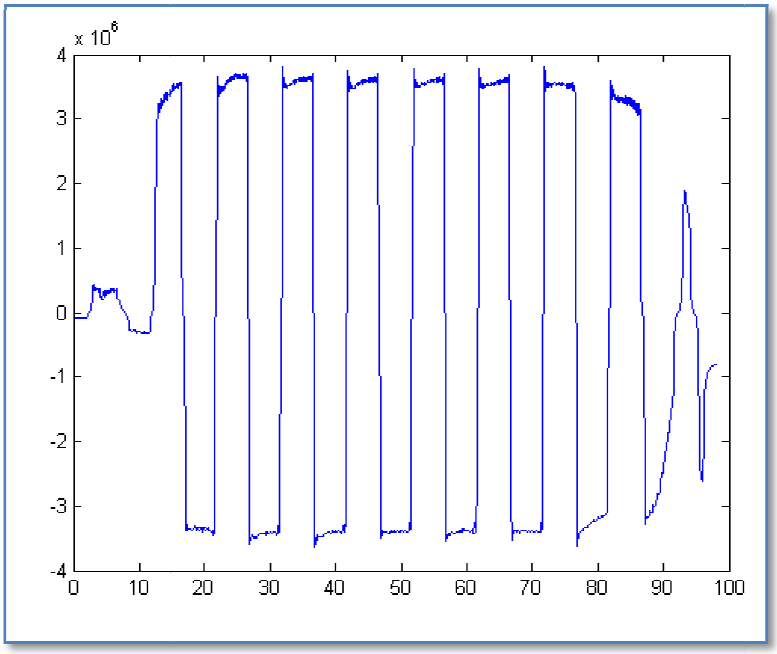

Figure 40: Pressure drop over MR valve for 0.1Hz 1A triangular wave input

From Figure 40 it can be seen that there is not a substantial amount of noise on the data, so only minor post test data filtering will be implemented. The two pressure transducers' values are also quite similar, showing that the calibration of the transducers works satisfactorily, yielding an approximately symmetric result, as was expected for this test setup. Figure 41 shows the pressure transducer readings for the same frequency and current inputs as the previous case, but with a sine wave for displacement being applied instead of a triangular wave.

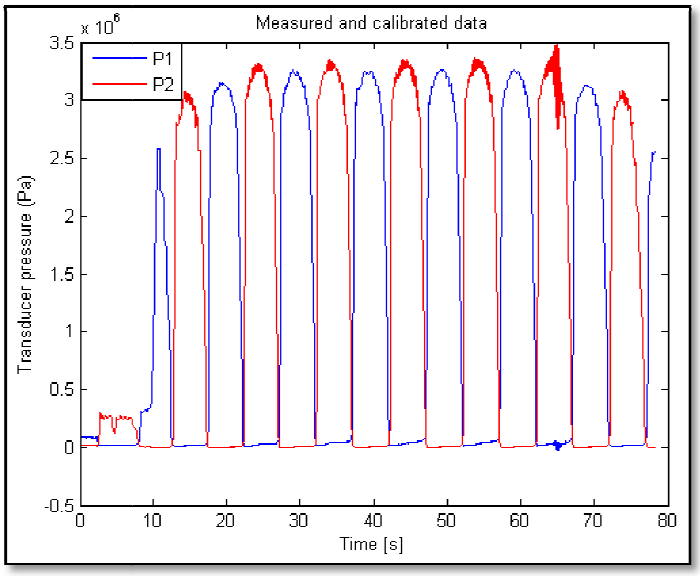

Figure 41: Pressure transducer measurements for 0.1Hz 1A sine wave

Now that the test setup, including the pressure transducers and displacement control circuit are proven to function the way expected we can start to perform the sweep of the tests for varying frequency and coil current after which the relevant pressure drop vs. flow rate characteristics may be investigated.

4.2.8. Pressure-drop testing

Triangular displacement wave tests were performed up to a safe operating frequency of 0.3Hz so that the most repeatable test results for pressure drop versus flow rate data may be obtained due to the constant flow rate for a triangular wave. Figure 42 shows the pressure drop vs. flow rate characteristic for a triangular wave test performed at 0.3Hz, 100mm amplitude and a 1A coil current. By performing a “comet” plot it was observed that most of the data sat at two specific locations, shown as the two points in the figure. A zoomed in view, Figure 43, of the plot shows the data all bundled at a point. The other data in the figure is the pressure drop measured as the actuator changes direction in its triangular wave, and is discarded. Thus, for a constant flow rate a constant repeatable pressure drop is witnessed.

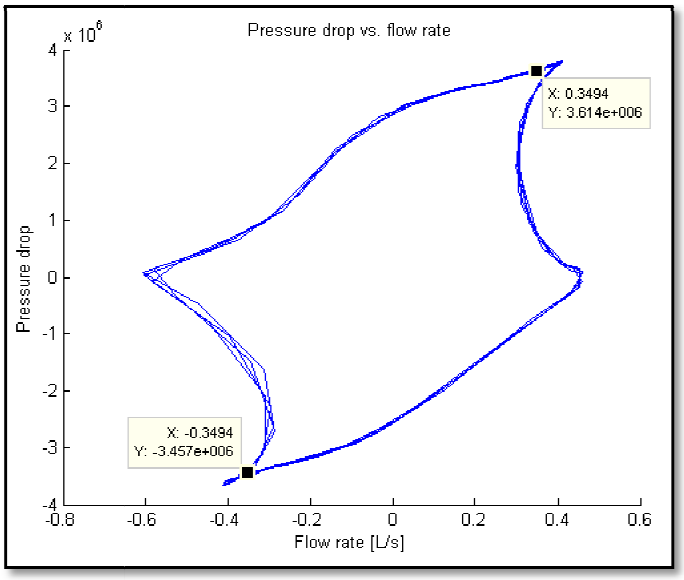

Figure 42: Pressure drop vs. flow rate for 0.3Hz 1A triangular wave

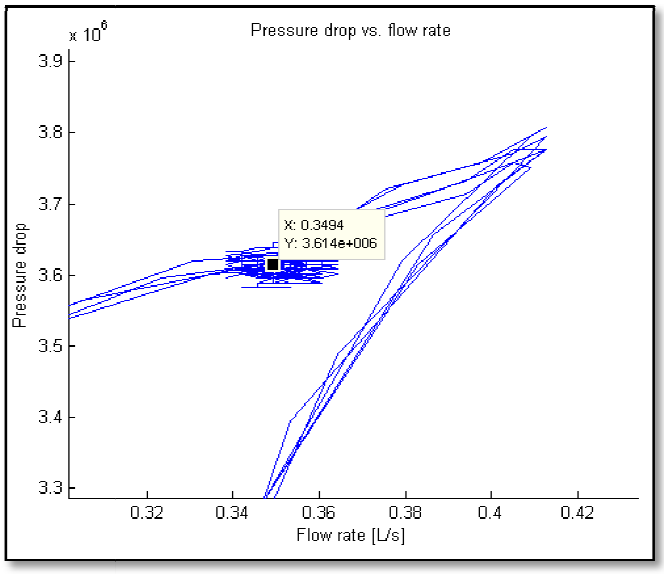

Figure 43: Zoomed in view showing a bundling of data at a specific location

By now performing this type of plot for the entire set of triangular wave test data it is possible to get a number of pressure drop vs. flow rate data points for a varying coil current. The triangular wave's application, as discussed earlier, has a limit to the frequency that it can be applied safely due to the shock at direction changing of the actuator that was to be kept to a minimum. Thus, for higher levels of flow rate testing a sine wave was implemented. Figure 44 shows the pressure drop vs. flow rate characteristic for a sine wave, performed at the maximum required frequency of 0.7Hz and saturation current of 2.4A. Only the central data values were used to only show the relevant information, and discard the coil start up behaviour.

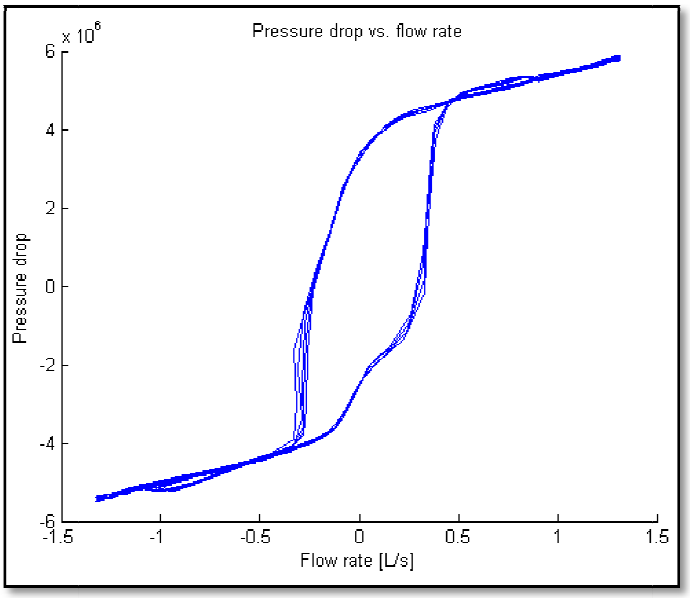

Figure 44: Pressure drop vs. flow rate for 0.7Hz, 100mm amplitude and 2.4A current

From these plots more pressure drop vs. flow rate information may be obtained for different values of coil current and this set of test results can be used to compare the performance of the MR valve to the theoretical model predictions, which is what will be discussed next.

4.2.9. Conclusion on results compared to theoretical model

With an elaborate set of data containing pressure drop as a function of flow rate and coil current these tests' results may then be compared to the theoretical model. Because the pressure drop is a function of mainly two variables it is decided to plot the test results on a 2-d graph keeping one of the variables constant.

Firstly the measured pressure drop as a function of coil current was plotted for constant flow rates against the theoretical model, as can be seen in Figure46 to Figure 51.

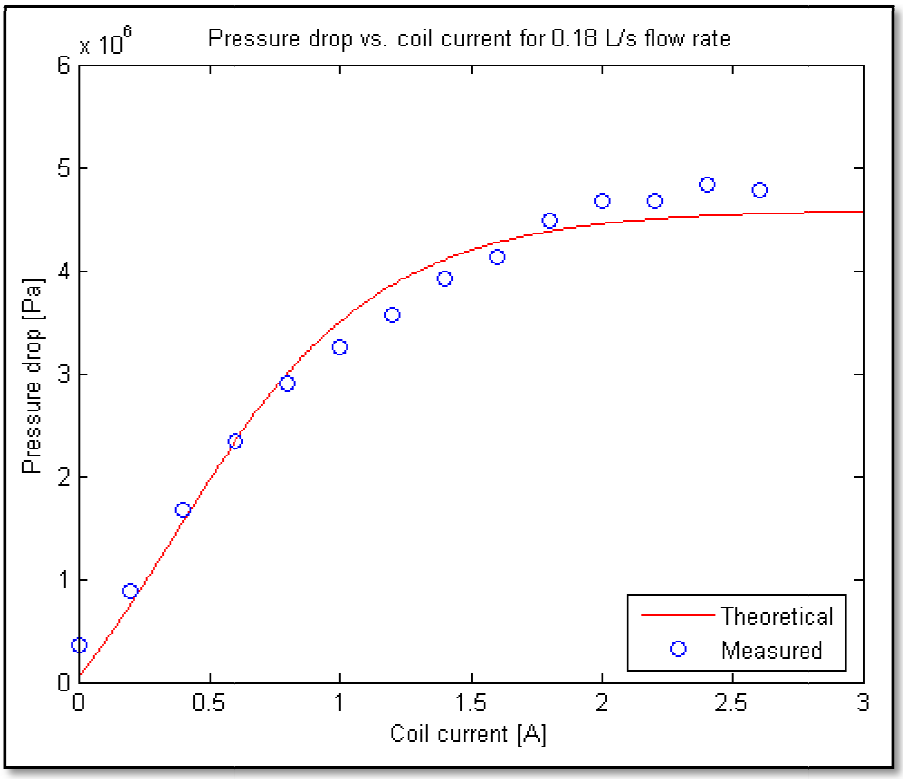

Figure 45: Pressure drop vs. coil current for 0.18 L/s

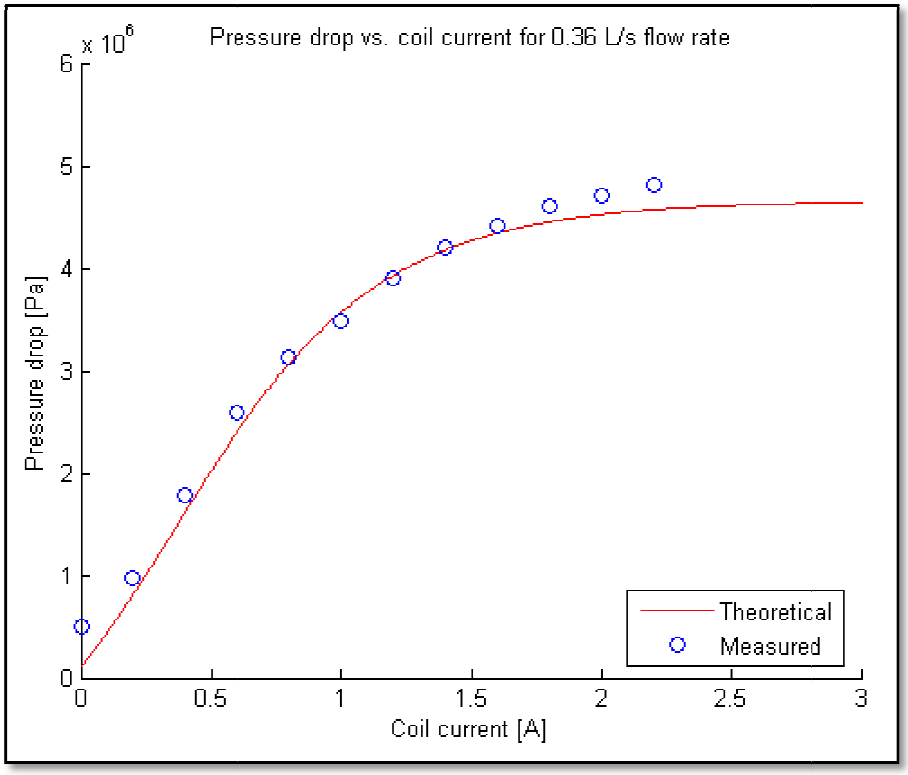

Figure 46: Pressure drop vs. coil current for 0.36 L/s

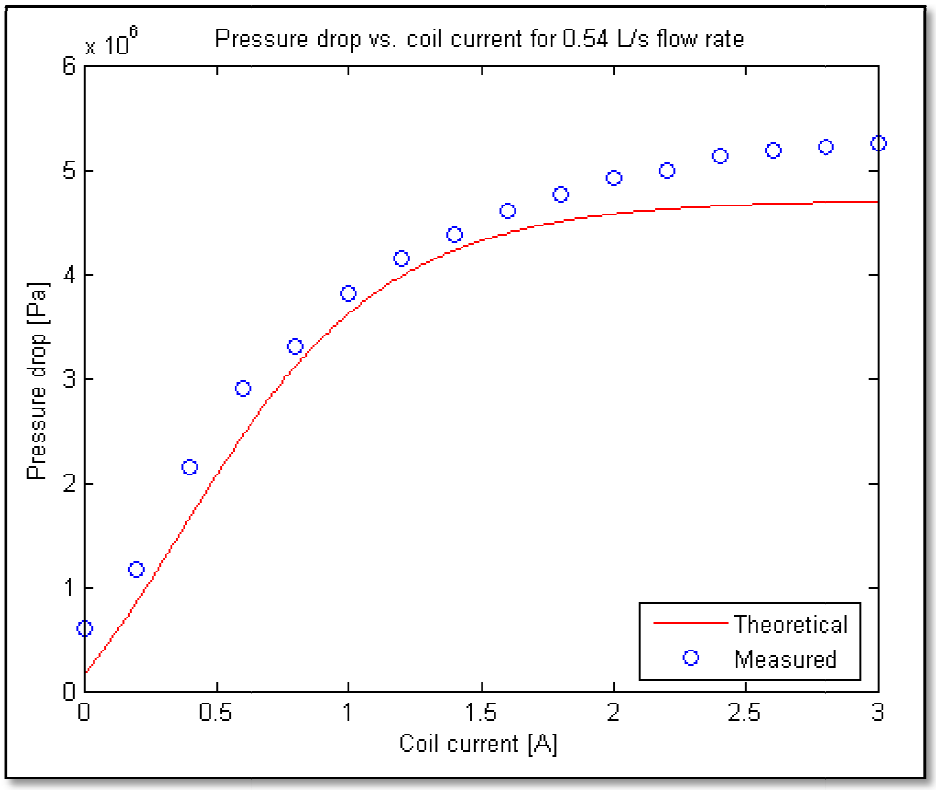

Figure 47: Pressure drop vs. coil current for 0.54 L/s

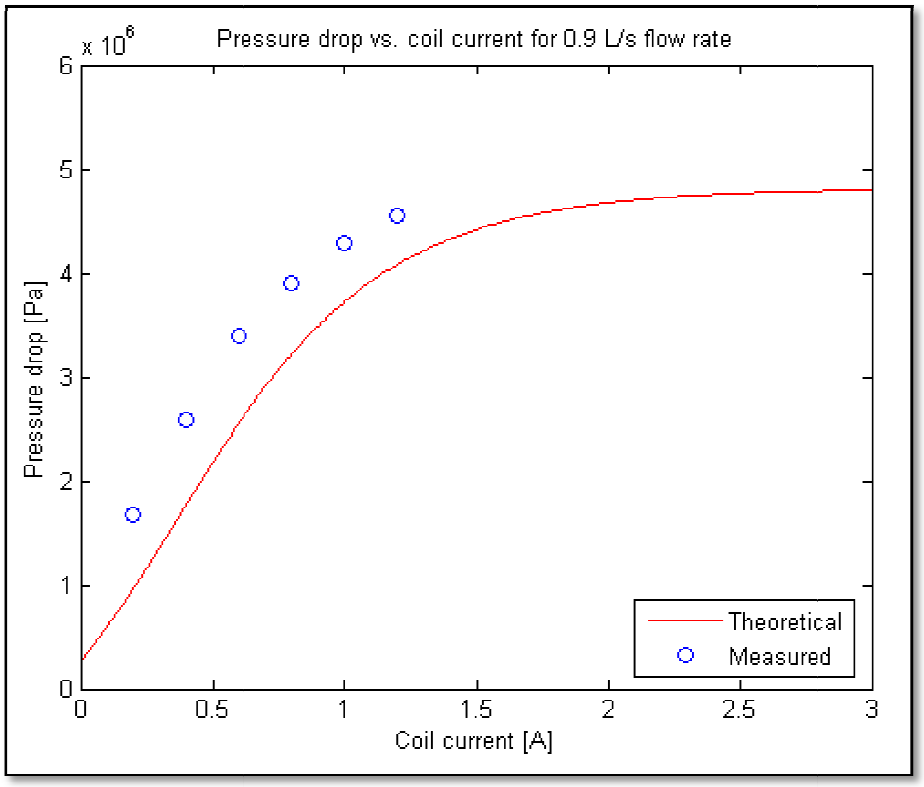

Figure 48: Pressure drop vs. coil current for 0.9 L/s

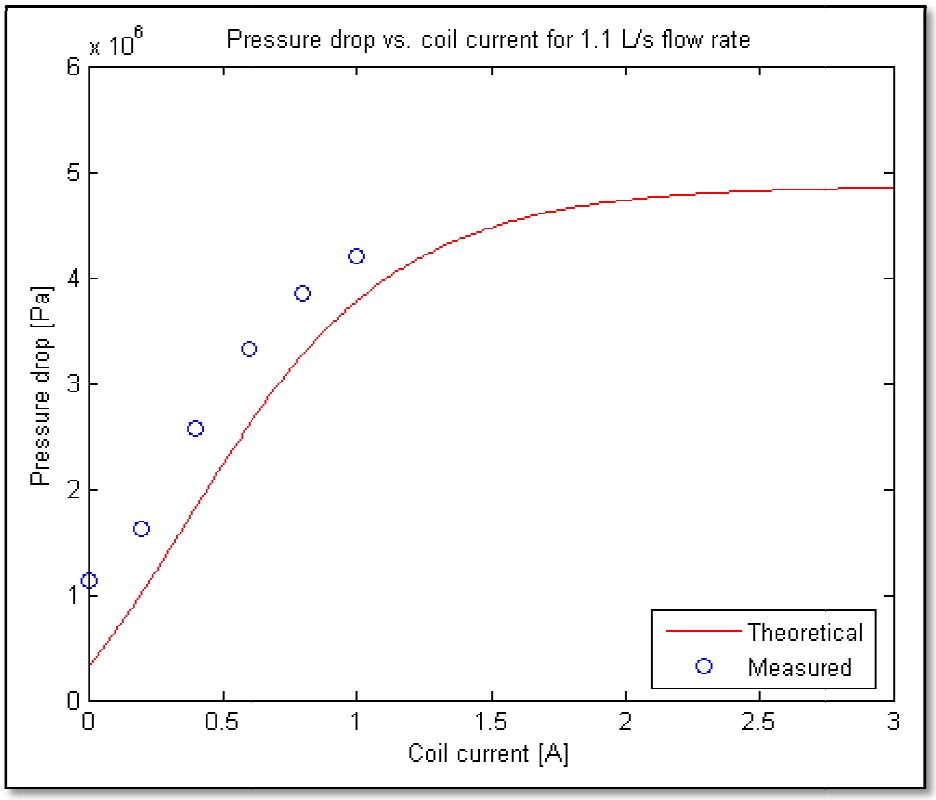

Figure 49: Pressure drop vs. coil current for 1.1 L/s

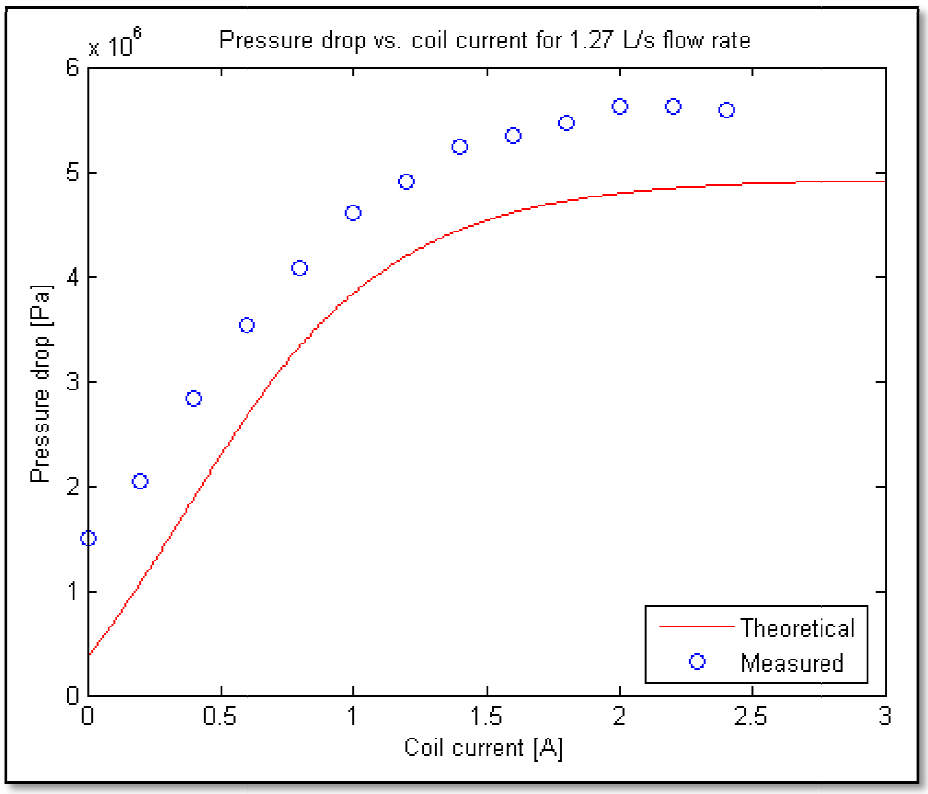

Figure 50: Pressure drop vs. coil current for 1.27 L/s

From Figure 45 to Figure 50 it can be seen that the theoretical model seems to follow the trend of the data accurately for low flow rates, but as flow rate is increased the model starts to deviate from the test results. This shows that the error is flow rate dependant.

The only variables that could influence the behaviour of the MR valve in this way is the viscosity of the fluid and the geometry of the MR valve. With the valve geometry quite accurately known it leaves the MR fluid viscosity as the culprit for the error in predictions. The assumed viscosity of the fluid was 0.1 Pa.s, with this an assumed value by comparison to an equivalent volume fraction commercial MR fluid, made by a different manufacturer, as the MR fluid manufacturer of the fluid used for this study did not supply a viscosity value. The actual value for the viscosity for the MR fluid used was now found by evaluating the pressure drop vs. flow rate curve for a high flow rate and zero current. An improved value for the viscosity was found by increasing the MR fluid viscosity incrementally until the theoretical model yielded off-state behaviour comparable to the experimental tests. The improved value for the viscosity was found to be 0.4 Pa.s with Figure 51 to Figure 56 showing the test results now compared to the theoretical model with an increased viscosity. Most of the tests were performed at a temperature of around 50°C; the effect of temperature is discussed in Section 4.4 to follow.

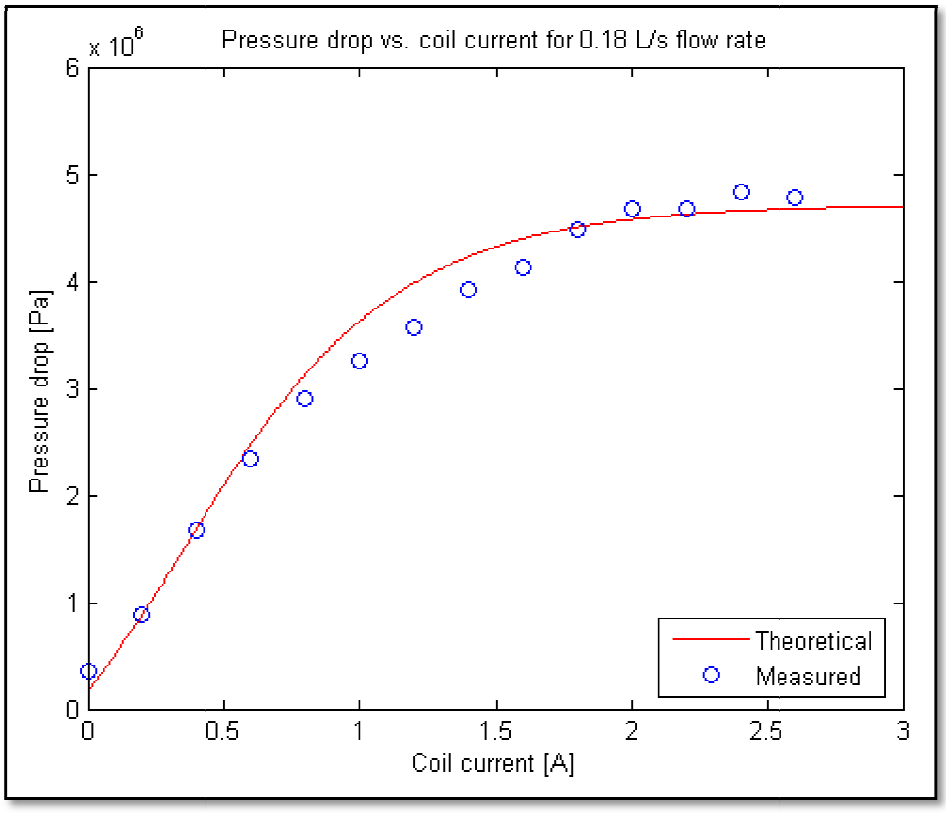

Figure 51: Pressure drop vs. coil current for 0.18 L/s improved viscosity

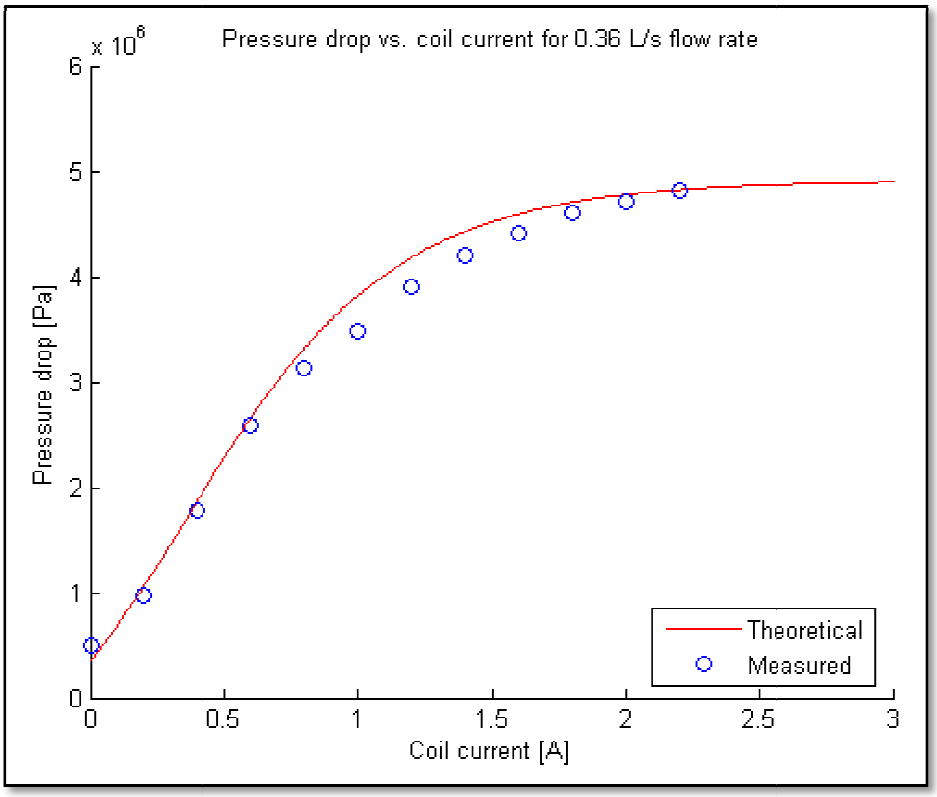

Figure 52: Pressure drop vs. coil current for 0.36 L/s improved viscosity

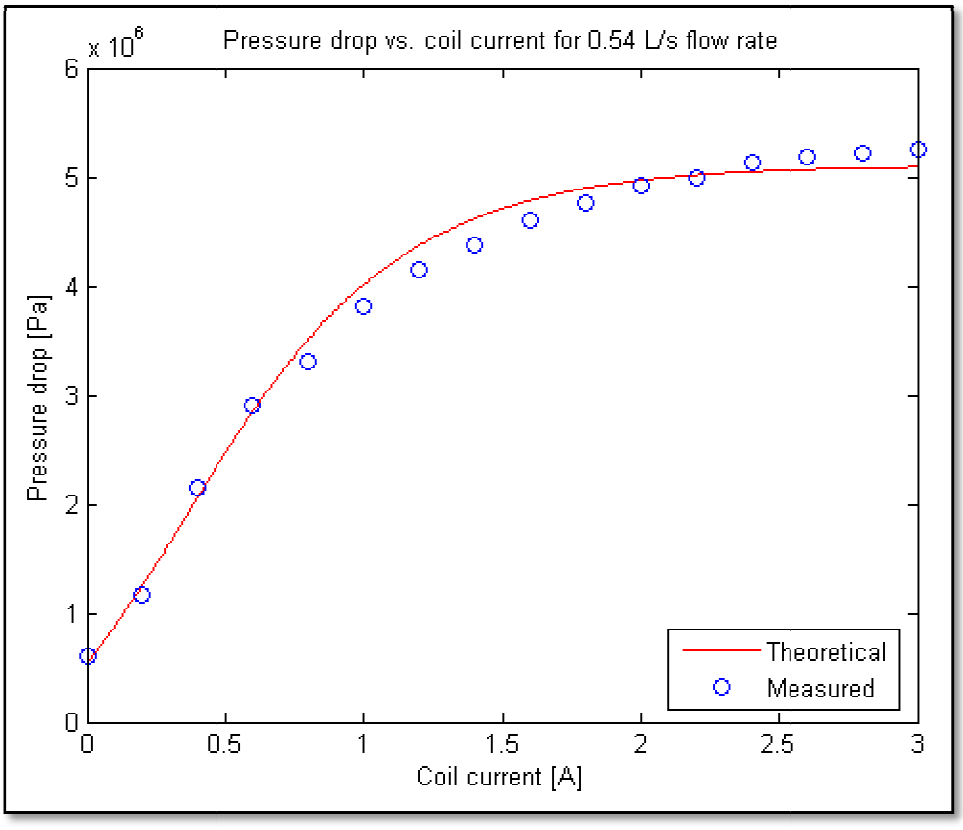

Figure 53: Pressure drop vs. coil current for 0.54 L/s improved viscosity

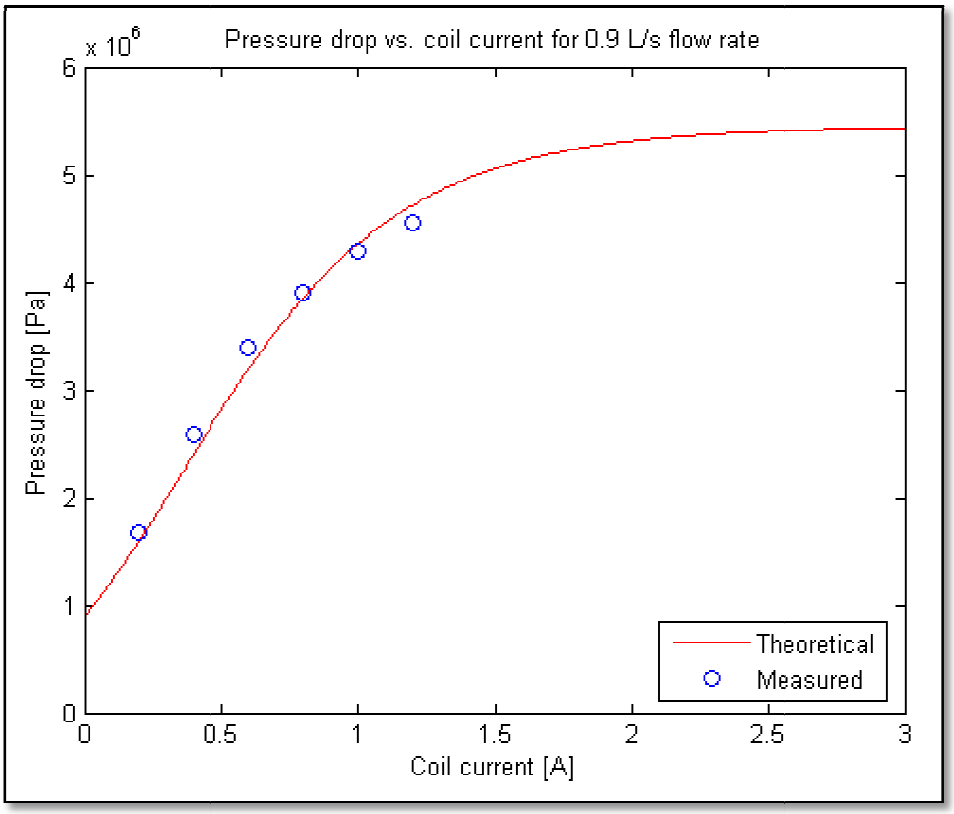

Figure 54: Pressure drop vs. coil current for 0.9 L/s improved viscosity

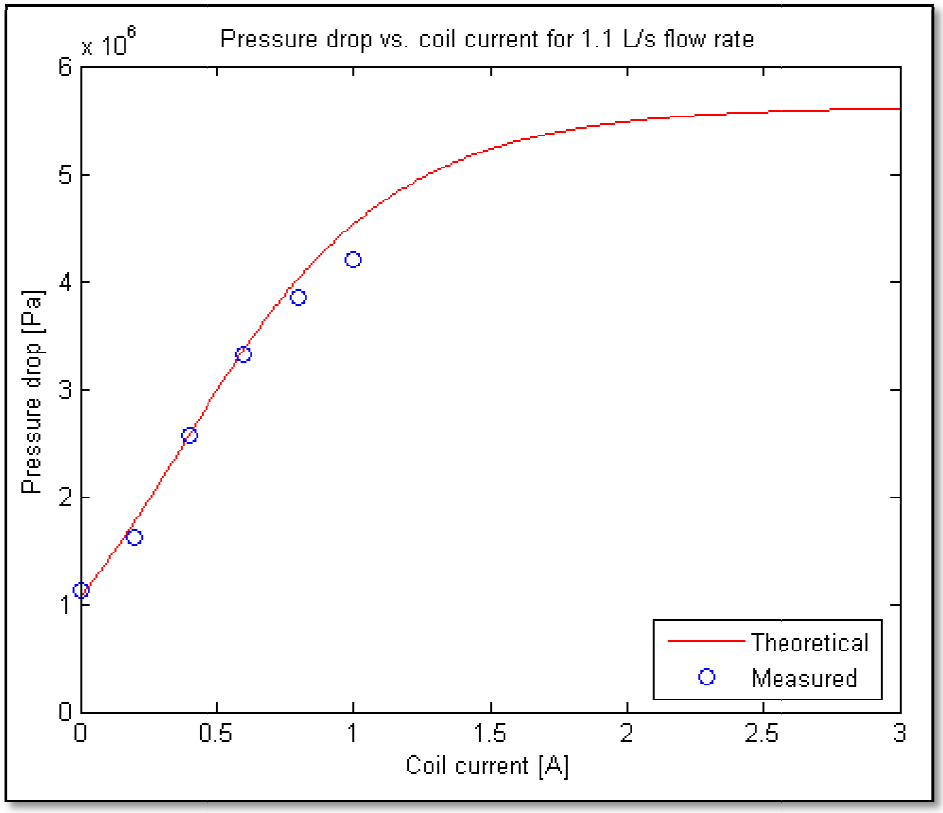

Figure 55: Pressure drop vs. coil current for 1.1 L/s improved viscosity

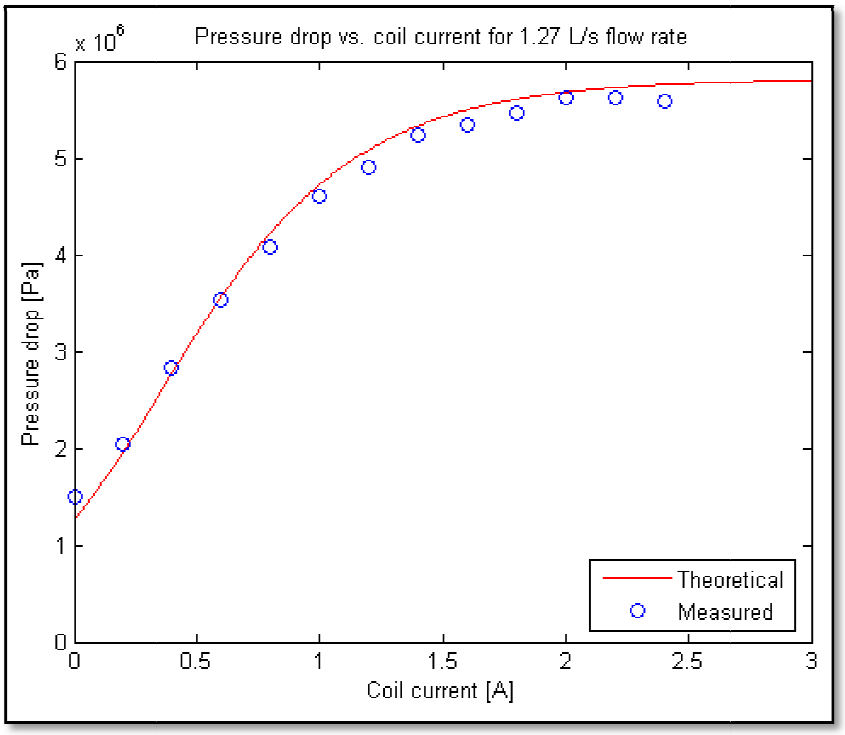

Figure 56: Pressure drop vs. coil current for 1.27 L/s improved viscosity

From Figure 51 to Figure 56 it can be seen that the theoretical model with the increased viscosity now predicts the data very well, with an average error determined to be less than 4.3 % and a maximum error found at some low flow rate data points of 16%. The average error is calculated by taking the average of the absolute value of error for all the data points.

This concludes the section on the testing for the pressure drop as a function of flow rate and coil current. The next section looks at the flow blocking ability of the MR valve.

4.3. Flow blocking ability and low flow rate testing

This section covers the low flow rate region in the pressure drop versus flow rate characteristic curve to determine the ability of the MR valve to block off flow of MR fluid. This is of special interest as one of the possible uses for the MR valve to be researched is the feasibility of replacing a positive flow blocking solenoid valve in the $4S_4$ with an MR valve, as was discussed in Section 1. This section firstly looks at the experimental setup's design, after which the equipment needed and testing procedures carried out are stated, followed by the results of the tests and a discussion thereof.

4.3.1. Experimental design and equipment required

To evaluate the ability of the MR valve to effectively stop any flow of fluid it will be required to measure the maximum pressure drop over the MR valve, as well as the corresponding flow rate of the fluid through the MR valve with the fluid in a magnetic saturation state. It was chosen to perform these tests at saturation current as it is at this value at that the highest ability of blocking off flow will be experienced.

If complete blocking of the flow of MR fluid does occur, the coil current will be lowered to determine which value of coil current is required to effectively block off a certain pressure drop over the valve.

4.3.2. Experimental procedure

The experimental procedure followed for the blocking ability tests differ only slightly from the pressure drop versus flow rate tests, in that the displacement input is changed to a constant force input. Using a constant force input will enable determining of pressure drop values that can be maintained for zero flow rates, if any, as well as quantifying the pressure drop vs. flow rate characteristics when very low flow rates are present.

To achieve constant force input to the actuator without forcing the actuator to its movement limits a square wave input was used. The force input for a 5kN force can be seen in Figure 57. The constant actuation force/pressure drop signal was started at 1.5kN actuation force to the cylinder, after which it was increased incrementally from there. The actuation force that was fed back to the servo hydraulic controller was measured at the actuator, so this force value does include the piston friction, which will be removed by using the pressure drop over the valve measured directly by the pressure transducers so as to also get an approximation to the piston friction experienced.

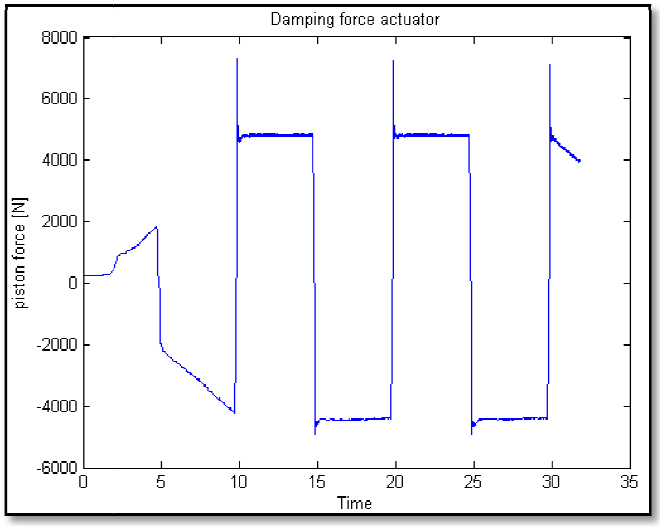

Figure 57: Square wave force input for flow blocking tests

After every test the actuator was displaced from its lowest to its highest position to ensure that the chains formed in the MR fluid inside the valve are properly broken down and the fluid in the valve mixed properly with other fluid. It was found that this is a necessary task as the MR fluid appeared to become stronger from one test to the next if the fluid was not properly circulated between tests. This phenomenon is confirmed by the theory presented by Tao, (2001), on the forming of columns in the MR fluid if an applied magnetic field is left on stationary fluid and time is given to settle.

4.3.3. Results and discussion of experiments

This section describes the results obtained for low flow rate testing of the MR valve. It was found that the proposed starting force of 1.5kN was not sufficient to overcome the piston friction in the hydraulic cylinder. After increasing the actuation force to 2kN the hydraulic cylinder started displacing fluid. It was now possible to set the current to a maximum value and find the flow rates corresponding to various applied actuation forces, i.e. pressure drops.

The tests performed using a constant, or square wave for force yielded a pressure drop vs. flow rate characteristic that is seen in Figure 58. Using a "comet" plot and zooming in to the regions where the data bundled together it was again found that the constant force data had been concentrated at small locations (Figure 59), with the other lines on the graph being due to the change in actuator force direction. These were the test results for a constant actuator force of 15kN and a maximum coil current of 3A for one complete cycle.

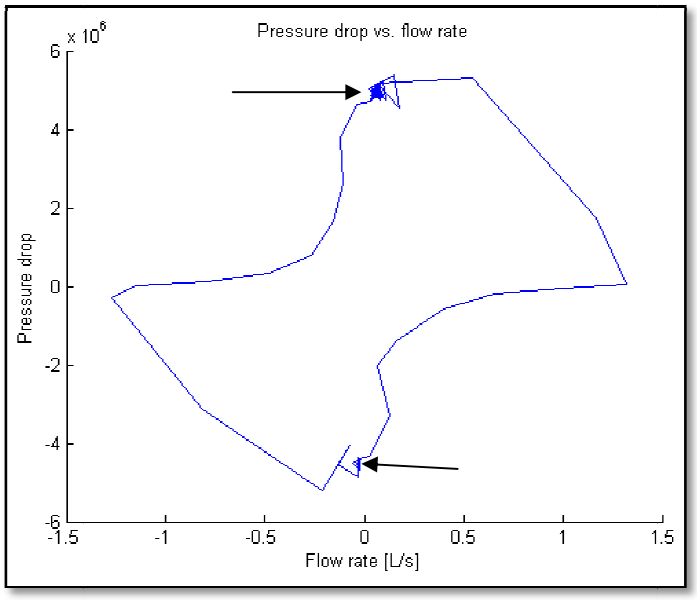

Figure 58: Constant force tests, 15kN actuator force

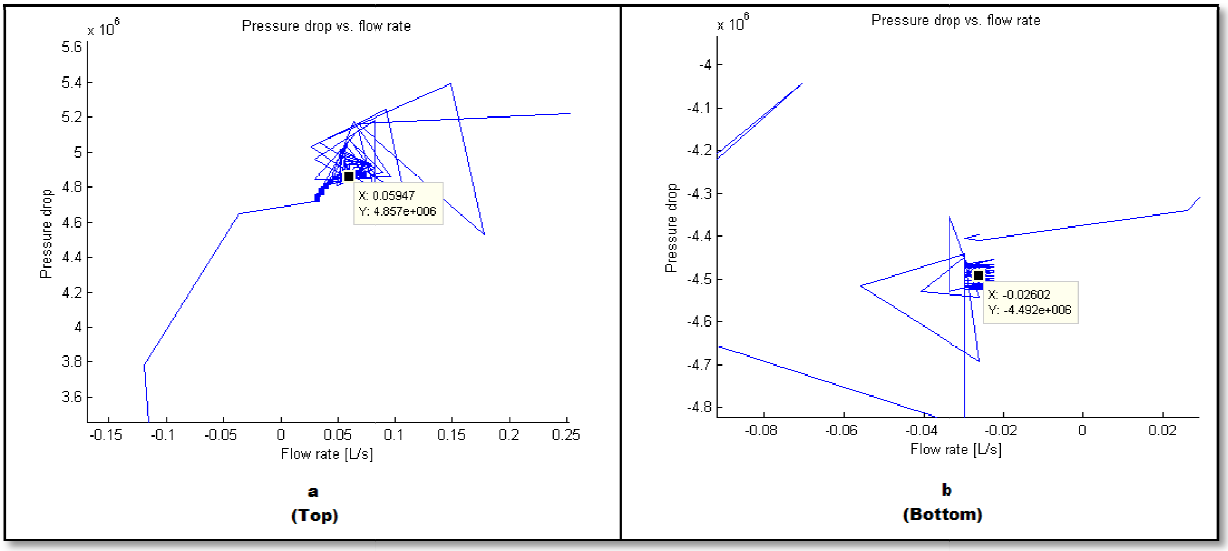

Figure 59: Zoomed in to locations of bundled data of Figure 58

Figure 59a and Figure 59b shows the concentrated regions where the actual pressure drop vs. flow rate data for Figure 58 lie, for the constant forces applied. These values are the ones used for the test comparisons. By reading a number of these small clusters' average values off the graphs a pressure drop vs. flow rate data set is obtained for the very low flow rate scenario. Figure 60 shows these data points plotted for saturation current at different levels of constant actuator force.

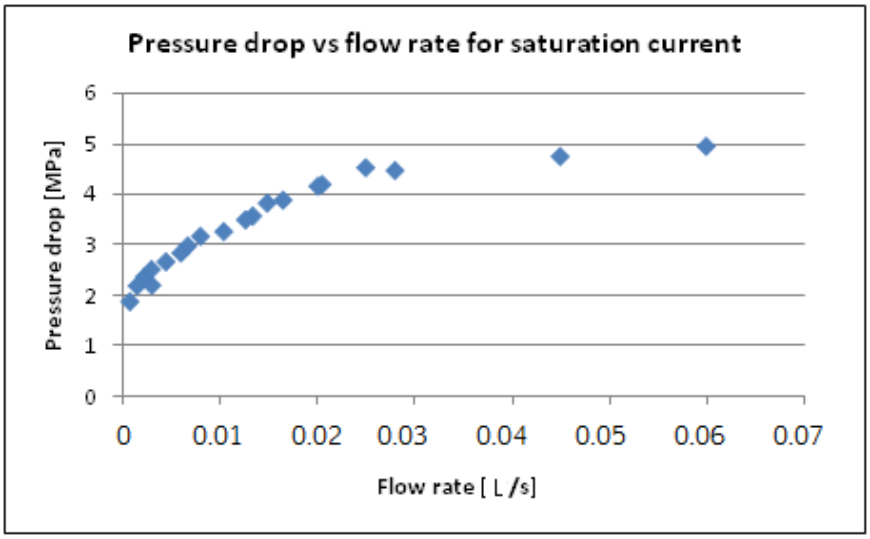

Figure 60: Minimum flow rate curve

Due to the piston friction and low velocity movement capabilities of the actuator the lower bound of flow rate was limited above a threshold value. It is noted in Figure 60 that the pressure drop as a function of flow rate does not reach zero, but rather goes down to a minimum value around 2MPa at the lowest flow rate that was tested. These test results are from the constant force tests. To evaluate the applicability of these pressure drop values a look was taken at the pressure drop vs. flow rate characteristics of some of the sine wave tests at very low flow rates. Figure 61 shows the pressure drop-flow rate data for the constant force tests as well as the 0.1Hz, 0.3Hz and 0.7Hz tests. The initial theoretical model's prediction based on an assumed value for the constant "a" from Section 3.1.4 is also shown, just as a reference.

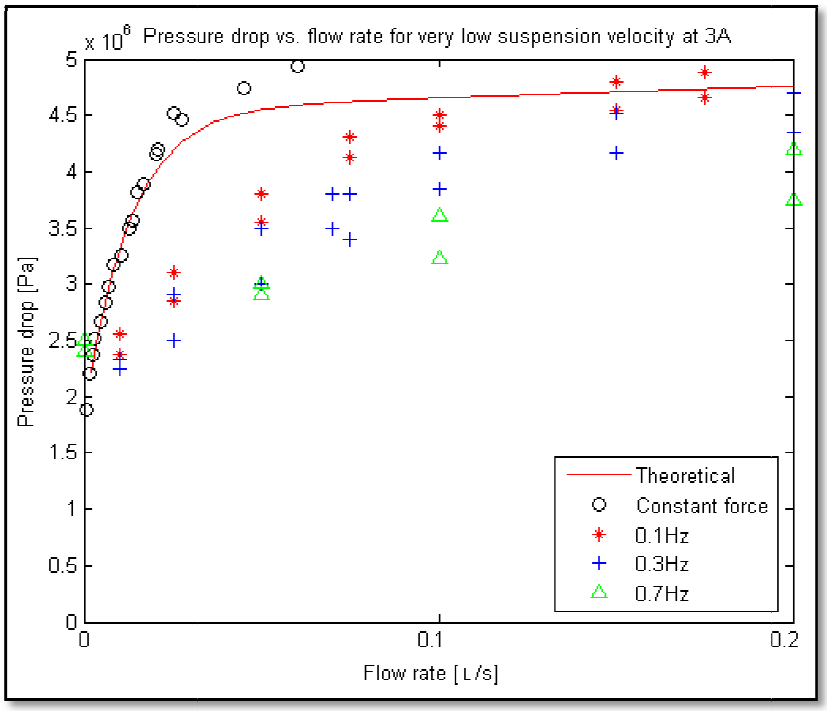

Figure 61: Low flow rate pressure drop data

What is interesting to note is that the low flow rate shear strength of the MR fluid is a function of the test's maximum fluid flow rate, thus it is a function of the history of the flow rate. This is a type of hysteresis effect that all MR fluid devices exhibit. What is also seen is that all these curves, although having different transient responses from the quasi-Newtonian to the Bingham behaviour do all exhibit a minimum value that they can resist before any flow will start occurring. This means that the MR valve does, for the purposes of the tests performed, have the ability to block off flow of MR fluid up to a certain pressure drop, after which fluid flow will start to occur. Figure 62 shows the minimum pressure drop as a function of flow rate for the MR valve. This is effectively the flow blocking ability of the MR device.

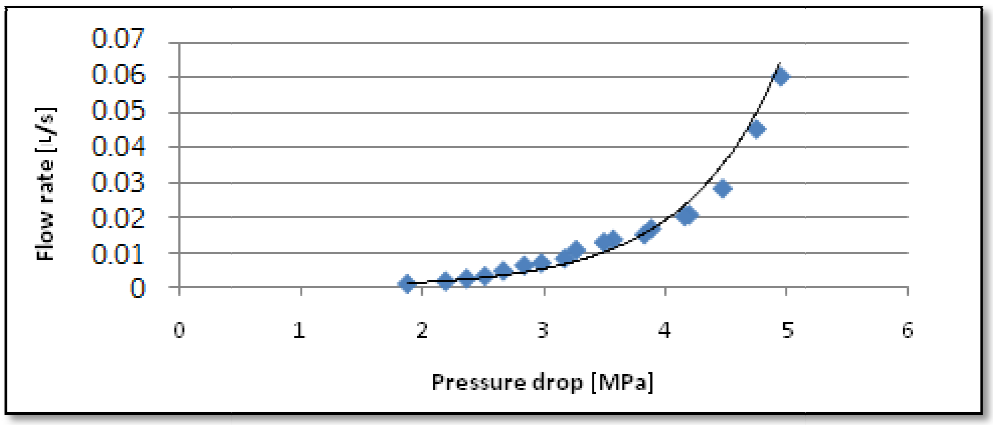

Figure 62: Minimum fluid flow rate for pressure drop

Although an accurate hysteresis model lies somewhat outside the scope of this research project it was decided to try to find a way of accurately predicting the behaviour of this MR valve using a curve fit to the test results. The low shear rate weakening behaviour of the MR fluid, as was

described in Section 3.1.3,as is seen in these figures, with the value for the exponent "a" as used in Eq. (19) seeming accurate in this case for the constant force tests, but not for the higher actuation frequency tests. It would now be necessary to determine the value of the exponent such that the low speed characteristics may be accurately predicted, i.e. an approximation to the exponent that determines the point at which the behaviour switches from quasi-Newtonian to Bingham can now be determined, also being a function of the history of the excitation of the fluid through the valve.

Because the weighing equation, Eq. (20), uses a constant "a" multiplied by the shear rate, it will be similar to use another constant value multiplied by the fluid flow rate, as the shear rate and flow rate are proportional to each other. The equation used in the program for predicting the transient response in Figure 61was stated as follows:

$$W_1 = e^{(-\text{constant} \times \text{flow rate})} \quad (23)$$

It is now necessary to rewrite this equation for the weighing factor such that it may take into account the hysteresis of the device. It was noted that a horizontal shift together with a change in the constant's value, both as a function of the flow rate, will yield the necessary correction to account for the hysteresis. The weighing equation is now modified as follows:

$$W_1 = e^{(-C1(\text{maximum flow rate}) \times \text{flow rate} \; - C2(\text{maximum flow rate}))} \quad (24)$$

It should be noted that C1 and C2 are functions of the maximum flow rate, and not the instantaneous flow rate, meaning that C1 and C2 will remain constant for a constant sine wave, although the weighing factor will vary according to the instantaneous flow rate. The best fits for the data were found using constants C1 and C2 as is stated in Table 2. It can be seen that these values are both a function of the maximum fluid flow rate (not the instantaneous flow rate).

Table 2: Low flow rate curve fit constants

Maximum Flow rate [m^3/s]	C1	C2
0	80000	0.5
1.8e-4	25000	0.6
5.4e-4	10000	0.7
1.27e-3	5000	0.8

Figure 63 shows these two constants plotted as a function of flow rate.

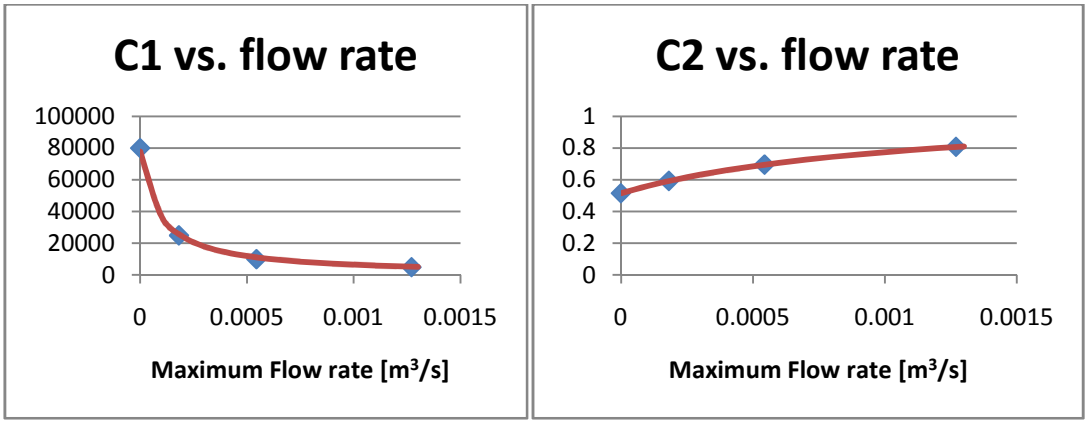

Figure 63: C1 and C2 curve fits

After performing a curve fit to the data using inverse functions to fit the data Eq. (25) and Eq. (26) for the two factors were obtained:

$$C1 = \frac{7}{(\text{maximum flow rate} + 9\times10^{-5})} \quad (25)$$

$$C2 = \frac{-6\times10^{-4}}{(\text{maximum flow rate} + 1.1\times10^{-3})} + 1.06 \quad (26)$$

The reason for choosing inverse functions for the curve fits is because the inverse function has the property that it will converge to a value, making it less sensitive to a change in flow rate for higher flow rates, where normal curve fits might diverge, or not give good correlations to the data. Off coarse the number of combinations of curve fits is infinite, and MR valve specific, but these values were found to fit the MR valve presented in this study well.

The effect of these equations can be seen in Figure 64to Figure66,that were plotted for sine waves having a frequency of 0.1Hz, 0.3Hz and 0.7Hz respectively with all having a 100mm amplitude. In each case the solid line is the theoretical model and the markers represent the measured results.

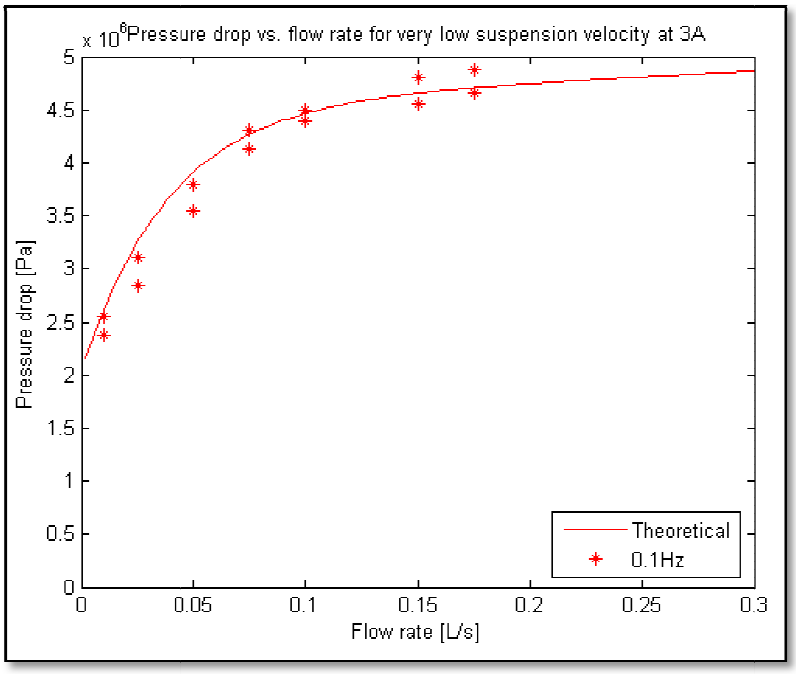

Figure 64: Low flow rate hysteresis modifying factors applied to 0.1Hz frequency

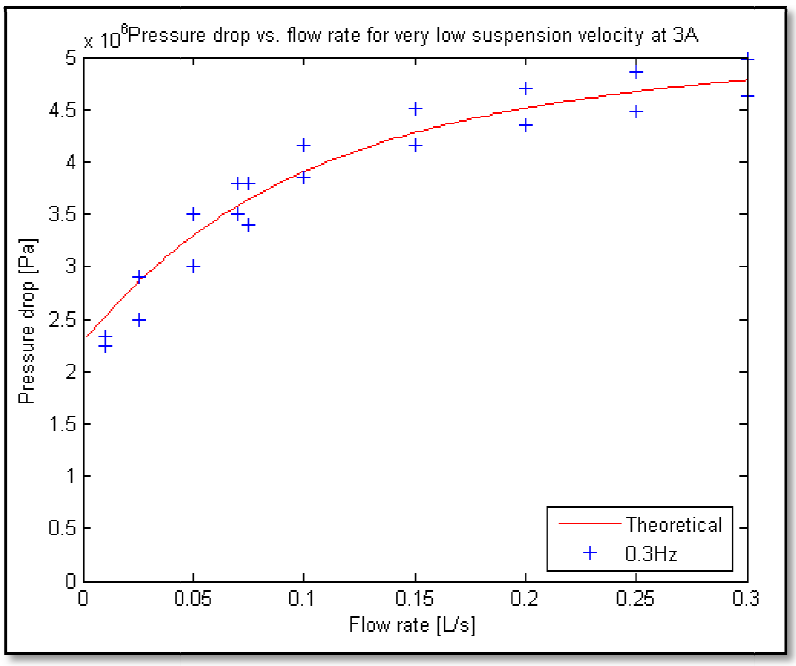

Figure 65: Low flow rate hysteresis modifying factors applied to 0.3Hz frequency

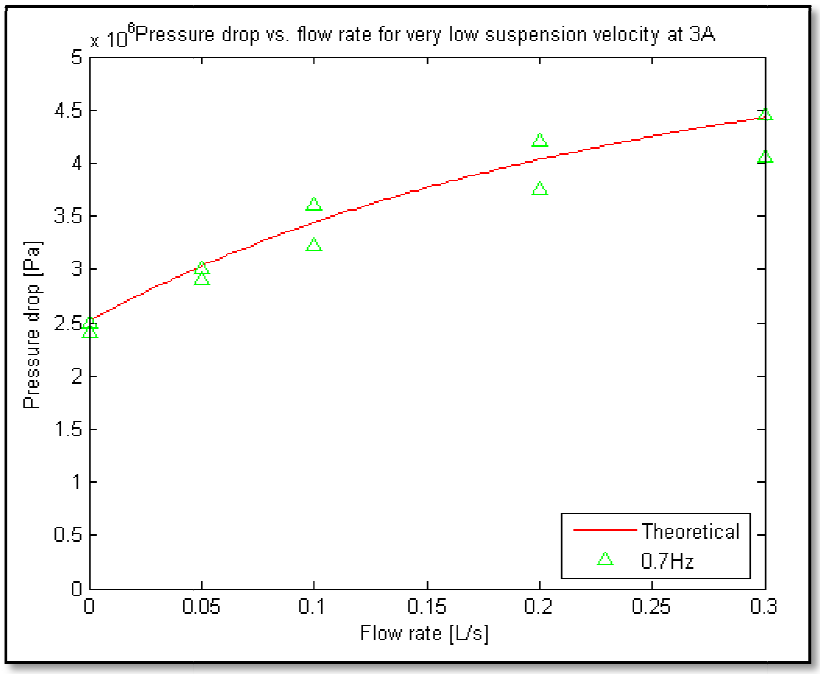

Figure 66: Low flow rate hysteresis modifying factors applied to 0.7Hz frequency

From the above figures it can be seen that the constants C1 and C2, used to determine the transition location do predict the hysteresis effect found in the tests, predicted the characteristics well.

4.3.4. Conclusion on blocking ability tests

By looking at the blocking ability tests performed it was seen that there exists a minimum threshold of pressure drop over the valve that can be maintained without a noticeable fluid flow through the valve. The MR device showed a "blocked" pressure drop of around 2MPa, with a noticeable fluid flow starting at pressures higher than that.

It was also noted that the theoretical model was able to predict the low flow rate pressure drop over the MR valve, provided that the variable as stated in section 3.1.4 is determined from testing. This is the variable that determines the transition from a quasi-Newtonian behaviour to the Bingham behaviour for low shear rates. It was found that this variable is a function of the history of the flow rate, and by appropriately obtaining a curve fit from testing it is possible to generate an equation that is able to accurately predict the pressure drop over the valve taking hysteresis into account as well. This variable is application specific, so it will have to be determined by testing for different valve geometries and fluids used.

4.4. Comparison to user requirements

With the theoretical model for the MR valve's pressure drop performance now validated for the entire range of flow rates and coil currents it is now possible to compare the MR valve presented in this study to the user requirements set forth at the start of the study.

Figure 67 shows a direct comparison of the optimised $4S_4$ system characteristics and the MR valve designed in this study. The top line represents the $4S_4$ system's high setting and the lower line the low setting. The colour band/rainbow across the figure is the operating range of the MR device. The operating location in the operating band is a function of coil current.

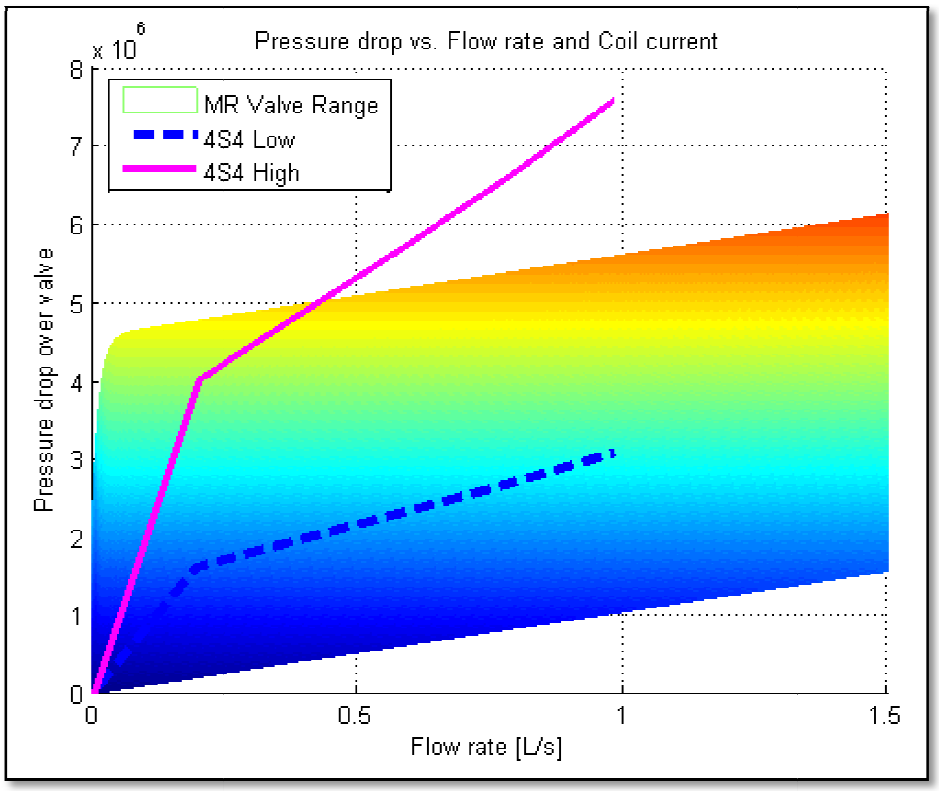

Figure 67: Comparison of MR valve and the optimised $4S_4$ system

It is noted for the optimised $4S_4$ high damping force case that the MR valve's pressure drop exceeds the performance of the current $4S_4$ system for flow rates less than 0.4 l/s, or 0.2m/s vehicle suspension velocity. After this point the optimised $4S_4$ characteristic shows a significantly higher rate of increase as compared to the MR valve for the pressure drop over the valve. At a flow rate of 1L/s the optimised $4S_4$ characteristic requires about 7.5 MPa pressure drop over the valve, which is 36% higher than the maximum pressure drop achieved by the MR valve presented in this study for the same flow rate. It should be noted however that the low flow rate characteristic of the MR valve is substantially higher than the optimised $4S_4$ system's capability, especially when approaching zero flow rate, yielding 4.5 MPa at a flow rate of 0.1 L/s, which is 2.25 times higher than the value for the optimised $4S_4$ system.

By looking at the $4S_4$ low setting it can be seen that the MR valve exhibits a much lower minimum damping than the $4S_4$ requirement. With the minimum damping of the MR valve much lower than the optimised $4S_4$ minimum value the vehicle's handling may be negatively affected. From Figure 67 one can see that the MR valve's whole performance range is lower than the optimised $4S_4$ required characteristic. This indicates that the geometry for the valve was not adequate to supply the necessary pressure drop characteristics as was required.

By changing the geometry in the theoretical model it was found that the new geometry for the valve that would fulfil the user requirements is a passage height of 2mm, a width of 40mm and a

length of 120mm, meaning that the only change required is to reduce the MR gap height. The geometry used is still the triple pass layout as the one that was conceived in this thesis. The predicted performance of the valve with the updated gap size can be seen in Figure 68.

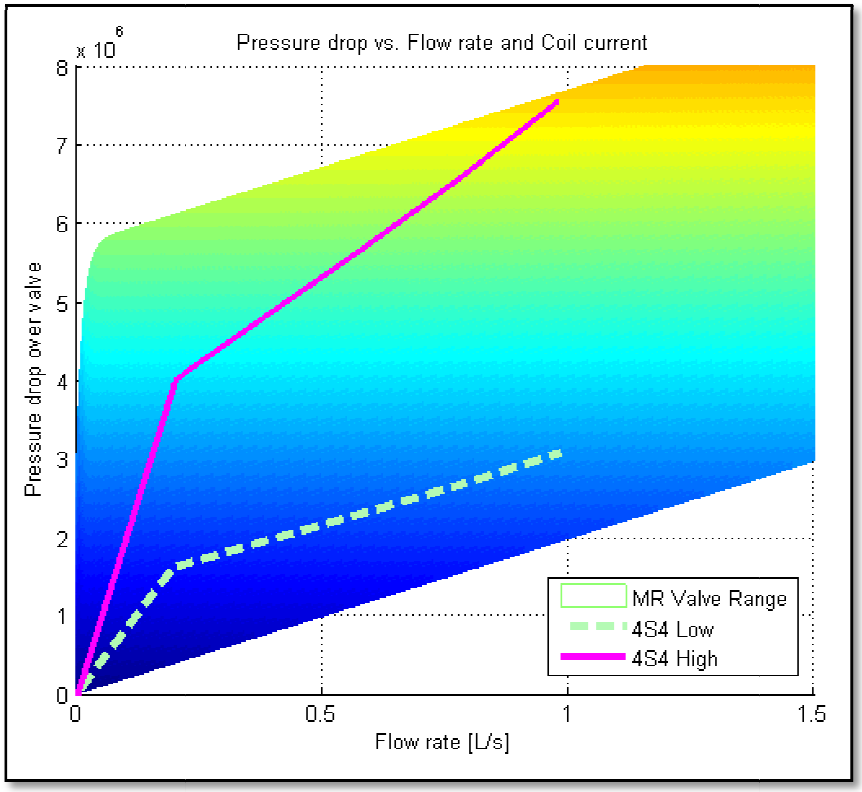

Figure 68: Performance of improved MR valve geometry

From Figure 68 it can be seen that the updated MR gap size now has an off-state characteristic slightly lower than the optimised $4S_4$ characteristic's low setting, with the high damping exceeding the optimised high damping value from zero flow rate up to around 1 L/s fluid flow rate. This means that the updated passage height moves the operating range to where it needs to be to adequately meet the suspension requirements.

This concludes the section on the pressure drop characteristics of the MR valve, next an investigation into the effect of temperature will be presented.

4.5. The effect of temperature

This section covers the effect of temperature on the performance of the MR fluid device. Although the MR effect has been documented to not be a strong function of temperature the pressure drop over a MR valve might very well be, due to the viscosity of the carrier fluid that is a strong function of temperature (Bhushan, 2002).

An accurate datasheet for the MR fluid showing viscosity as a function of temperature was not available, meaning that the temperature dependant characteristics needed to be determined from testing.

Figure 69 shows the pressure drop as a function of coil current for an excitation frequency of 0.2Hz with the blue crosses representing a cold test (33°C) and the red dots a warmed up test (50°C). The theoretical model assumed a temperature of 50°C. Figure 70 shows the force velocity curves for both the cold and the hot tests.

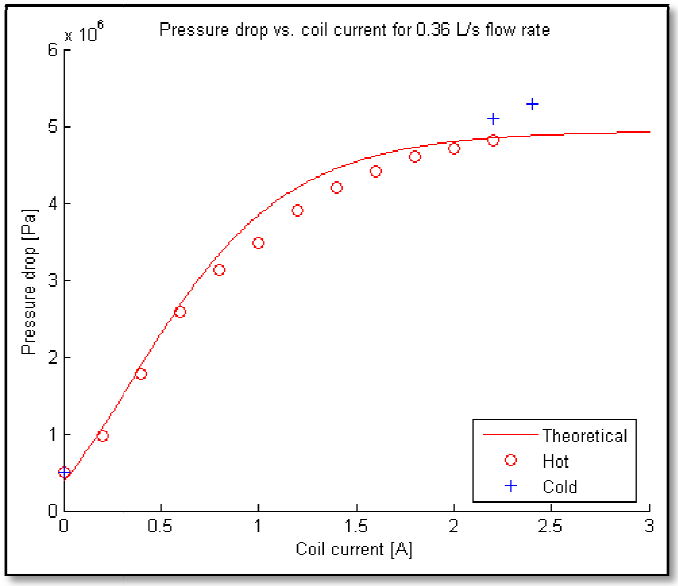

Figure 69: Pressure drop vs. current for hot and cold tests at 0.2Hz

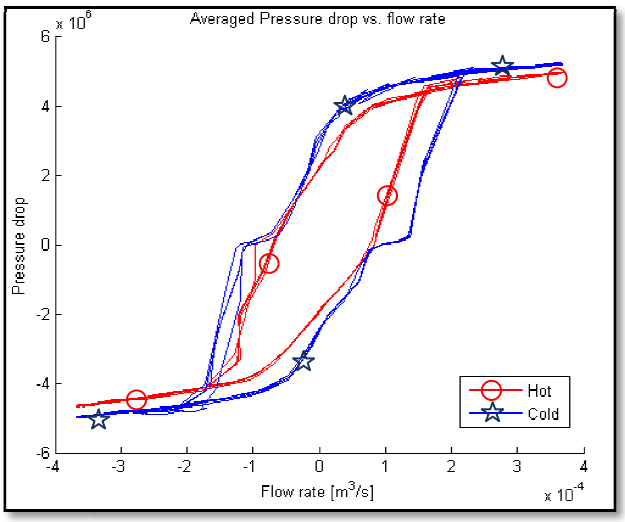

Figure 70: Pressure drop vs. flow rate for both the cold and hot tests performed at 0.2Hz

From Figure 69 and Figure 70 one can see that the temperature only influences the pressure drop by about 6 percent from cold to hot in the above test. It is however still recommended to model the temperature in the theoretical analysis so that a more accurate model may be achieved, especially when looking at the off-state of operation, when lacking the effect of a change in viscosity with temperature will yield a greater error. The temperature difference for the above tests was 17°C, with the cold temperature being 33°C and the hot state 50°C.

The temperature of the fluid was not recorded live for each and every test, but rather a thermal image was taken of the hydraulic cylinder at intervals between tests to get an estimate of the temperature of the fluid. Figure 71 shows a screenshot of the thermal imager taken of the hydraulic cylinder for the test 0.7Hz 2.4A.The long vertical heated (glowing) item in the figure is the

hydraulic cylinder, reading a maximum cylinder temperature of 63°C. Figure 72 shows the temperature of the MR valve body, reading a temperature of just under 62°C. These temperatures were some of the highest measured during the entire testing phase, with the temperatures for the lower frequency excitations, and thus lower energy dissipation tests being between 40°C and 50°C.

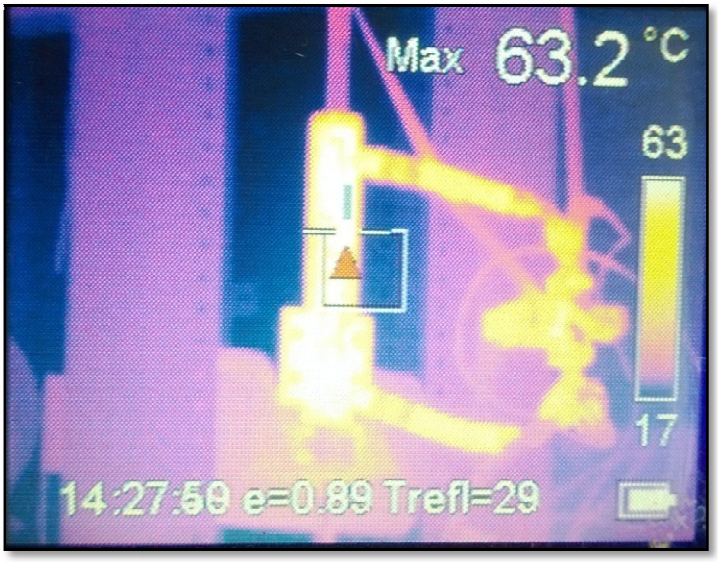

Figure 71: Thermal image of the hydraulic actuator for 0.7Hz 2.4A after some time of testing

Figure 72: Thermal image of MR valve after some time of testing

By viewing the thermal image for a specific test and finding the viscosity that will result in an accurate fit to that test, a temperature-viscosity relationship, as is shown in Table 3has been found.

Table 3: Viscosity vs. temperature for the MR fluid

Viscosity [Pa.s.]	Temperature [°C.]
0.35	68
0.36	62
0.37	52.5
0.56	38
0.6	35

A simple expression for the viscosity-temperature dependence for a fluid is given by Bhushan, (2002), as

$$\eta = \eta_0 \times e^{\left[\beta\left(\frac{1}{T}-\frac{1}{T_0}\right)\right]} \quad (27)$$

In Eq.(27) η is the actual fluid viscosity, at temperature T and reference temperature $T_0$and reference viscosity $\eta_0$respectively. Now, using the information in Table 3together with Eq. (27) the constants and reference values were obtained and the viscosity-temperature relation plotted. Figure 73 shows this equation plotted for the MR fluid used, with η_0 = 0.36, T_0 = 62°C and β determined to be 43.4.

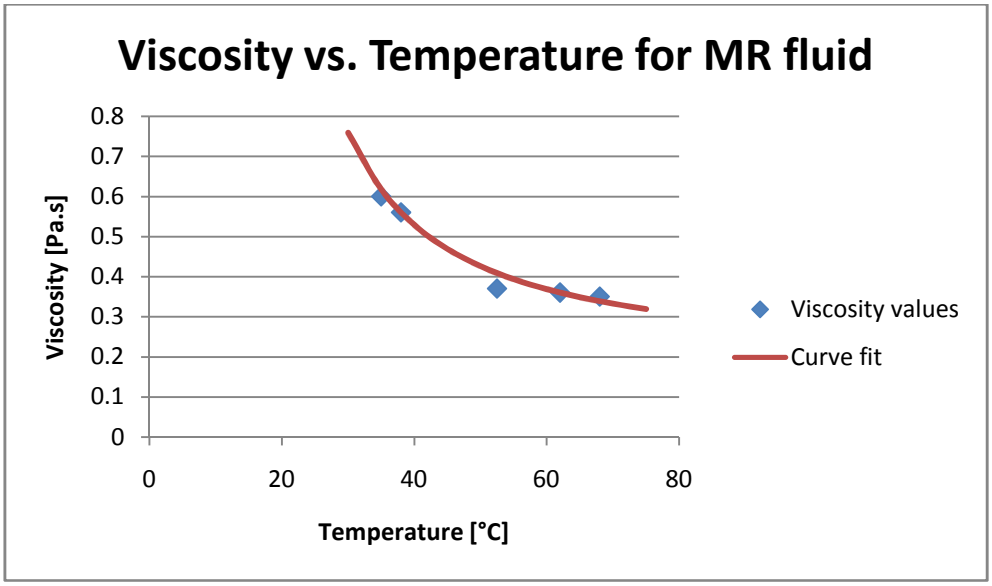

Figure 73: MR fluid determined viscosity as a function of temperature

With the curve fit showing a good fit for the viscosity as a function of the temperature of the MR fluid used it can now be concluded that the theoretical model can account for the viscosity of the MR fluid used as a function of temperature in the MR valve. Figure 74shows tests performed at 0.2Hz 2.2A using a 33°C and a 50°Ccylinder temperature respectively, the theoretical predictions for the two temperatures measured are also included. From Figure 74 it is seen that the theoretical model is now successful in predicting the pressure drop over the MR valve.

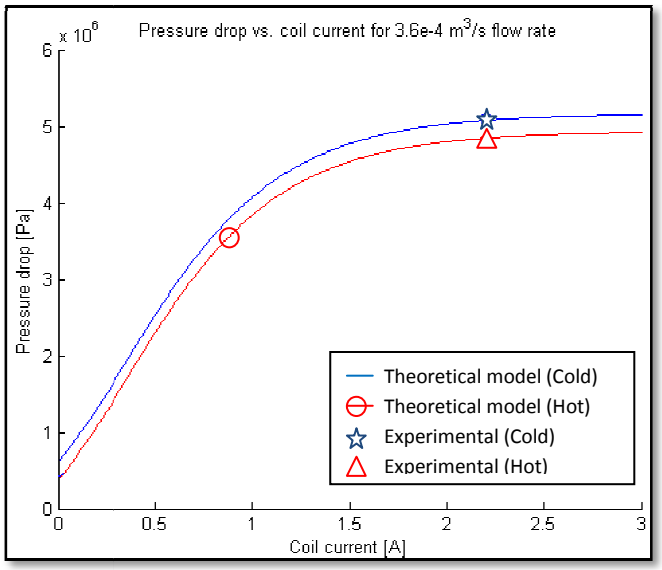

Figure 74: Cold and hot test data with theoretical predictions as function of temperature

From the study on the effect of temperature it was noted that temperature does in fact influence the pressure drop over the MR valve. With temperature varying from 33°C to 50°C a difference in pressure drop of around 6% was noted. This shows that temperature does not cause vast changes in the MR device performance in its normal operating temperature range, but is something that should be accounted for if accurate predictions are required, or if the device is operated at temperatures far from its normal operating temperature of 50°C.

This now concludes the section on the effect of temperature on the performance of the MR device. Next, the effect of piston friction in the damper is discussed.

4.6. Piston friction

This section investigates the effect of piston friction in the proposed MR suspension discussed in this study. Piston friction does not influence the pressure drop of the MR fluid over the valve, but it does influence the effort required to displace a suspension system comprising of a hydraulic cylinder and MR damper as the one that is proposed in this study, and therefore an investigation into the effect of piston friction will be conducted.

The tests performed in this study, that were discussed in Section 4.2, made use of a double acting hydraulic cylinder to displace the MR fluid. Pressure transducers were placed on either side of the valve to measure the pressure drop over the valve. By measuring the pressure drop in this way the effect of the piston friction was intentionally excluded from those results. To investigate the friction of the piston in the hydraulic cylinder a load cell was used to measure the force input from the servo hydraulic actuator to the hydraulic cylinder used to pump the MR fluid. By calculating the force required to pump the fluid using the known piston area of the hydraulic cylinder and measured pressure drop over the MR valve, and subtracting that force from the load cell between the servo hydraulic actuator and the hydraulic cylinder one is able to obtain an estimate for the piston friction experienced in the device.

The absolute value of the friction-velocity characteristic evident from testing with varying parameters is plotted in Figure 75. It may be noted that the piston friction may be approximated by using a quadratic equation with a non-zero vertical axis offset. Figure 75 shows the piston friction for tests performed with the best fit curve to estimate the friction as a function of velocity for all the test frequencies performed.

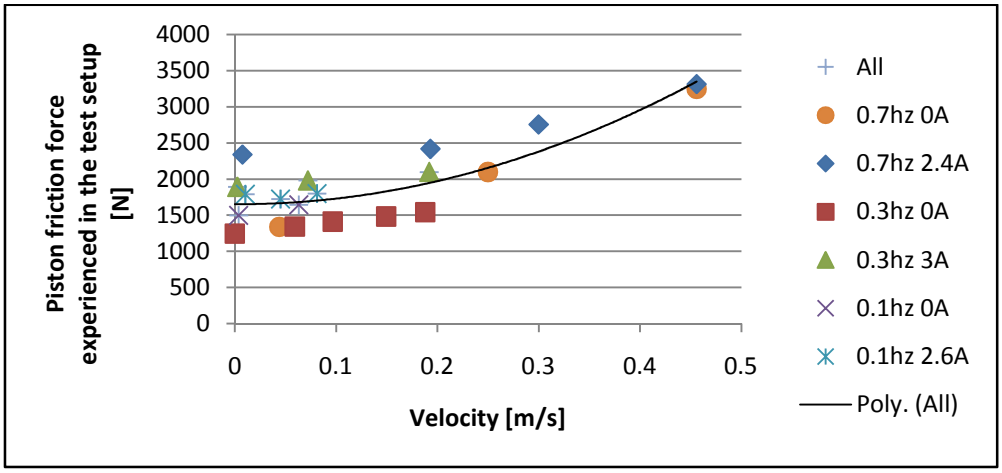

Figure 75: Piston friction as a function of velocity for different coil currents and excitation frequencies

Using this crude method, an approximation to the piston friction in the hydraulic cylinder may be obtained from the test data. It is to be noted that this is a rough estimation to the piston friction in the hydraulic cylinder. The actual friction in the final suspension will have to be determined by testing of the specific hydraulic cylinder that will be used as it is a function of the tightness of the fit between the various parts and the total length of seal material used, as well as a function of the pressure inside the cylinder and the speed of excitation.

To be able to use this information in the design of a MR suspension, the best possible method of obtaining a theoretical estimate for the piston friction is by scaling the data obtained by these tests to the appropriate cylinder size. This has been done by looking at the effective seal and sliding ring lengths of both the hydraulic cylinder used in the testing, as well as the $4S_4$ suspension cylinder itself. The seals and sliding rings are the main contributors to the friction experienced as they are the only components that make physical contact with each other, and all other small frictions like shearing of the fluid between the piston and cylinder wall is neglected. The piston friction in a design may now be scaled from the characteristic of the measured friction in the test setup's hydraulic cylinder, using a scale factor equal to the ratio of the hydraulic cylinder seal length compared to the $4S_4$ suspension's seal length. This value was found to be close to 2.1, meaning that the $4S_4$ hydraulic cylinder should approximately experience 2.1 times less friction force than the cylinder used in the experiments, for a given velocity.

4.7. Response time of the MR valve

A property of MR valves that make them very attractive for use in semi-active dampers is their ability to rapidly and reversibly change their damping as a function of the electromagnet's electric current. It should be stated that the main focus of this study was on the design of the valve for the MR fluid, and not on designing the optimally reactive magnetic circuit.

For the MR valve presented in this study the maximum flow rate that was tested was 1.27 Litre/second. With a passage cross-section of 2.5mm x 40mm it means that the maximum velocity of the fluid through the MR valve is determined to be 12.7 m/s. By using this velocity, it is calculated that the time that a particle in the fluid will spend in the 40mm long magnetised single passage is 3.15ms. With no diminishing effect in the pressure drop evident from testing at higher fluid flow rates, it is assumed that the response time of the fluid is not dependant on the fluid, as it has the ability to react fully to the magnetic field in the small time frame as calculated above. This shows that the response time of the fluid is a function of the magnetic field supply itself.

The reaction time of the MR device that was focussed on in this study is thus a function of the time it takes the electromagnetic circuit to develop its magnetic field. The magnetic field strength is directly proportional to the electric current flowing through the coil. Thus, if the coil current is logged as a function of time from a completely off state up to a saturation point for the applied voltage the reaction time of the MR valve can be determined for that voltage.

Figure 76 shows the coil current plotted as a function of time for different applied voltages, ranging from 10v up to 31v.

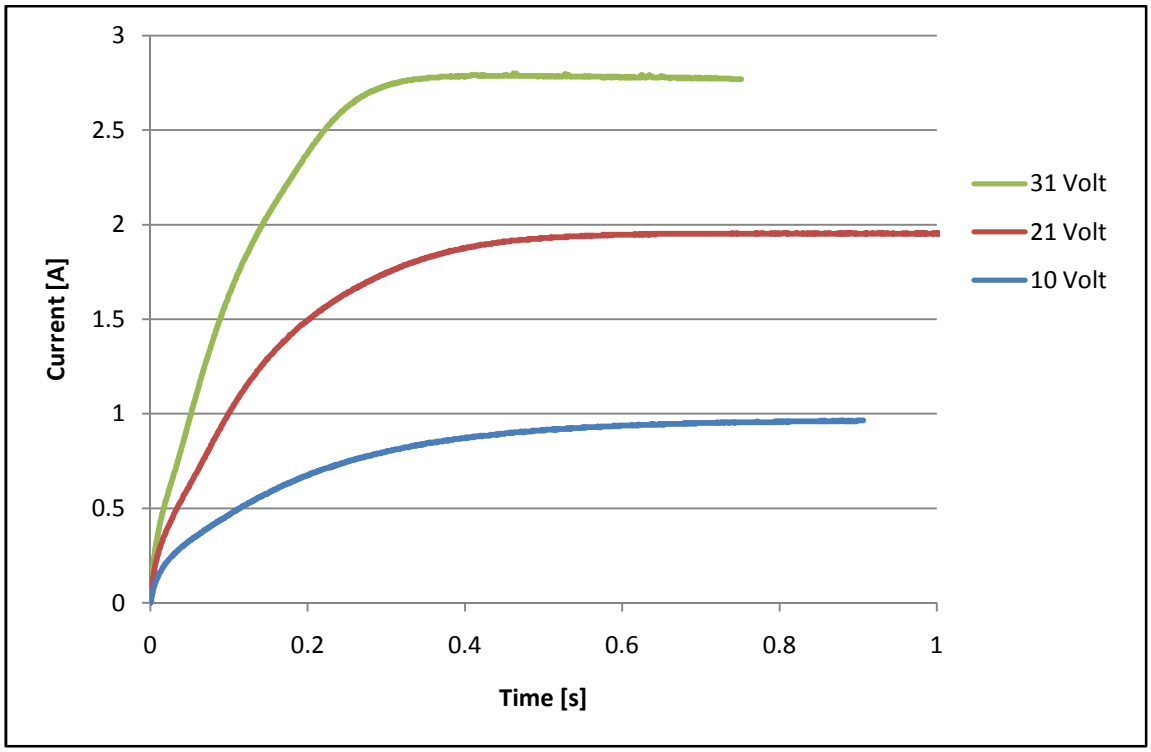

Figure 76: Reaction time of electric coil for different applied voltages

From Figure 76 it is seen that the reaction time for the electric coil is a function of the applied voltage. For 10v about 1 second is needed to develop a saturated electric current of 1A, where the saturation time for 31v is around 0.25 seconds. The upper voltage for the tests was limited by the amount of batteries available at the time of testing, as well as the maximum current that the measuring equipment allowed. From the pressure drop tests it was seen that the MR fluid started saturating at coil currents higher than 2A, with a definitive saturation seen at around 3A coil current. From the tests performed at 31v (3A saturated) the time required to almost saturate the MR fluid, i.e. the time to reach 2A is 0.15 seconds (150ms).

The reaction time of the electromagnetic circuit can be enhanced by using smarter control algorithms. In an electromagnet the voltage to current ratio is not constant for varying coil currents. If a constant voltage is suddenly applied to an electromagnet the current flowing through the electromagnet will lag behind and gradually increase to its maximum value as the current through an inductor cannot change instantaneously (Alexander & Sadiko, 2002). This phenomenon was seen in the tests performed, depicted in Figure 76. Even though the current cannot change instantaneously the rate at which the current changes can be forced higher by applying a higher potential initially to the electromagnetic coil, thus reducing the reaction time of the MR device. The residual magnetic field can also be reduced at a higher rate if the current in the coil is reversed to force the residual magnetic field in the core to diminish quicker, which can decrease the time for the MR valve to return to its “off-state”.

4.8. Sealing of the valve body

The whole valve body was manufactured by hand on normal manually operated machinery. The valve design that was used for the testing had many seal interfaces that had to be perfectly manufactured and assembled to seal effectively. This led to some small leakage that started to occur between the magnetic core and the valve body. This kind of minor leakage will not be acceptable when a valve like the one designed in this research study is to be used commercially. An improved design was conceived which reduces the number of sealing interfaces from about twenty, down to only one. For this to be implemented the whole valve body needs to be CNC machined from a solid block of a non-ferrous metal such as the aluminium used for the valve body in this study, with only the access from the main cover being left to seal against the main lid. Such an improved valve is shown in the isometric view Figure 77, with the single o-ring type seal to be used also shown. The only disadvantage of this design is that there is a short piece of non-ferrous metal in the path of the magnetic field, effectively giving the magnetic flux an “air gap” that needs to be jumped, however this could be accounted for by implementing a sufficiently strong magnetic source.

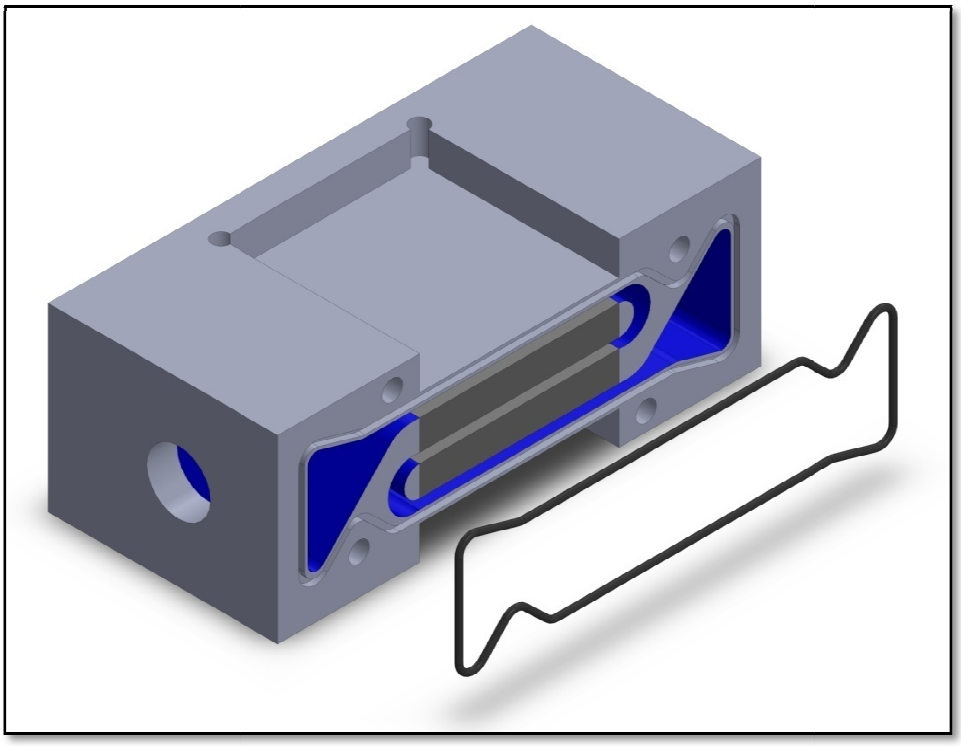

Figure 77: Improved MR valve seal design

5. Conclusions and Recommendations

This chapter presents the conclusions that can be drawn from this research study, based on the theoretical models that have been developed, and the testing that has been performed. The MR valve that has been developed in this study is a valve mode damper with the passage geometry of 40mm x 120mm and a height of 2.5mm, using a triple pass layout.

5.1. Pressure drop characteristic

The main aspect of interest in this study has been an investigation of the pressure drop characteristics of the proposed MR valve. The pressure drop is modelled as a function of two main input parameters; the fluid flow rate and magnetic field intensity. It has been observed from the tests performed that the original estimate for the viscosity of the MR fluid was inaccurate, and it is found that an increase from a value of 0.1Pa.s to 0.4Pa.s fits the experimental data quite accurately for normal operating temperatures. With this increase in the fluid viscosity the entire range of pressure drop characteristics as a function of fluid flow rate shifts upwards, which is especially noticeable in the off-state pressure drop over the MR valve that increases substantially.

It is found that the model developed for predicting the pressure drop over the valve as a function of coil current and flow rate, for the moderate flow rates tested in this study, delivers very accurate results with the error on average being less than 5%. The viscosity of the fluid is the only variable that needs to be modified in the theoretical model to account for the effect of fluid temperature. Temperature has been accounted for by using a fluid viscosity model, with some parameters derived from testing.

With the theoretical model verified to be accurate in predicting the pressure drop of the valve, a comparison can be made between the MR valve developed in this study and the user requirements. It is seen that the initial design for the MR valve yields a pressure difference from the off-state to the on-state that is comparable to the user requirements, but this whole range of pressure drops is lower than the requirements. Using the theoretical model, an improved geometry for the valve has been generated and the proposed MR valve should have the ability to comply with the user requirements with respect to the required pressure drop characteristics. The new geometry of the MR valve includes a passage height of 2mm, width of 40mm and a total length of 120mm, again divided into three 40mm long passages stacked one on top of the other in the s-pattern as discussed in this study.

5.2. Low flow rate and flow blocking ability

One of the user requirements for this research project has been to try to determine whether it would be possible to use the MR valve designed to block off the flow of fluid so that the solenoid valve controlling the suspension spring rate in the $4S_4$ system may be removed and its function taken over by a MR valve.

From the test results, it has been found that it is in fact possible to reduce the flow rate to quite close to zero, as long as the pressure drop over the MR valve is below a threshold value. It is shown that the initially designed MR valve can effectively withstand a pressure drop of around 2MPa without a measureable fluid flow. If the pressure drop over the valve is increased, the MR fluid will start to flow.

For the accurate modelling of the pressure drop as a function of fluid flow rate, it has been necessary to determine some variables that control the transition characteristic from where the fluid goes from the low shear rate quasi-Newtonian behaviour to the normal Bingham model. Equations have been derived for these variables and appropriate curve fits have been performed with satisfactory results.

If the improved MR valve geometry with a passage height of 2mm is evaluated for the flow blocking ability, the theoretical model predicts that the valve will now be able to effectively block off flow up to a pressure of 2.8 MPa, which is a 40% increase as compared to the initially designed MR valve presented in this study.

5.3. Passage geometry

The geometry of the MR passage used in this study is determined by building of a theoretical model that predicts the pressure drop over the passage as a function of fluid flow rate and coil current. With the information gathered through this study an improved geometry of the MR device has been identified. This improved geometry is expected, according to the theoretical model, to meet the requirements as set forth by the optimised $4S_4$ system in both the high and low settings. As stated in Section 5.1 above, the geometry of the passage that will yield the required range of damping from the off-state to the on-state is a passage height of 2mm, a width of 40mm and an overall length of 120mm.

5.4. Magnetic core modelling

A mathematical model has been built that solves for the magnetic field strength as a function of core material, fluid properties and MMF input to the electromagnetic coil. Tests have been performed, showing that the theoretical model is accurate if the core is not yet in its magnetic saturation region or close to a zero value, which might be influenced by hysteresis.

This model is implemented and the test results for the MR valve's pressure drop as a function of coil current verify that the proposed model yields accurate results. The wire used for the electromagnet is chosen such that it can withstand a current of up to 3.6A. The model also indicates that the maximum current that the wire can accommodate is more than sufficient to saturate the core. From the test results for the MR fluid it is found that the fluid itself shows saturation at around 2.4A. This shows that the magnetic core used in this study is actually too large, meaning that a smaller electromagnet would also be able to yield the same results with the benefit of being smaller in physical size.

5.5. Temperature effects and piston friction

From testing, it is found that temperature does not have a noticeable effect on the MR fluid's magnetic field dependant shear strength. It is noted that the theoretical model accurately predicts the pressure drop over the valve for low flow rates, even though the value for viscosity at that stage is off by a factor of 4, showing that the low flow rate on-state performance is not a strong function of fluid viscosity/temperature, but more of a function of the MR effect.

It is, however, found that the effect of temperature at increased flow rates does influence the accuracy of theoretical predictions significantly. The analytical model is adapted to account for the viscosity as a function of temperature. The results show that it is possible to account for the viscosity change as a function of temperature if some reference values for the MR fluid are known from testing. This enables accurate prediction of the performance of the MR valve as a function of temperature. If need be, a more accurate model for the temperature dependence of the fluid viscosity may be obtained by further testing.

The piston friction is measured for various tests and is found to have a quadratic behaviour with respect to flow rate. A fit to the friction data is performed to yield an averaged equation that is able to give an approximation to the friction that a typical piston would experience. The approximate value for piston friction can be used in the initial design stage of a MR suspension. In order to accurately model the friction, however, additional information such as the seal lengths, slide ring lengths and the fit between parts which are all design specific are required, and need to be investigated for the specific case that is being considered.

5.6. Reaction time

An aspect of specific interest to the designers of MR dampers is the reaction time of such a device. Designing the MR valve magnetic circuit for the best reaction time lay somewhat outside the scope of this project, although significant conclusions can be drawn from the tests performed. By evaluating the flow rate of the MR fluid through the valve it is concluded that the reaction time of

the MR fluid cannot be very dependent on the fluid itself, as the valve yields the pressure drop characteristics as predicted by the theoretical model, even at the high end of the flow rates that were tested. At the highest flow rate, the time that the fluid would spend in the magnetised MR gap was found to be around 3ms. It can be concluded that the reaction time of the MR damper presented in this study is mostly dependant on the magnetic circuit that supplies the magnetic flux to the fluid.

The shortest response time for the MR valve to increase from zero magnetic field up to an almost saturated value for an applied voltage of 31v was determined to be 150ms. This is slower than the solenoid valves that are currently used in the $4S_4$ which have a reaction time of 40-100ms (Els, 2006). The rate of change in the magnetic field, and hence the rate of change in damping for a MR valve, can be increased by implementing better control strategies that are able to momentarily over-power the electromagnetic coil to force the current in the coil to increase at a higher rate. One limitation to this is that the voltages should still be within safe power levels so as to not cause any harm in the event of a short-circuit.

The core material that has been used is AISI 1018 steel. If a shorter reaction time is required than the times mentioned above, it would also be possible to change the core material to one with better magnetic properties as compared to AISI 1018. By making use of a laminated core the rate of change in the magnetic field can also be increased, with the drawback of increased cost and a higher complexity of the magnetic circuit.

5.7. Sealing of the valve

The valve design that is used for the testing in this study has many seal interfaces that, after some time and pressure, started to leak the MR fluid's carrier fluid. This leakage problem can be solved by implementing an improved design that reduces the number of sealing interfaces. If this design is implemented in another study, the sealing problem should be solved.

5.8. Research outcomes

This section reflects on the initial research objectives that have been set at the start of this project, discussed in Section 1. The following may be concluded:

1. From the tests performed, it has been seen that it is possible to use MR fluid to yield a variable damping, which could be used in an appropriately designed controllable damper.
2. The tests show that the MR valve is capable of delivering the required range of damping that is required by the $4S_4$ system if an appropriate geometry of the valve is implemented.
3. It is found that it is possible to block off the flow of MR fluid up to a pressure drop of 2.8MPa (with the improved design), after which MR fluid does start to flow. This means that it will be possible to remove solenoid valve 3, as shown in Figure 1, and achieve the flow blocking capability by means of the MR valve, within limits.

Thus, the research outcomes are seen to answer the questions outlined in Chapter 1. The final theoretical model has proven to be accurate, and some valuable insight has been developed into the design of the MR valve. A list of recommendations is provided in the next section.

5.9. Recommendations

This section discusses some recommendations that can be made for further research into the MR valve discussed in this study:

1) The overall package size of the MR valve can be reduced so as to reduce the size of the magnetic circuit for feasible implementation into the $4S_4$ system.
2) The magnetic field distribution can be modeled using a Finite Element (FE) software package to improve on the field distribution accuracy in and around the MR passage, which will enable analysis into the effect that different parameters may have on the valve's performance.
3) The time response can be further investigated, and possibly improved by studying the MR valve in detail so as to yield a higher level of control to the $4S_4$ system.
4) The MR valve should be incorporated in the $4S_4$ suspension and thoroughly tested.
5) Further testing of the MR valve and the $4S_4$is required as part of the vehicle testing in order to move to the next phase of development for the device investigated in this study.

6. References

Alexander, C.K., Sadiko, M.N.O. (2002). *Fundamentals of electric circuits*, 2nd edition. McGraw Hill.

Alireza Farjoud, M. A. (2011). Nonlinear modeling and testing of magneto-rheological fluids in low shear rate squeezing flows. *SMART MATERIALS AND STRUCTURES* .

Ay, R., Golnaraghi, M. F., Khajepour, A. (2000). *Investigation on a Semi-Active Hydro Mount Using Mr Fluid.* Braunschweig, Germany: RTO MP-051.

Bhushan, B. (2002). *Introduction to tribology.* John Wiley & Sons.

Carlson, J.D., Jolly, M. R. (2000). MR Fluid, foam and elastomer devices. *Mechatronics 10* , 555-569.

Carlson, J. D. (2004). *Lord Corporation.* Retrieved 2009, from Lord corporation corporate website: www.lord.com

Carlson, J. D. (2005). MR fluids and devices in the real world. *International journal of modern physics B* , 1463-1470.

Els, P.S., Theron, N.J., Uys, P.E., Thoresson, M.J. (2007). The ride comfort vs. handling compromise for off-road vehicles. *Journal of terramechanics vol 44* , 303-317.

Els, P.S. (2006, July). The ride comfort vs. handling compromise for off-road vehicles. Unpublished Phd. Thesis. www.upetd.up.ac.za/thesis/available/etd-07152008-102911/

Gillespie, T.D. (1992). *Fundamentals of vehicle dynamics.* SAE.

Goncalves, F. D. (2005). *Characterizing the Behavior of Magnetorheological Fluids at High Velocities and High Shear Rates.* Blacksburg, Virginia.

Hersman, S., Hu, K., Sunday, D., & Yang, L. (2006). Flow of magnetic-rheological fluids.

Jansen, L. M., & Dyke, S. J. (2000). Semi-Active Control Strategies for MR Dampers:A Comparative Study. *ASCE journal of engineering mechanics, 126* (8), 795-803.

Jingnan, L., Hongyu, S., Aitao, T., & Ping, X. (2003). Operational model of magnetorheological transmission. *Proc. of SPIE, 5253*, 901-904.

Jolly M.R., Bender, J.W., Carlson, J.D. (1998). Properties and applications of commercial Magnetho rheological fluids. *SPIE 5th annual international simposium on smart structures and materials* , 12-17.

Klingenberg, D. (2001). Magnetorheology: Applications and challanges. *AIChE, 47* (2), 246-249.

Land Rover Evoque's magnetic attraction. (2011, April 8). Retrieved February 13, 2014, from Automotive engineer: www.ae-plus.com

Levin, M. L., Polesskii, D. E., Prokhorov, I. V. (1997). Some features of the magnetorheological effect. *Journal of engineering physics and thermophysics, 70* (5), 769-772.

Li, W. H., Du, H. (2003). Design and Experimental Evaluation of a Magnetorheological brake. *The international journal of advanced manufacturing technology, 21*, 508-515.

Lord.com. (2013). *LORD Magneto-Rheological (MR)*. Retrieved February 13, 2014, from Lord Corporation: www.lord.com

Lord_Corporation. (2008). *MR 180 kN Damper*. Retrieved 08 17, 2009, from http://www.lord.com/Home/MagnetoRheologicalMRFluid/Products/MR180kNDamper/tabid/3365/Default.aspx

Lord-Corporation. (2008). *Primary Suspension*. Retrieved 08 17, 2009, from http://www.lord.com/Home/MagnetoRheologicalMRFluid/Applications/PrimarySuspension/tabid/3329/Default.aspx

Magneride. (2014, January 31). Retrieved February 13, 2014, from Wikipedia: en.wikipedia.org/wiki/MagneRide

Metzger and Willard. (2011). *Moody diagram*. Retrieved September 12, 2011, from Metzger & Willard inc. website: http://metzgerwillard.com

Occhiuzzi, A., Spizzuoco, M., Serino, G. (2003). Experimental analysis of magnetorheological dampers for structural control. *Smart materials and structures, 12*, 703-711.

Olabi, A. G., Grunwald, A. (2007). Design and application of magneto-rheological fluid. *Materials and Design 28* , 2658–2664.

Poynor, J. C. (2001). Innovative Designs fo rMagneto-Rheological Dampers.

Sen, P.C (1997). *Principles of Electric Machines and Power Electronics, 2nd ed.* Kingston, Ontario, Canada: John Wiley & Sons.

Spencer, B. F., Dyke, S. J., Sain, M. K., & Carlson, J. D. (1996). Phenomenological Model of a Magnetorheological Damper. *ASCE Journal of Engineering Mechanics* .

Susan-Resiga,D., Vékás, L., Susan-Resiga,R. (2007). A RHEOLOGICAL MODEL FOR MAGNETO-RHEOLOGICAL FLUIDS.

Tao, R. (2001). Super-strong magnetorheological fluids. *Journal of physics: Condensed matter* , 979-999.

Thoresson,M.J., Uys, P.E., Els, P.S., Snyman, J.A. (2009). Efficient optimisation of a vehicle suspension system, using a gradient-based approximation method, Part 2: Optimisation results. *Mathematical and Computer Modelling 50* , 1437-1447.

Uys, P.E., Els P.S., Thoresson, M.J.(2007). Suspension settings for optimal ride comfort of off-road vehicles travelling on roads with different roughness and speeds. *Journal of terramechanics vol 44* , 163-175.

Wray, A. C., Hoogterp, F. B., Garabedian, S., Anderfaas, E., & Hopkins, B. (2003). *Magneto-Rheological fluid Semi-Active suspension performance testing.* Michigan: TARDEC.

Wray, A. C., Jimenez, A. R., Anderfaas, D. E., Hopkins, B., & LeNoach, P. (2005). *Magneto-Rheological fluid Semiactive suspension system performance testing on a stryker vehicle.* Michigan: TACOM.

Xianzhou Zhang, W. L. (2008). *Study on magnetorheological shear thickening fluid.* Wollongong, Australia: School of Mechanical, Materials and Mechatronic Engineering, University of Wollongong.

Yang, G, Spencer, B.F Jr., Carlson, J.D., Sain, M.K., (2002). Large-scale MR fluid dampers: Modelling and dynamic performance considerations. *Journal of Engineering Structures vol 24,* 309–323.